UC Berkeley
UC Berkeley Electronic Theses and Dissertations

Title
Control of Strand Scission by Type IIA Topoisomerases

Permalink
https://escholarship.org/uc/item/4cb1b5f3

Author
Schmidt, Bryan Harris

Publication Date
2012

Peer reviewed|Thesis/dissertation

Control of Strand Scission by Type IIA Topoisomerases

By

Bryan Harris Schmidt

A dissertation submitted in partial satisfaction of the

requirements for the degree of

Doctor of Philosophy

in

Molecular and Cell Biology

in the

Graduate Division

of the

University of California, Berkeley

Committee in charge:

Professor James M. Berger, Chair
Professor Jamie H. D. Cate
Professor Bryan A. Krantz
Professor Matthew B. Francis

Fall 2012

Abstract

Control of Strand Scission by Type IIA Topoisomerases

by

Bryan Harris Schmidt

Doctor of Philosophy in Molecular and Cell Biology

University of California, Berkeley

Professor James M. Berger, Chair

Topoisomerases are a family of essential enzymes that disentangle chromosomes and manage DNA supercoils, and are targets of a broad class of successful antibiotics and anticancer therapeutics. The type IIA topoisomerases operate by a complex ATP-dependent strand passage mechanism in which the enzyme transports one DNA segment through a transient, enzyme-mediated break in a second DNA segment. To understand the mechanism of DNA cleavage by type IIA topoisomerases, I used a suicide DNA substrate to crystallize the DNA binding and cleavage core of the enzyme covalently bound to DNA through its active-site catalytic tyrosine. The crystal structure revealed that type II and IA topoisomerases employ a novel variation of canonical two-metal ion phosphoryl-transfer chemistry to achieve DNA cleavage. Additionally, the suicide DNA substrate enabled me to determine the first structure of a fully-catalytic type IIA topo II-DNA-nucleotide complex. The structure revealed the overall doubly-domain swapped architecture of the enzyme. This organization produces an unexpected interaction between the bound DNA and a conformational transducing element in the ATPase domain, which is critical for both DNA-stimulated ATP hydrolysis and global topoisomerase activity. The data indicate that the ATPase domains pivot about each other to ensure unidirectional strand passage and that this state senses bound DNA to promote ATP turnover and enzyme reset. Lastly, the DNA-bound structure of one of the two human topo II isoforms, topo IIα, underscores the coupling between the DNA cleavage active site configuration with both metal ion occupancy at the cleavage center, as well as the dimerization status of a key dissociable interface over 50 Å away. The structure also highlights amino acid differences in the drug-binding pocket between the two human isoforms that could serve as differentiating features for developing more selective anti-topoisomerase agents. The work presented in this dissertation helps to explain years of biochemical studies, unifies many elements of topo II mechanism and its control by allostery, and has implications for both understanding large ATP-dependent DNA-remodeling molecular machines as a whole, as well as understanding the means by which small molecules target these enzymes for clinical benefit.

TABLE OF CONTENTS

Chapter 4 – The structure of a DNA-bound human topoisomerase IIα: conformational mechanisms for coordinating inter-subunit interactions with DNA cleavage

Chapter 5 – Concluding Remarks

Acknowledgments

Special thanks to my family and friends, who have supported me tremendously along the entire way. Everyone in the Berger lab has been helpful; in particular I would like to thank Ken Dong, Allyn Schoeffler, and Kevin Jude for answering so many questions and teaching me so much. I would also like to thank Tim Wendorff, who worked with me on the human topo IIα structure and was instrumental in both the experimental work and the intellectual analysis. James Berger was invaluable in his insight, support, and guidance; I feel very fortunate to have had him as my graduate adviser. Committee members Bryan Krantz, Jamie Cate, and Matt Francis were very helpful with their comments, advice, and support. The work described in this thesis was supported by the NIH. Lastly, I want to thank Debbie Thurtle for all her love and support.

Chapter 1 – Introduction to Type IIA Topoisomerases

(Portions of this chapter are adapted from: Vos S.M., Tretter E.M., **Schmidt B.H.** and Berger J.M. (2011). Nat Rev Mol Cell Biol 12(12),827-41)

The inherent challenges of the double helix
The extended, double-helical structure of DNA presents a stable way of storing and sequestering genetic information. However, it also poses a particular set of challenges to living organisms. Chromosomes must be folded and compacted in an orderly manner to fit within the confines of the cell. Additionally, nucleic-acid transactions such as transcription and replication, which require access to nucleotide sequence information, necessitate duplex melting events that overwind or underwind (i.e. supercoil) nucleic acid segments. For example, DNA will become overwound, or positively supercoiled, in front of a replication fork or transcription bubble. Supercoiling, if left unresolved, interferes with DNA replication and gene expression. Furthermore, DNA repair and replication generate entanglements between chromosomal regions that can lead to potentially mutagenic or cytotoxic DNA strand breaks.

Nature's solution to these problems is a class of enzymes known as topoisomerases. Endowed with an ability to cut, shuffle, and religate DNA strands, topoisomerases can add or remove DNA supercoils and disentangle snarled DNA segments. How topoisomerases carry out such complex functions has long been a significant question of biochemical and biophysical interest. In addition, topoisomerases remain a subject of intense interest because a remarkable diversity of natural and synthetic agents block topoisomerase function for therapeutic gain.

Classification of topoisomerase families
At first glance, a bewildering number of different topoisomerase classes exist. This abundance underscores the diversity of both topoisomerase function and evolution. However, the topoisomerase collection is not as complicated as it first appears. For example, all topoisomerases identified to date contain a nucleophilic tyrosine, which they use to promote strand scission. This creates a transient, covalent enzyme–DNA linkage that helps prevent the inadvertent formation of DNA nicks and breaks. Moreover, topoisomerases can be divided into just two primal classes, type I and type II, based on whether they cleave one strand of DNA (type I) or both strands (type II). These two classes are further categorized by subtype – "A," "B," or "C" – based on: the protein structure of the topoisomerase and the primary DNA sequence relationships between topoisomerases, the disposition of a given topoisomerase to cleave at either 5' or 3' DNA linkages, and whether metal ions are involved in strand breakage and rejoining. Enzymes with an odd Roman numeral (for example, "I" or "V") after their name fall into the type I class, whereas those with an even-numbered Roman numeral after their name

are type II class. A comparison of the different subtypes of topoisomerases is presented in **Table 1.1**.

Why are there so many different types of topoisomerases? One reason is that these enzymes have specialized functions to address particular aspects of genome maintenance. Different topoisomerases have different substrate specificities (for example, favoring positively supercoiled DNA vs. negatively supercoiled DNA, or favoring single-stranded DNA over double-stranded DNA.) Whichever topoisomerase might be used to address a particular need for the cell, to effect changes in DNA topology it must break at least one strand of DNA. Upon strand scission, there are two general mechanisms for topoisomerases. In one scheme, the rotary mechanism, one intact strand is held in place while the other nicked strand has a free end that is allowed to rotate around it. This "swivelase" scheme is used by the type IB and IC families. The other scheme is the strand passage mechanism, where DNA is actively passed through a break in another piece of DNA (either single-stranded in type IA, or double-stranded in type II topoisomerases).

Overview of the type IIA topoisomerase family

As with their type IA counterparts, type IIA topoisomerase employ an active strand passage mechanism for effecting topological changes in DNA (**Figure 1.1**). Type IIA topoisomerases share certain catalytic domains used for DNA cleavage in common with the type IA family(Aravind et al., 1998; Berger et al., 1998). However, type IIA enzymes differ in that they cleave both strands of a DNA duplex and pass a second intact duplex through the transient break(Liu et al., 1980; Mizuuchi et al., 1980), and they use ATP to power strand passage(Gellert et al., 1976; Goto and Wang, 1982). These activities allow type IIA topoisomerases to resolve both negative and positive supercoils, as well as to disentangle long intertwined chromosomes and DNA (catenanes). Type IIA topoisomerases are found throughout all cellular organisms, as well as in some viruses and organelles, and can be partitioned into three homologous subfamilies – eukaryotic topo II, bacterial topo IV, and bacterial and archaeal gyrase – that each exhibit distinct functional properties(Forterre et al., 2007; Schoeffler and Berger, 2008).

Structure and mechanism of type IIA topoisomerases

In prokaryotes, type IIA topoisomerases are A_2B_2 type heterotetramers. In eukaryotes, the two halves of the enzyme are fused into a single chain that assembles as a homodimer. Structural biology has been a useful tool in understanding the arrangement of topoisomerase domains and elucidating their reaction cycles. Although no full-length type IIA topoisomerase has been imaged at high resolution, X-ray crystal structures of the individual domains have proven useful in our understanding of mechanism and substrate binding. In particular, they reveal that there are three primary dimerization interfaces, or "gates." The first of these interfaces resides in the N-terminal ATPase domain.

The ATPase of type IIA topoisomerases belongs to the GHKL family, named after gyrase, Hsp90, histidine kinases, and MutL proteins(Dutta and Inouye, 2000). The ATPase Bergerat fold connects to another domain, called the transducer, which in turn connects to the core DNA-binding and cleavage center of the enzyme. The transducer is thought to relay conformational states from the ATPase domain down to the rest of the enzyme. The first structure of a type IIA ATPase was determined for *E. coli* gyrase in the presence of a non-hydrolyzeable ATP analogue, AMPPNP(Wigley et al., 1991). This structure (and subsequent ones reported for the yeast and human enzymes(Classen et al., 2003; Wei et al., 2005)) show the ATPase to adopt a heart-shaped dimer. A domain swapping event at the extreme N-termini acts *in trans* as a lid to complete the binding pocket for nucleotide. In the center of the dimer is a central cavity that is thought to accommodate a segment of DNA, although the cavity seen in eukaryotic ATPase structures is significantly smaller than those seen in their prokaryotic counterparts.

The transducer connects to the core of the enzyme, beginning with the TOPRIM domain, named after topoisomerase and DnaG primase families, although it is also found in RecR proteins and OLD family nucleases(Aravind et al., 1998). This domain participates in DNA binding, and also has a conserved motif of acidic residues that coordinates divalent cations. Metal ions are essential for religation in both the type II and IA families; however, metal ions are only essential for DNA cleavage in the type II but not IA family(Goto et al., 1984). The TOPRIM is connected to the remaining core of the enzyme – called the DNA-binding and cleavage core – which binds to DNA and also contains the catalytic tyrosine. The tyrosine resides in the Winged Helix Domain (WHD), historically named CAP domain because of its similarity to catabolite activating protein. The TOPRIM domain of one protomer acts *in trans* with the WHD of the other protomer to form a bipartite active site(Dong and Berger, 2007). This active site region comprises the second of three gates, the "DNA gate." The core region then gives way to two long alpha helices that comprise the "legs" of the enzyme, featuring the third and final dimerization interface, the C-gate.

In the type IIA reaction cycle, one double-stranded DNA (termed the "G-segment") is bound and cleaved by the enzyme, while a second duplex (the "T-segment") is transported through the break(Roca and Wang, 1994). G-segment breakage is catalyzed by the two symmetrically-related tyrosines(Tse et al., 1980; Worland and Wang, 1989), in conjunction with the TOPRIM fold, forming a transient covalent topoisomerase•DNA cleavage complex. Strand passage is coordinated by the ATPase domains(Brown et al., 1979; Gellert et al., 1979; Lindsley and Wang, 1993b) which use ATP binding and hydrolysis to promote T-segment capture, stimulate G-segment cleavage, and coordinate successive opening and closing of the gates(Roca and Wang, 1992, 1994; Williams and Maxwell, 1999a, b). The cleavage of the G-segment by tyrosine constitutes an important focus of my research for two primary reasons. First, outstanding

questions remain concerning the biophysical understanding of the DNA cleavage mechanism. Second, the covalent cleavage state is the target for a large number of successful therapeutic agents that target topoisomerases.

Topoisomerase inhibition

Although indispensible for supporting viability, topoisomerases present cells with a fundamental problem: they can be inadvertently inactivated, or their DNA cleavage activity can be corrupted, resulting in cytotoxic or mutagenic DNA breaks. In the case of aberrant cleavage, the evolution of repair systems, such as the Tdps(Cortes Ledesma et al., 2009; Nitiss et al., 2006; Pouliot et al., 1999; Zeng et al.), serve to deal with this molecular problem. However, nature and humans have been able to exploit topoisomerase inactivity and stalling through diverse means to kill cells, at times for tangible therapeutic benefit.

A number of proteins and protein-like factors specifically inhibit topoisomerase activity, particularly in bacteria. These proteins range from toxins that control plasmid stability (CcdB)(Bernard and Couturier, 1992; Smith and Maxwell, 2006) to agents that are involved in microbial competition (microcin B17)(Vizán et al., 1991) and antibiotic resistance (Qnr and MfpA)(Hegde et al., 2005). Such factors have varied modes of action that include attenuating the DNA binding activity of topoisomerases, or promoting their ability to cleave DNA.

On the biomedical side, topoisomerase inhibition has proven to be a highly versatile and useful approach for therapeutic intervention. Small-molecule agents targeting topoisomerases fall into two broad classes based on their mode of action: "inhibitors," which attenuate enzyme activity, and "poisons", which stabilize DNA-cleavage complexes (see **Figure 1.2** for a partial list of type II topoisomerase antagonists). Although many of the most significant therapeutics (for example, epipodophyllotoxins, quinolones, and camptothecin derivatives) have been used for decades, only relatively recently have their mechanisms of action been understood in molecular detail. For instance, camptothecin, and its derivatives such as Topotecan, poisons that target type IB topoisomerases, bind at the enzyme active site in the presence of cleaved DNA (Staker et al., 2002), impeding both DNA religation and the relaxation of supercoils. Fluoroquinolones, which are used primarily as antibiotics but also can exhibit anti-tumor properties (Elsea et al., 1992; Hoch et al., 2009), appear to act in a similar manner, binding between the 5' and 3' end of a cleaved DNA strand to prevent resealing and release of the DNA by the topoisomerase(Bax et al., 2010a; Laponogov et al., 2010; Laponogov et al., 2009; Wohlkonig et al., 2010). For type II topoisomerases, compounds that block ATPase activity (novo and cholorobiocins(Lewis et al., 1996; Tsai et al., 1997), bisdioxopiperazines(Classen et al., 2003), radicicol(Corbett and Berger, 2006)), DNA binding (simocyclinone D8)(Edwards et al., 2009), or DNA cleavage (NTBI GSK299423)(Bax et al., 2010a) have all been found and captured with X-ray crystallography in the presence of their respective targets. Together, these findings not only highlight the molecular

determinants that enable drug binding and explain their inhibitor properties, but further demonstrate that there is a rich abundance of molecular scaffolds capable of inhibiting topoisomerases (**Figures 1.1, 1.2**). A hopeful, but presently unrealized, goal for these combined efforts is to point the way toward design of new inhibitors that show improved patient tolerance and can circumvent emerging problems with drug-resistance.

Outstanding questions

Despite decades of study, fundamental questions concerning topoisomerase function and mechanism remain unresolved. For example, despite the identification of the nucleophilic tyrosine residue decades ago, a complete picture of the DNA cleavage mechanism by type II and IA topoisomerases has remained persistently out of reach. Cleavage is known to require divalent metal ions, in particular magnesium, but how many metal ions bind, where they bind, and the roles they play are unclear. Additionally, while crystal structures of the isolated ATPase domain and the DNA binding and cleavage core have been determined, the overall architecture of the full-length enzyme, and how spatially-segregated ATPase and DNA-binding centers communicate with each other, remain undefined. Also, while *S. cerevisiae* topo II has been a successful structural model since the structural determination of its DNA binding and cleavage core in 1996 by Berger *et al*, there is increasing interest in the structures of the two human isoforms, topo IIα and topo IIβ , as these are the targets of anticancer topoisomerase poisons. Lastly, while several structures have emerged in recent years reporting topo II bound to DNA and a poison, there remain questions about what determines the specificity of each drug, how they target primarily eukaryotic or prokaryotic topoisomerases, and how their molecular scaffolds might be modified to overcome increasing drug resistance and secondary malignancies. Each chapter in this thesis will address these outstanding questions, primarily by both structural determination via X-ray crystallography and by biochemical assays.

Table 1.1 – Comparisons of the five identified topoisomerase families

Topo type:	IA	IB	IC	IIA	IIB
Number of strands cleaved	1	1	1	2	2
Representatives	Topo I, Topo III, Reverse gyrase	Topo I	Topo V	Topo II, Topo IV, Gyrase	Topo VI
Mechanism	Strand passage	Rotary	Rotary	Strand passage	Strand passage
Phosphotyrosyl connection	5'	3'	3'	5'	5'
ATP requirement	No (reverse gyrase, yes)	No	No	Yes	Yes
Divalent cation requirement	Mg^{2+} and Zn^{2+}	None	None	Mg^{2+}	Mg^{2+}
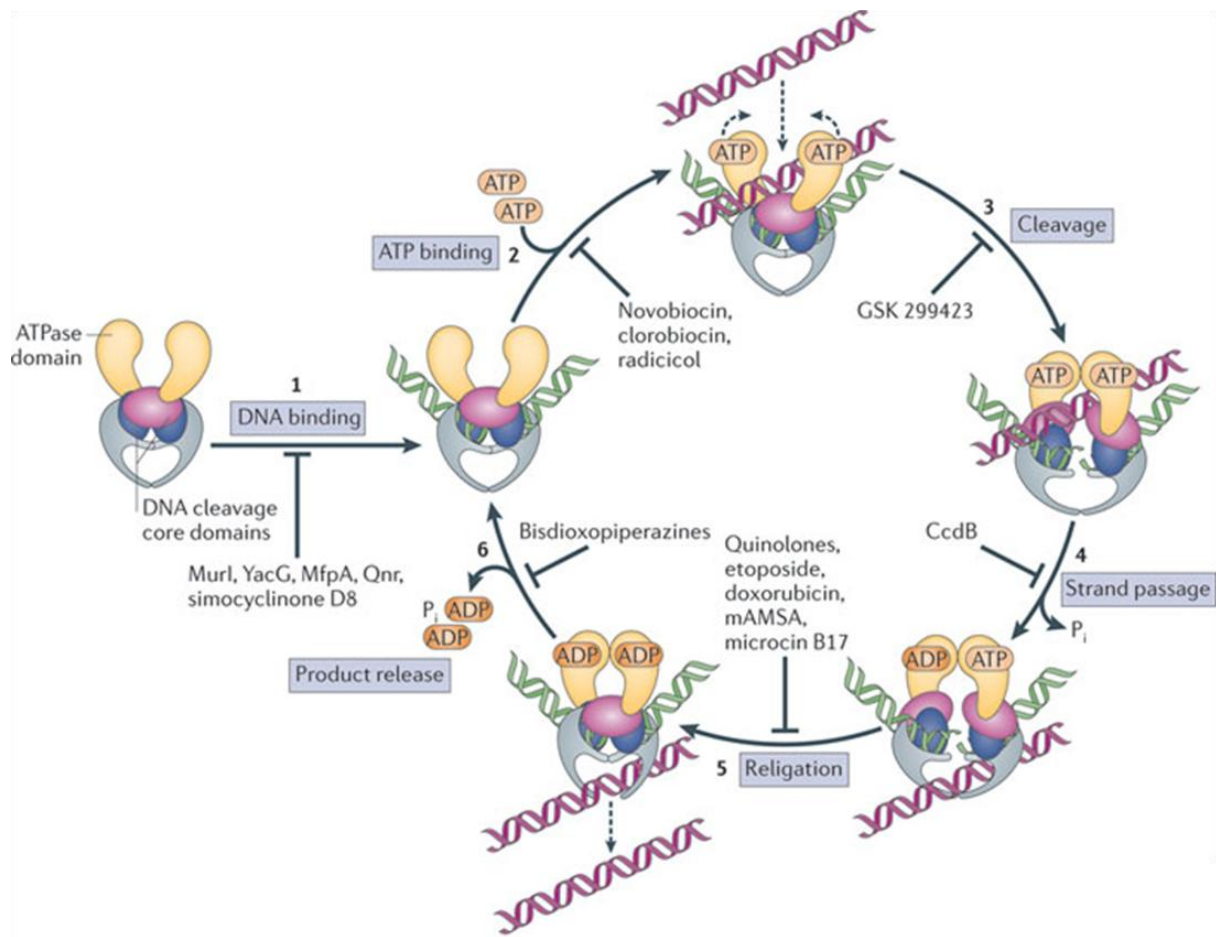
Figure 1.1 – Type IIA topoisomerase catalytic cycle and its points of inhibition
The type IIA topoisomerase reaction cycle and all points at which exogenous agents can disrupt function. During catalysis, the topo initially binds one duplex DNA segment (step 1). Following binding, the topo can then associate with a second duplex DNA segment. ATP binding (step 2) stimulates cleavage and opening of the first DNA (step 3), and passage of the second DNA segment through the transient opening (step 4). The broken strands are then religated (step 5), and the product is released (step 6). Agents are identified that interfere with each step, as indicated, but only a partial list of inhibitors and poisons is given here.
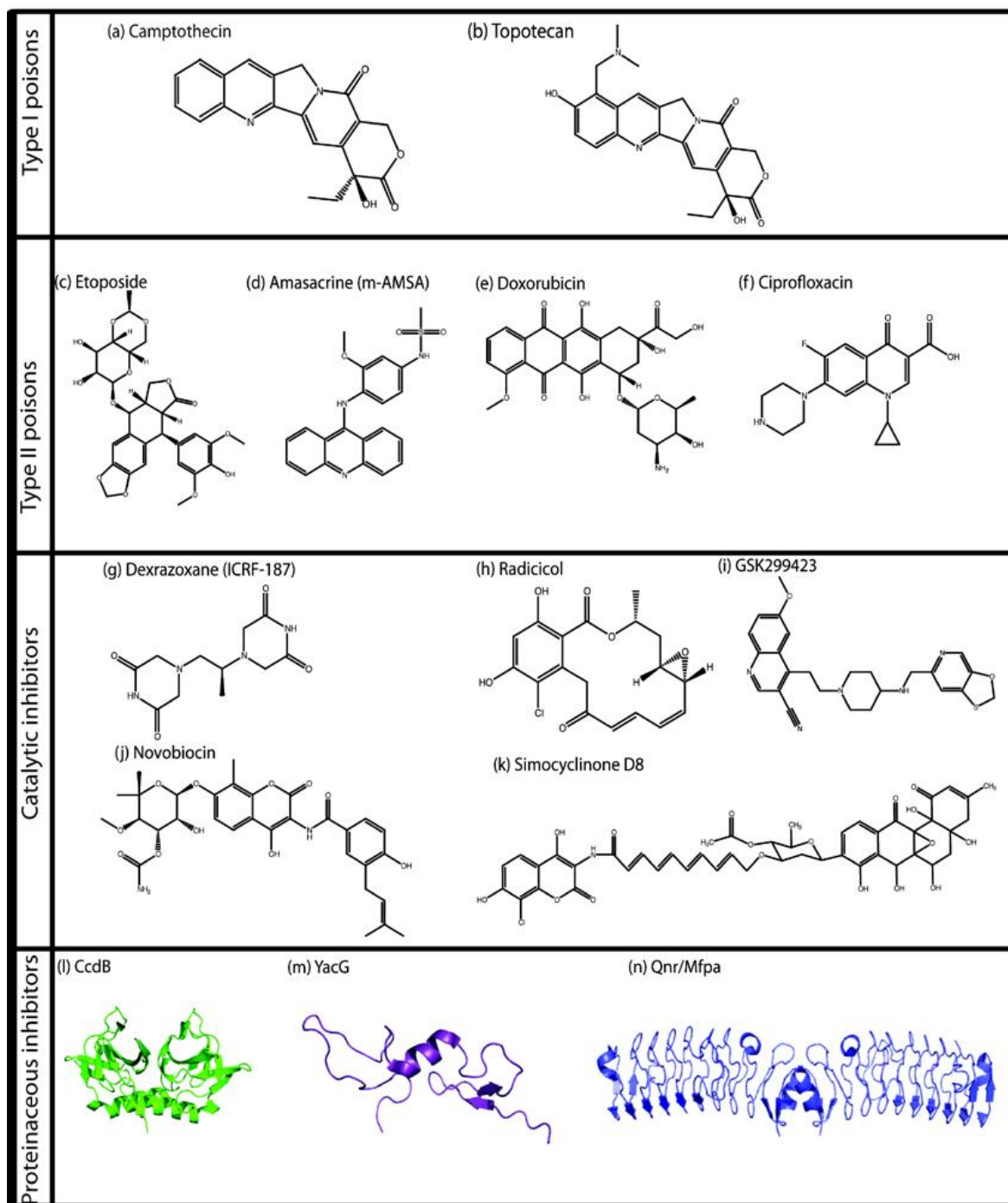
Figure 1.2 – Diversity of anti-topoisomerase agents
The chemical or ribbon structures of a very limited collection of known topoisomerase inhibitors and poisons is shown.

Chapter 2 – A Novel and Unified Mechanism for DNA Cleavage by Type IIA and IA Topoisomerases

(Portions of this chapter are adapted from: **Schmidt, B.H.**, Burgin, A.B., Deweese, J.E., Osheroff N. and Berger J.M. (2010). Nature 465, 641-644.)

Introduction

One of the key events during the catatlytic cycle of all topoisomerases is cleavage of the DNA phosphodiester backbone. For type II topoisomerases, it has been well established that a pair of dimer-related tyrosines, together with divalent cations, catalyze G-segment cleavage(Goto et al., 1984; Goto and Wang, 1982; Worland and Wang, 1989). Although a wealth of structural and biochemical efforts have illuminated key aspects of the type II topoisomerase mechanism, a biophysical understanding of their control of DNA cleavage chemistry has remained persistently out of reach. The first DNA-bound type II topoisomerase structure showed how these enzymes engage and bend substrate duplexes(Dong and Berger, 2007), but used a nicked DNA substrate to capture a pre-cleavage intermediate that could not provide insights into the chemistry of strand scission. Critically, the spacing seen between the catalytic tyrosine and the DNA backbone in this structure was too far apart (~6Å) to accommodate nucleophilic attack. The structure also exhibited only a single magnesium ion in the active site, whereas biochemical studies have implicated two in promoting strand scission (Deweese et al., 2009; Noble and Maxwell, 2002; West et al., 2000).

To attempt to visualize a more catalytically informative state, I determined the crystal structure of a *bona fide* topo II-DNA cleavage complex. Because type II topoisomerases disfavor cleavage when bound to short oligonucleotides, I used bridging phosphorothiolate chemistry to create a suicide substrate that leaves a free thiol as a leaving group instead of the usual 3'-OH (**Figure 2.1**). The thiol is insufficiently nucleophilic towards a tyrosyl phosphate group and unable to support religation(Burgin et al., 1995). This approach has been used at the 5'-ribose position to trap and image a type IB topoisomerase, which cleaves at the 3' end of a phosphodiester bond, bound to DNA(Redinbo et al., 1998).

Results and Discussion

Structure of a covalent complex

To form an irreversible cleavage complex with a type II topoisomerase, which cleaves at the 5' DNA end, the principal DNA binding and cleavage domain of *S. cerevisiae* topo II (residues 408–1177) was incubated with a DNA substrate containing a nick at one cleavage site and a 3'-bridging phosphorothiolate at the other (**Figure 2.2a-b**). Crystals grew in 20% 1,4 butanediol and 100 mM sodium acetate pH 4.5. Following co-crystallization, the structure of this complex

was determined to 2.5 Å resolution using molecular replacement. Electron density permitted building and refinement of a model to an R_{work}/R_{free} of 23.9%/25.9% (**Figure 2.2c, Table 2.1**), and showed clear evidence for a covalent 5' link between DNA and the active-site tyrosine (Y782) resident in topo II's winged helix domain (WHD) (**Figure 2.2a, d**).

Because a non-palindromic DNA sequence was used for co-crystallization (**Figure 2.2b**), and because the topo II–DNA dimer crystallized on a crystallographic dyad, electron density for the DNA corresponded to an average of the two half-sites. To account for this superposition, I modeled the DNA density as two alternate oligonucleotide segments, each present at half-occupancy; the covalent phosphotyrosine linkage was treated similarly (note: this approach has been used in similar circumstances with a STAT-1–DNA complex(Chen et al., 1998)). Refinement of this hybrid DNA model with a single protein chain produced significantly improved $2F_o$-F_c maps, gave rise to far less F_o-F_c difference density, and substantially decreased both R_{work} and R_{free}. Interestingly, $2F_o$-F_c and simulated-annealing composite omit maps not only showed features of both DNA sequences (**Figure 2.3**), but also revealed electron density corresponding to only one catalytic tyrosine rotamer and a single 5' DNA-end position (**Figure 2.2d**). Thus, even though only one active site can exist in a *bona fide* cleavage state with DNA (because the substrate contains only a single bridging phosphorothiolate modification), the nick is coordinated in essentially the same manner as the phosphotyrosyl bond. Formation of this state may arise from the high cooperativity observed between the topoisomerase active sites during DNA cleavage *in vitro*(Zechiedrich et al., 1989).

The structure of the complex shows the constellation of amino acids required to form a cleavage-competent active site. However, given the known metal dependence for DNA cleavage by type II topoisomerases(Goto and Wang, 1982), there was a surprising lack of electron density for these cofactors, despite the presence of 5 mM $MgCl_2$ in the protein buffer. Suspecting this absence might be due to the low pH (4.5) of crystallization, I solved a second structure of an isomorphous crystal soaked at a higher pH (6.5) with zinc chloride (Mg^{2+}, Mn^{2+} and Ca^{2+} did not produce sufficiently high diffraction, and glutaraldehyde cross-linking was required to stabilize the crystals for pH exchange). Soaking strategies have been used successfully to gain insights into other divalent cation-dependent polymerase and phosphodiesterase systems such as RNaseH and DNA polymerase I(Nowotny and Yang, 2006; Wang et al., 1996). Anomalous difference maps for this structure, which was determined by molecular replacement to 3.0 Å resolution, show clear evidence for two zinc ions (7σ peaks) in the active site (**Figure 2.4**). As anticipated from previous studies of topo II and its related bacterial counterpart, DNA gyrase, the ions are coordinated by highly-conserved acidic residues within the enzyme's topoisomerase/primase (TOPRIM) domain(Aravind et al., 1998), with E449 and D526 contacting metal A, and D526 and D528 engaging metal B (**Figures 2.2a and 2.4**).

A surprising metal ion configuration

In classical two-metal phosphoryl transfer reactions, one ion activates a catalytic water or ribose hydroxyl for nucleophilic attack, whereas the other coordinates a leaving group(Steitz and Steitz, 1993; Yang et al., 2006). Both cofactors stabilize a pentavalent transition state. Because of the frequent occurrence of this mechanism across many unrelated biomolecular systems, I was surprised to observe that the metal organization in topo II does not recapitulate such a configuration (**Figure 2.5**). Metal A interacts with both a non-bridging oxygen of the phosphotyrosine and the 3'-ribose position (**Figure 2.4**), and is thus well positioned to assist with transition state chemistry. However, metal B sits farther afield, contacting only a non-bridging oxygen of the (-1/-2) phosphate upstream of the cleavage site.

Despite the surprising deviation from a canonical two-metal arrangement, several lines of evidence indicate that the structure observed here recapitulates a catalytically relevant configuration. Replacement of an invariant arginine (R781), which contacts the phosphotyrosine moiety, markedly reduces DNA cleavage and relaxation activity(Liu and Wang, 1998), except when substituted with lysine(Okada et al., 2000). Metal binding at either the A or B locus has been seen in different type II topoisomerase structures (**Figure 2.4**)(Bax et al., 2010b; Dong and Berger, 2007; Laponogov et al., 2010; Nichols et al., 1999; Wohlkonig et al., 2010; Wu et al., 2011), and mutation of associated liganding groups severely compromises strand scission in both eukaryotic and bacterial enzymes(Deweese et al., 2009; Noble and Maxwell, 2002; West et al., 2000). The relative position of the metal-binding cluster with respect to DNA and the active-site tyrosine is further supported by: (1) patterns of thiol-dependent DNA cleavage seen in cysteine-mutagenesis and metal-ion rescue experiments consistent with the bonding arrangement seen here(Deweese et al., 2009; Noble and Maxwell, 2002); (2) the formation of an ion pair between two highly-conserved amino acids (D530 and R690) required for wild-type function(Liu and Wang, 1998); and (3) a new role for an invariant histidine (H736), which engages the (-1) phosphate bound by metal B. Finally, in the metal-free structure, the thio-ribose 3'-SH adopts a C2' endo (B-form DNA) sugar pucker non-optimally oriented for promoting religation, whereas in the zinc-bound structure, the thiol flips to a C3' endo state (A-form) similar to its neighboring nucleotides, moving within 2.0 Å of metal A and taking an in-line position with respect to the phosphotyrosyl linkage.

Collectively, these interactions indicate that type II topoisomerases use a distinct variation of canonical two-metal mechanisms (**Figure 2.6a**). In this scheme, one ion (metal A) partakes directly in transition state stabilization and in promoting the leaving and attacking of the ribose 3'-OH during DNA cleavage and religation. The other (metal B) plays a role in anchoring the DNA. The reason why type II topoisomerases may have lost the need for a second metal in performing chemistry is probably due to (1) the lower pK_a (~10–11) of the attacking tyrosine nucleophile during cleavage, which makes it easier to deprotonate compared to water or an

incoming ribose hydroxyl (pK_a ~13–15), and (2) the acquisition of a positively-charged arginine, which takes the place of the second metal to assist with transition state stabilization and to depress the pK_a on the tyrosine. Consistent with this reasoning, basic side-chain groups are not typically found to coordinate directly the reactive phosphate in classic two-metal ion systems.

The structure of the cleavage complex further reconciles the type II topoisomerase strand-scission mechanism with that used by type IA topoisomerases, a group of enzymes that cleave single, rather than double, DNA strands. Previous studies have noted that both types of topoisomerases use the same collection of active site residues and conserved domains to cut DNA(Berger et al., 1998). Moreover, both type II and IA topoisomerases form 5'-phosphotyrosyl bonds and require metal ions for full activity(Domanico and Tse-Dinh, 1991; Goto et al., 1984). However, one perplexing difference between the two families is that DNA cleavage by type IA topoisomerases is not strictly metal-dependent: although religation requires metal ions, their presence is needed only to stimulate, but not execute, strand scission(Goto et al., 1984). Comparison of the type II and IA topoisomerase active sites reveals the existence of an extra lysine in type IA topoisomerases that contacts the scissile phosphate (**Figure 2.6b**)(Changela et al., 2001). This lysine is found in all IA enzymes, although it switches between two adjacent locations in topo I and topo III paralogs (**Figure 2.7**). Significantly, mutation of this lysine in topo I abrogates metal-independent cleavage(Strahs et al., 2006), indicating that this basic amino acid is able to promote strand scission by fulfilling the role of metal A. Moreover, because this amino acid is incapable of polarizing the resultant 3'-OH, it would not be expected to support religation. Consistent with this reasoning, an aspartate to asparagine (D117N) mutant in topo I creates a dominant lethal enzyme that does not efficiently religate DNA, even in the presence of metals(Cheng et al., 2009), probably because a key metal-A binding residue is disrupted and hence favors lysine-mediated cleavage. Thus, the structure unifies previously conflicting lines of evidence to establish a common cleavage mechanism between two distantly-related and functionally distinct topoisomerase families.

Coordinating C-gate dimerization with DNA cleavage status
Finally, the cleavage-complex structure reveals a new molecular connection by which DNA breakage is coordinated with the association and dissociation of inter-subunit interfaces during catalysis to prevent the accidental formation of double-strand DNA breaks. One major difference between a previous, non-covalent DNA-topo II structure and the covalent complex is that the primary dimer interface of the enzyme (the 'C-gate') switches from a dissociated, or "open" state to an associated, or "closed" configuration (**Figure 2.8a**). Comparison of the structures reveals why: formation of a covalent attachment between Y782 and DNA occurs with the coincident movement of the active site tyrosine up toward the DNA from its uncleaved position by ~6 Å (**Figure 2.8b**). This movement is made possible by a rocking of the winged helix domains (**Figure 2.9a**), which in turn tugs on a long linker and a small α-helix (residues

12

797–802) that engages a set of distal coiled–coil 'lever arms' through a conserved salt-bridge network (D799, R1001 and R1008) (**Figure 2.9b-c**). Motions at this elbow joint have been shown previously to open and close the DNA-binding regions of topo II (**Figure 2.9d**)(Berger et al., 1996; Fass et al., 1999; Morais Cabral et al., 1997). Here, however, formation of the phosphotyrosyl bond acts like the drawstring on a latch to pull the coiled coils inward, driving C-gate closure. This transition highlights how the status of the active site is communicated to a gating element over 50 Å away, and shows that type IIA topoisomerases retain a molecular 'trapdoor' as a failsafe to ensure that protein–protein interactions are maximized at times when DNA is cleaved (**Figure 2.10**). Such tight control over DNA cleavage and inter-subunit associations helps explain how the fidelity of the type II topoisomerase breakage/rejoining reaction is maximized to protect the genome from the aberrant formation of potentially damaging and cytotoxic DNA lesions during supercoiling management and chromosome disentanglement.

Subsequent controversy over metal ion placement and chemical roles
Since these results were published, there has been some controversy in the field over how metal ions participate in the type II topoisomerase cleavage reaction. The debate focuses on two key aspects of these cofactors: their positional placement, and their occupancy. Insofar as position, a computational modeling group led by Marco De Vivo at the Italian Institute of Technology submitted a Brief Communication Arising to *Nature* contesting our one-metal mechanism approximately one year ago. A summary of the data, as presented to us by the authors in an email correspondence, follows here; however, at the time of writing this thesis, the work from De Vivo has not been published, either in *Nature* or elsewhere.

In their manuscript, the authors use molecular dynamics to investigate divalent metal-ion coordination during DNA cleavage in topoisomerase II. Starting with my crystal structure of yeast topo II covalently bound to a broken DNA segment, the authors replaced the zinc ions with magnesium and severed the phosphotyrosyl linkage between the enzyme and DNA *in silico*. Subsequent rounds of molecular dynamics simulations showed a shift of the two magnesium ions into a coordination-geometry similar to that seen for canonical two-metal ion phosphoryl transfer chemistry. In their coordination, metal B has moved to where I see metal A, while metal A has moved to a new position (**Figure 2.11**). Based on this result, the authors conclude that yeast topo II uses the same chemical approach as the canonical two-metal scheme(Steitz and Steitz, 1993), which differs from that described in the topoisomerase literature so far. Although the findings are intriguing, the authors either do not discuss or simply dismiss multiple lines of experimental evidence that run counter to the outcome of their simulations. At the same time, the authors make no effort to biochemically test whether Mg ions indeed can bind at the new metal binding site suggested by their theoretical simulations.

Insofar as structural data, the authors focus exclusively on the yeast topo II model; however, there currently exist 15 different structures of type II topoisomerases bound to DNA. Almost all of these were published after mine, and they collectively derive from seven separate papers and four independent groups(Bax et al., 2010b; Dong and Berger, 2007; Laponogov et al., 2010; Laponogov et al., 2009; Schmidt et al., 2010; Wohlkonig et al., 2010; Wu et al., 2011). While there is debate in the field as to whether the metal ion sites seen in these structures can be simultaneously occupied (see below), in no instance has any metal been reported to bind at the new site highlighted by the authors' MD simulations, even though high concentrations of Mg ions were present in the many of these crystallization conditions.

The authors refer repeatedly to their scheme as the "reactant state," which they define as having both *uncleaved* DNA and bound magnesium ions, and which is repeatedly claimed to have not been observed in experimental data. Insofar as having two Mg ions occupy their sites, the authors are correct that there are no experimental data showing such; however, this particular omission hurts, rather than helps, their case for physiological relevance. With respect to having an intact DNA and one associated metal ion, the statement is not true – one paper describes just such a co-crystal structure(Laponogov et al., 2010), with the lone Mg ion occupying a position corresponding to the B site. Another paper also features uncleaved DNA, along with a catalytic Y→F mutation(Bax et al., 2010b), and again only a single ion binds at the metal B position (in this instance, Mn).

The model proposed in the manuscript also is at odds with the existing biochemical literature on topo II. In particular, the authors' MD runs lead R781 to break its contact with the scissile (+1) phosphate, and instead move over to interact the adjacent +2 phosphate. However, numerous crystal structures have shown that this amino acid always contacts either the scissile phosphate or the scissile phosphotyrosyl linkage (**Figure 2.4**) (providing one or the other is present in the co-crystallized DNA), while biochemical studies also have implicated this residue in directly DNA cleavage(Liu and Wang, 1998; Okada et al., 2000). An analogous arginine/scissile-phosphate interaction is preserved in the distantly-related type IA topoisomerases (**Figure 2.6a**), and likewise is critical for function, further implicating this residue in supporting the chemistry of DNA cleavage/religation. The authors do not explain this discrepancy, nor do they discuss the biochemical implications of the marked active site reorganization that occurs during their simulations in general. In structures where R781 is seen to contact the scissile phosphate/phosphotyrosyl bond, it sits very close to the new metal binding site that appears during the authors' MD simulations (**Figure 2.11a**); it seems likely that when this amino acid leaves the active site during the simulation, the uncompensated negative charge in the region simply attracts a magnesium ion to take its place.

The metal arrangement in the de Vivo computational model, however, does make a specific, testable prediction. In particular, during the MD simulations, a conserved serine (S452) engages the new metal ion position that appears in place of R781. Since this interaction has not been observed structurally or validated biochemically, I turned to site-directed mutagenesis to probe its validity. In the experiment, I mutate S452 to cysteine, and then subject the mutant to a standard DNA cleavage assay(Osheroff and Zechiedrich, 1987). If the serine were to contact a metal ion, then substituting manganese for magnesium would be expected to either rescue or increase cleavage activity due to the thiophilicity of manganese ions for thiol groups. This approach has been used previously to identify metal-liganding residues in type IIA topoisomerases (Deweese et al., 2009; Noble and Maxwell, 2002). However, when I performed the experiment with the S452C mutant, I found that the manganese substitution did not affect DNA cleavage levels (**Figure 2.12**). This result indicates that S452 probably does not contact a metal ion, further casting doubt on the outcome of the MD simulations and the concept that type II topoisomerases use two metal ions to promote chemical transformations during DNA cleavage.

The second debate over the role of metal ions in topo II DNA cleavage concerns their occupancy. The empirical evidence is in good agreement with the idea that there are two metal binding sites, and that only one of them is directly catalytic. However, my structure is the only one reporting two metals bound at the active site, while all others show just one metal, either at the A or B site. This has led some of the authors to posit that one dynamic metal ion moves between the two sites(Bax et al., 2010b; Laponogov et al., 2010). This controversy will be explored in more detail in Chapter 4.

Methods
Topo II expression and purification
Residues 408–1177 of *S. cerevisiae* topoisomerase II were expressed as a fusion with an amino-terminal tobacco etch virus (TEV) protease-cleavable hexahistidine tag. Overexpression was carried out in *S. cerevisiae* strain BCY123 grown in complete supplement mixture dropout medium lacking uracil (CSM URA) supplemented with lactic acid and glycerol for carbon source and galactose for induction (6 h at 30 °C). Induced cells were collected by centrifugation, flash frozen in liquid nitrogen and lysed by grinding under liquid nitrogen. Ground cell powder was resuspended in lysis buffer (300 mM KCl, 20 mM Tris (pH 8.5), 10% glycerol, 20 mM imidazole (pH 8.0), 1 mM phenylmethylsulphonyl fluoride) and centrifuged to clarify the lysate. Protein was purified by tandem nickel-affinity and ion-exchange chromatography (nickel-chelating Sepharose and HiTrap SP, GE), followed by removal of the His$_6$ tag with His-tagged TEV protease(Tropea et al., 2009) and passage over a second nickel affinity column to remove uncleaved protein and the protease. The protein was then run over a gel-filtration column (S-

300, GE) equilibrated in 10% glycerol, 500 mM KCl and 20 mM Tris (pH 7.9). Peak fractions were pooled and concentrated to over 20 mg ml^{-1}.

Covalent complex assembly and purification

Both standard and phosphorothiolate oligonucleotides were synthesized on an ABI synthesizer. Phosphorothioamidite for producing the 3'-bridging phosphorothiolate was synthesized as reported(Deweese et al., 2008; Sabbagh et al., 2004). After synthesis, DNAs were purified by urea-formamide PAGE. For producing the cleavage complex, oligonucleotides were incubated for 60 min at room temperature at a 1:1 molar ratio with protein in 100 mM KCl, 10 mM Tris (pH 7.9) and 5 mM MnCl$_2$. Unreacted DNA and protein were separated from the complex by passing the sample over a gel filtration column (S-300, GE) and cation exchange column (HiTrap SP, GE) connected in series and equilibrated with 100 mM KCl and 20 mM Tris (pH 7.9). The gel filtration column removed unbound DNA from the protein, whereas unbound protein and the DNA-cleavage complex were separated by the cation-exchange column. The protein–DNA complex was then concentrated to 3.5–6 mg ml^{-1}.

Crystallization and structure solution

Crystals were grown at 18 °C in hanging drops by mixing 1 µl protein solution with 1 µl well solution containing 20% 1,4-butanediol and 100 mM sodium acetate (pH 4.5). For collection, crystals were looped and flash frozen in liquid nitrogen without additional cryoprotection. Data were collected at Beamline 8.3.1 at the Advanced Light Source (ALS) at Lawrence Berkeley National Laboratory(MacDowell et al., 2004) and reduced using HKL2000(Otwinowski and Minor, 1997). Initial phases were calculated by molecular replacement (MR), using the DNA binding and cleavage core without the coiled–coil arms (residues 419–1004) of a non-covalent topo II–DNA complex (PDB ID code 2RGR)(Dong and Berger, 2007) as a search model for PHASER(McCoy et al., 2007). There is one monomer per asymmetric unit, with a canonical topo II homodimer recapitulated by a crystallographic dyad. All model building was carried out in COOT(Emsley et al., 2010), followed by refinement using PHENIX(Adams et al., 2010). Structure validation was assisted by MolProbity(Chen et al., 2010). Figures were rendered using PyMOL. Ramachandran angles, as calculated by Procheck, are 90.6% most favored, 8.9% additionally allowed, 0.5% generously allowed, and 0% disallowed for the apo structure. For the Zn-soaked structure, these values are 89.0%, 10.0%, 0.9% and 0%.

Metal soaks

During building and refinement of the first model, I saw no evidence for metal ion factors within the active site. I suspected that the absence of metal ions might be due to the relatively acidic crystallization conditions (pH 4.5), which would favor protonation and hence charge

neutralization of the acidic residue cluster within the TOPRIM domain that comprises the principal cation-binding site. Initial attempts to raise the pH of drop-grown crystals directly resulted in crystal dissolution, so I cross-linked the crystals by adding glutaraldehyde to the well solution (final concentration 0.09%), and allowing cross-linking to occur through the vapor phase for 16 h. I then changed the crystal pH by moving the cover slip with the drop over a new well in which the acetate buffer was adjusted to pH 6.5; crystals were again allowed to equilibrate through the vapor phase overnight. Metal salt solutions were added either during this final step, or for 1–5 min before crystal collection.

Tables

Table 2.1 Data collection and refinement statistics

	Apo	Zn
Data collection		
Space group	$P2_122_1$	$P2_122_1$
Cell dimensions		
a, b, c (Å)	86.05, 92.42, 116.73	86.06, 91.85, 115.93
α, β, γ (°)	90, 90, 90	90, 90, 90
Resolution (Å)	50 - 2.5	50 - 3.0
R_{sym}	5.4 (64.2)	10.2 (53.8)
$I / \sigma I$	34.5 (3.6)	10.6 (2.1)
Completeness (%)	100.0 (100.0)	91.4 (94.0)
Redundancy	7.8 (8.0)	4.3 (4.4)
Refinement		
Resolution (Å)	50 - 2.5	50 - 3.0
No. reflections	33330	29106
R_{work} / R_{free}	23.9 / 25.9	24.4/27.4
No. atoms		
Protein/DNA	7000	7000
Ion	0	8
Water	113	20
B-factors		
Protein/DNA	78.4	88.9
Ion	n/a	123.0
Water	47.7	53.0
R.m.s. deviations		
Bond lengths (Å)	0.009	0.007
Bond angles (°)	1.2	1.2

*Values in parentheses are for highest-resolution shell.
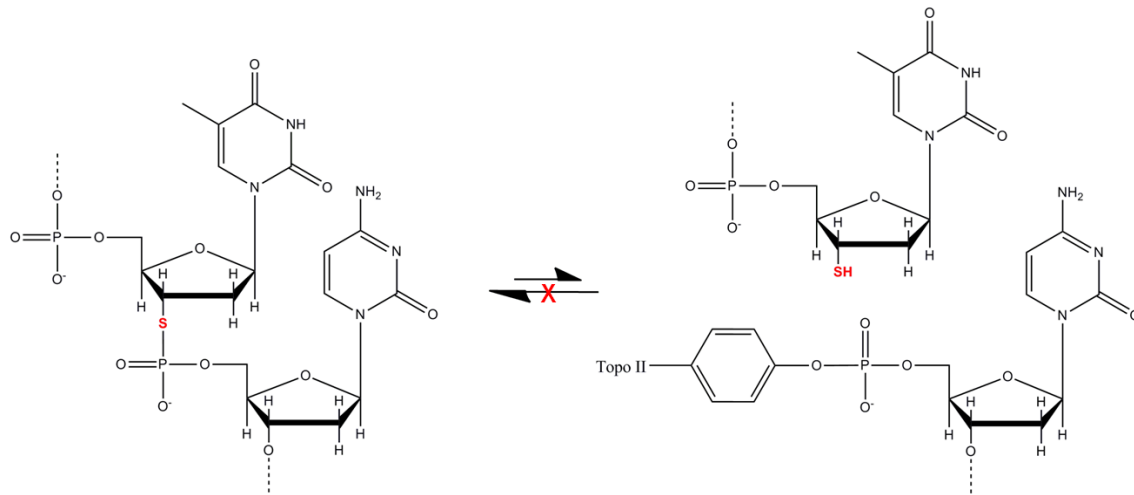
Figures

Figure 2.1 – Phosphorothiolated DNA acts as a suicide substrate for topo II
In phosphorothiolated DNA, a bridging oxygen is replaced with a sulfur atom. When topo II cleaves at the scissile phosphate, the leaving group is a 3'-thiol instead of a 3'-OH. This traps the covalently tethered enzyme-DNA complex.
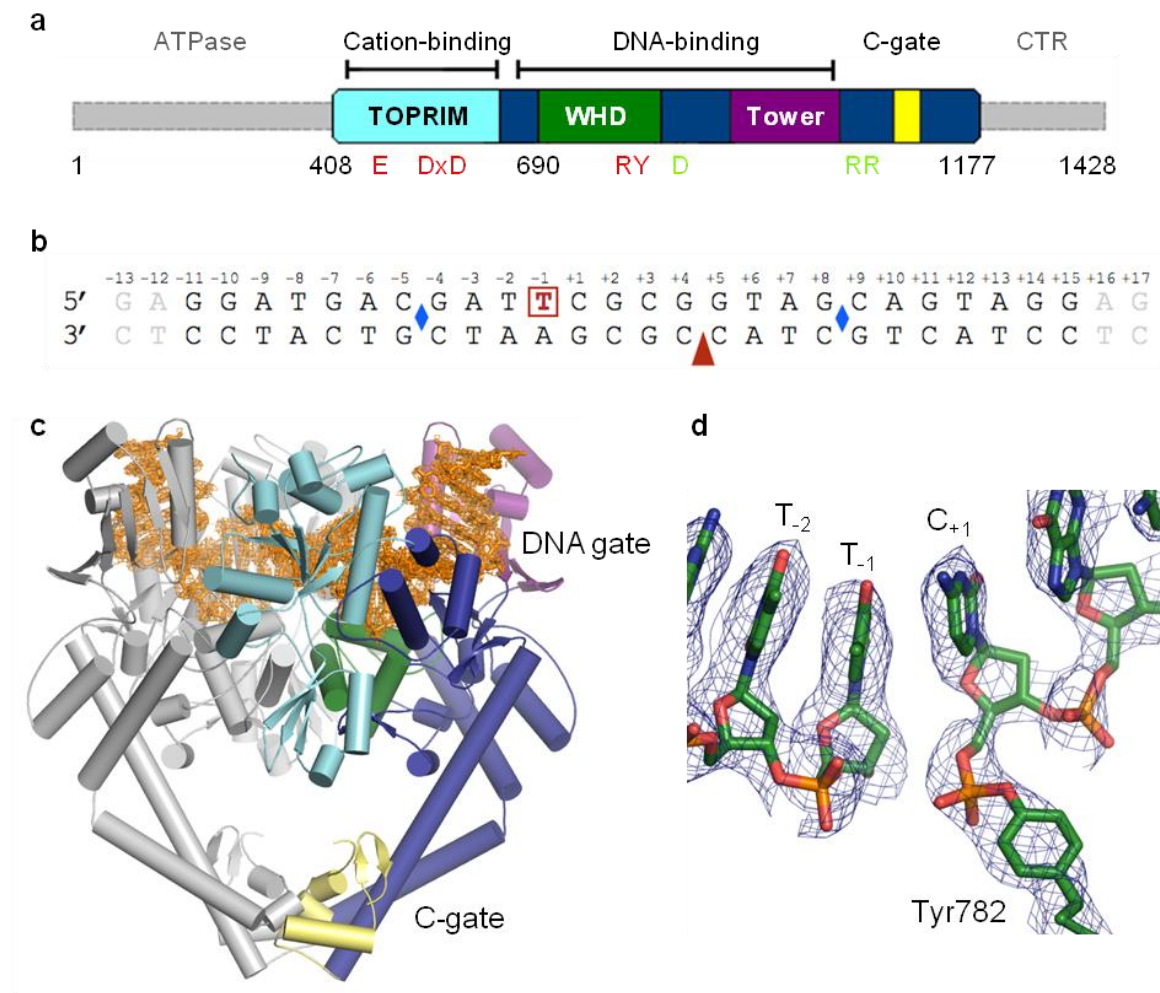
Figure 2.2 - Structure of a topo II-DNA cleavage complex

a) *S. cerevisiae* topo II domain arrangement. Functional regions are colored and labeled. Active-site residues are red; 'trapdoor' residues green.

b) DNA substrate. One strand (top) contains a 3'-bridging phosphorothiolate between the -1/+1 positions (red, boxed). Two complementary strands (bottom) adjoin at a nick (red arrowhead). Blue diamonds indicate DNA bend points. The terminal two base pairs (gray) are disordered.

c) The cleavage complex. One topo II monomer is colored as in (**a**). $2F_o$-F_c density (1σ contour, orange) is shown around the DNA.

d) The 5'-phosphotyrosine link modeled into a simulated-annealing composite omit map (1σ contour).
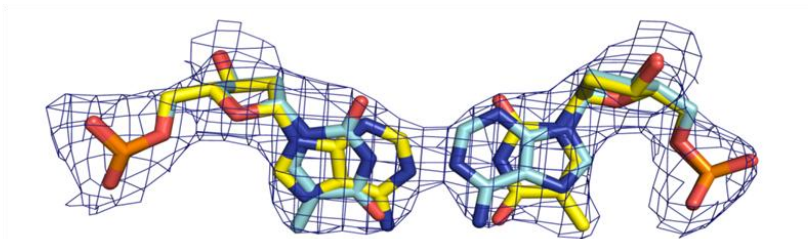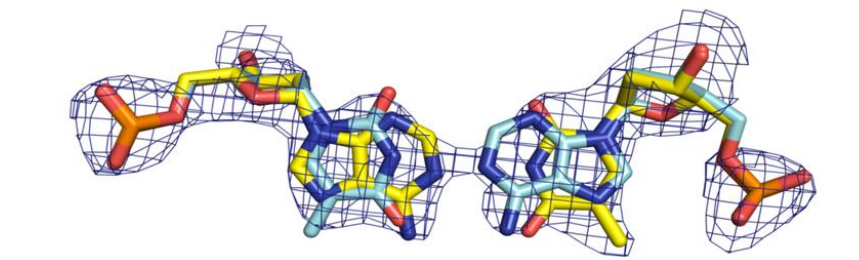
Figure 2.3 – Modeling of alternate DNA half-sites
a) 2Fo-Fc maps showing representative electron density (1σ contour) around positions T+6/A and A/T-2 base pairs (see Fig. 1b for numbering) highlights the averaged features of the DNA resulting from the operation of the crystallographic dyad.
b) Same as (**a**), but showing simulated-annealing composite omit maps at 1σ contour.
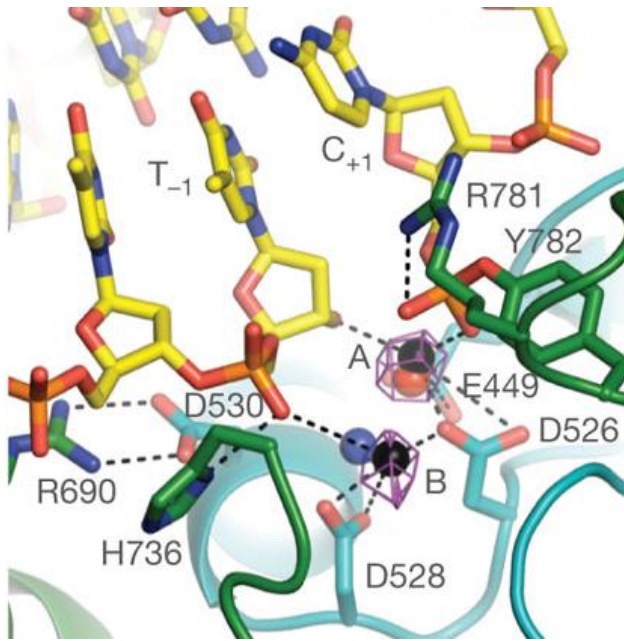
Figure 2.4 – A cleavage-competent active site
Close-up showing DNA (yellow), catalytic amino acids (cyan, TOPRIM; green, winged helix domain) and metal coordination (black spheres). A Zn-anomalous difference map is shown as purple mesh (5σ contour). The two modelled zinc ions are spaced 3.5 Å apart. Hydrogen bonds and metal interactions are displayed as dashed lines. Both non-bridging phosphotyrosyl oxygens are liganded, one by metal A and the other by R781. Mg^{2+} ions seen in a non-covalent topo II–DNA complex(Dong and Berger, 2007) and in the DNA-free topo VI A-subunit(Nichols et al., 1999) are shown as blue and red spheres, respectively.
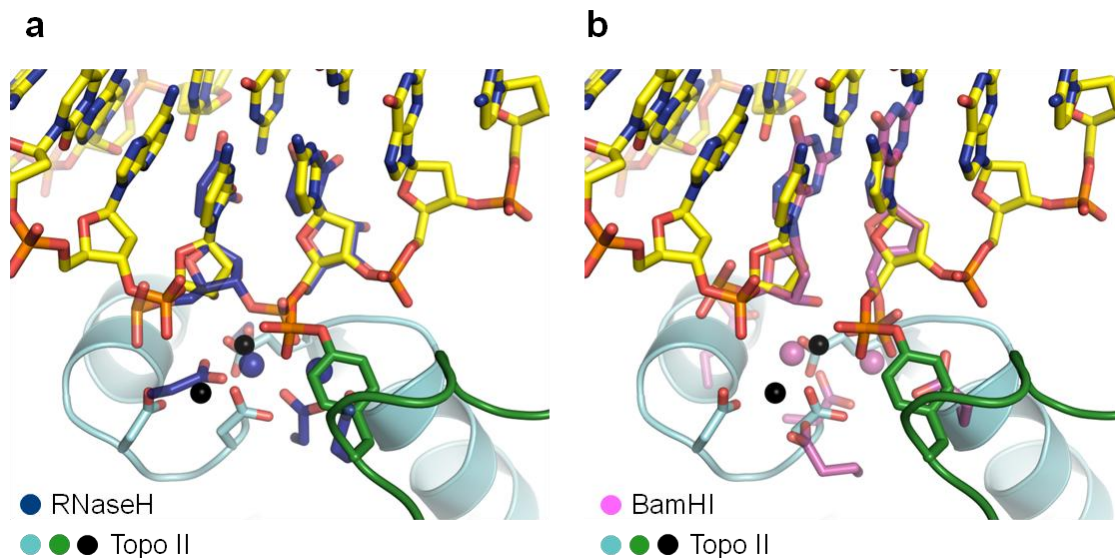
Figure 2.5 – Comparison of the topo II active site with classic two-metal systems
a) Superposition of the covalent-complex active site (cyan/green/yellow) with ribonuclease H (RNaseH, dark blue) bound to uncleaved RNA(Nowotny et al., 2005). The two magnesium ions seen in RNaseH (blue spheres) straddle the scissile phosphate; one resides close to the metal A position seen in the topo II model (black spheres).
b) Superposition of the covalent-complex active site (cyan/green/yellow) with the BamHI restriction endonuclease (pink) bound to cleaved DNA products(Viadiu and Aggarwal, 1998). As with RNaseH, both metal ions (pink spheres) straddle the scissile phosphate; again, one is situated in a position analogous to metal A (black spheres) in the present structure.
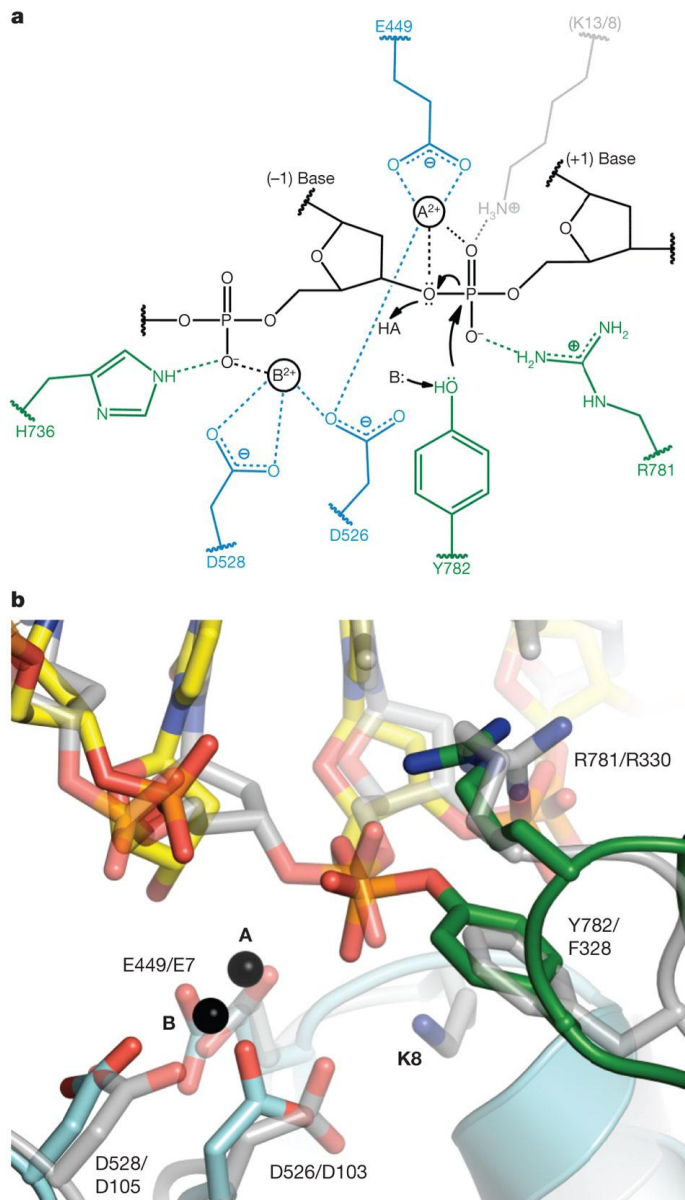
Figure 2.6 – DNA cleavage by type IIA and IA topoisomerases
a) Proposed cleavage mechanism. The general base (B:) and acid (HA) are unknown, but may be metal-associated waters. Metal A and R781 stabilize the transition state; metal B and H736 anchor the (-1) phosphate. Amino acids (blue, TOPRIM; green, winged helix domain) are labeled on the basis of positions in yeast topo II, except for a lysine residue present in type IA (but not type II) topoisomerases (gray, *E. coli* topo I/III numbering).
b) Type IA/IIA topoisomerase active site superposition. A DNA-bound (and uncleaved) topo III structure(Changela et al., 2001) (gray) is overlaid on topo II complex (cyan/green). Catalytic residues are labeled (yeast topo II/*E. coli* topo III numbering).

Topo I

	Glu9	Lys13

```
E. coli         KALVIVESPAKAKTINKYLGSDY
H. influenza    KSLVIVESPAKAKTINKYLGSQY
A. aeolicus     MELFIVESPTKAKTIQKFLGKGF
T. maritime     KKYIVVESPAKARTIKSILGNEY
M. genitalium   KNLVVIESPNKVRTLKQYLPSDE
S. aureus       DNLVIVESPAKAKTIEKYLGKKY
R. prowazekii   MKLVIVESPAKAKTINKYLQDEF
```

Topo III

	Glu7 Lys8

```
E. coli         MRLFIAEKPSLARAIADVLPKPH
H. sapiens      TVLMVAEKPSLAQSIAKILSRGS
S. cerevisiae   KVLCVAEKNSIAKAVSQILGGGR
H. influenza    MRLFIAEKPSLARAOADVLPKPH
B. subtilis     KTVVIAEKPSVGRDLARVLKCHK
S. aureus       KSLILAEKPSVARDIADALQINQ
S. typhi        MRLVLCEKPSQGRDIAKFLGATO
P. multocida    MRLFIAEKPSLARAIADVLPKPH
V. cholera      TRLFIAEKPSLARAIADALPKPH
```

Figure 2.7 – Alignment of active site residues for type IA topoisomerases
The presence of a conserved lysine in the type IA topoisomerase active site is highlighted in red.
The lysine alternates between two adjacent positions between topo I (TopA) and topo III
(TopB) paralogs. The metal A-binding glutamic acid is highlighted in cyan. *E. coli* amino acid
numberings are indicated.
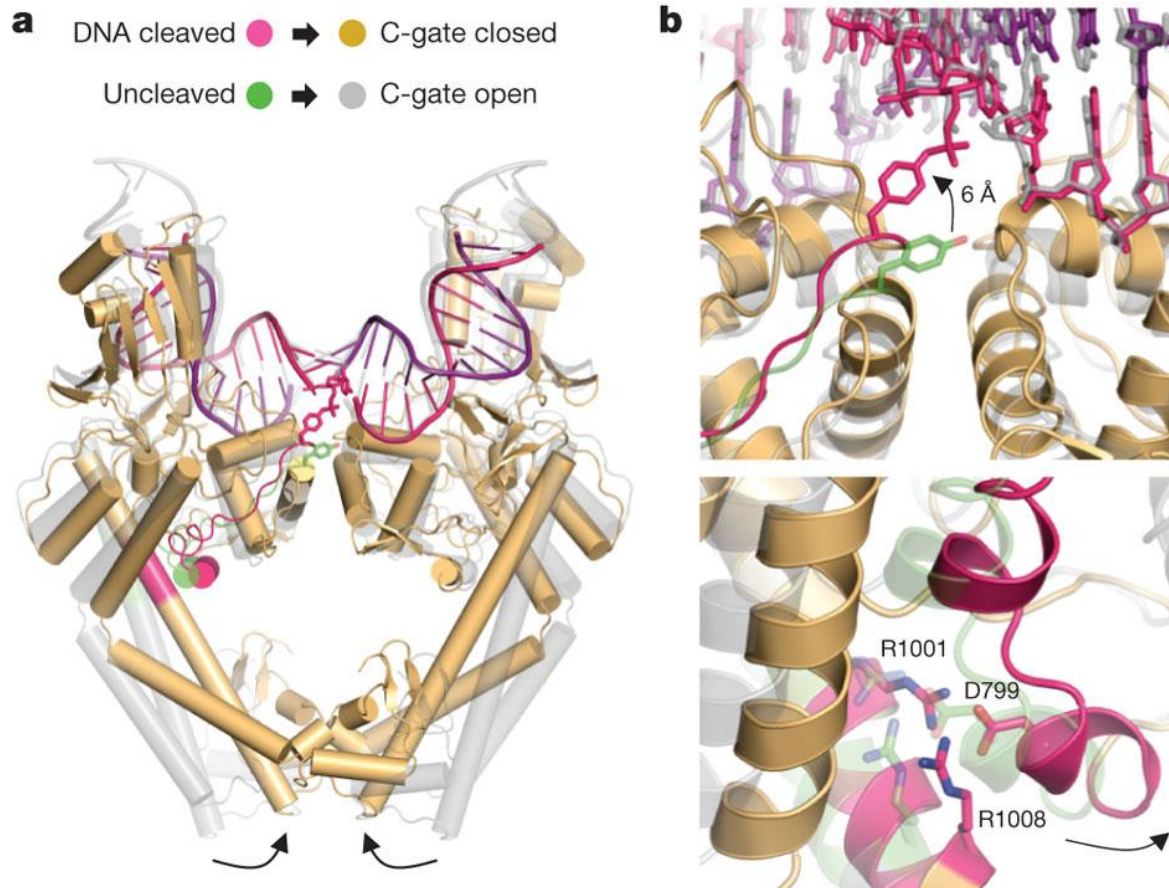
Figure 2.8 – Cleavage-dependent control of C-gate dynamics

a) Superposition of non-covalent (grey)(Dong and Berger, 2007) and cleavage (orange) complexes between topo II and DNA reveal how C-gate opening and closure is linked to active site status. The connection from the active-site tyrosines to the coiled–coil arms is colored green/magenta. For clarity, the TOPRIM domains are hidden.
b) Close-up of positional shifts. Upper panel, upward movement of the active-site tyrosine upon becoming attached to the DNA. Lower panel, concomitant inward movement of the coiled–coil joint through a conserved salt bridge network.

a
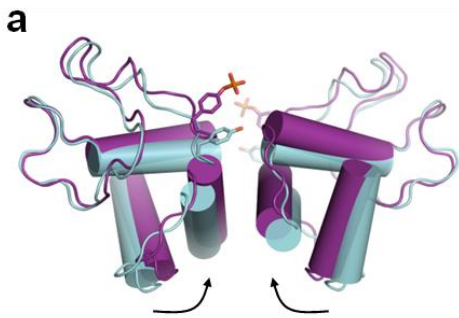
b

<pre>
                                              Asp799
Top2   S. cerevisiae   TELNKLTRKIFHPA**D**DPLYKYI
Top2   S. pombe   TALSPLARVLFNSN**D**DQLINYQ
Top2α H. sapiens   TMLSSLARLLFPPK**D**DHTLKFL
Top2α M. musculus   TMLSPLARLLFPPK**D**DHTLRFL
Top2   D. melanogaster TIMSPLTRLIYHPL**D**DPLLDYQ
Top2   A. thaliana   TKLSPVTRILFPKD**D**DLLLDYL
GyrA   E. coli   IRLAKIAHELMA**D**LEKETVDFV
GyrA   A. aeolicus   AKLSPLAVEMLT**D**IDKDTVDFQ
GyrA   M. tuberc.   ARLTPLAMEMLR**E**IDEETVDFI
ParC   E. coli   SRLSKYSELLLS**E**LGQGTADWV

                            Arg1001   Arg1008
Top2   S. cerevisiae   EFYYV**R**LEYYQK**R**KDHMSERLQ
Top2   S. pombe   EFYEV**R**LRTYQR**R**KEHMVNELE
Top2α H. sapiens   DFFEL**R**LKYYGL**R**KEWLLGMLG
Top2α M. musculus   DFFEL**R**LKYYGL**R**KEWLLGMLG
Top2   D. melanogaster EYYKL**R**REYYAR**R**RDFLVGQLT
Top2   A. thaliana   EFFDL**R**FEYYEK**R**KETVVKNME
GyrA   E. coli   AFVRH**R**REVVTR**R**TIFELRKAR
GyrA   A. aeolicus   EFIKH**R**LEVILRR**R**SKYFLKKVQ
GyrA   M. tuberc.   YYVDHQLDVIVR**R**TTY**R**LRKAM
ParC   E. coli   EWLVF**R**RDTVRR**R**LNYRLEKVL
</pre>

c
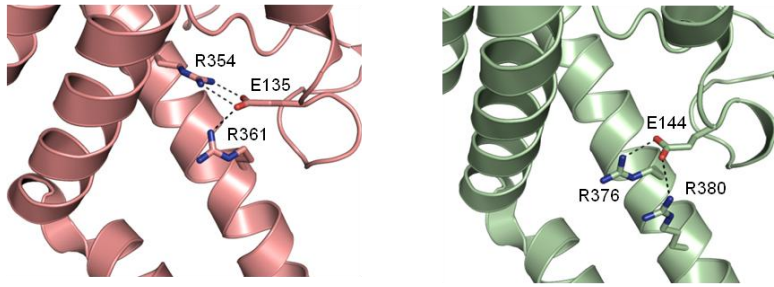
d
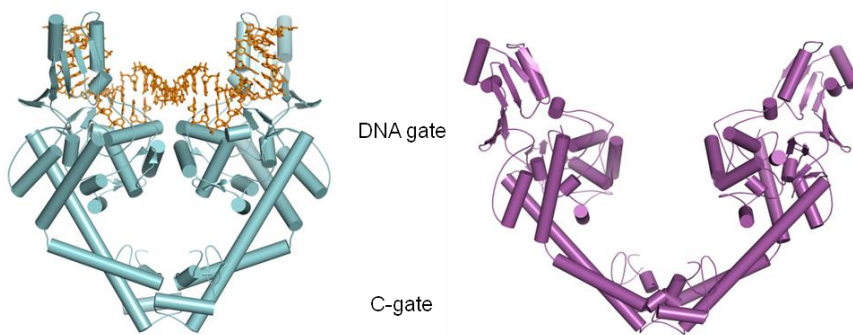
Figure 2.9 – Type IIA topoisomerase gating motions
a) Superposition of the winged helix domains for the covalent-complex structure (magenta) on the prior non-covalent structure (cyan)(Dong and Berger, 2007). Movement of the active site tyrosine is enabled by an inward rocking of the WHD.
b) Alignment of the salt-bridge network that links active site status to C-gate dynamics. Although the alignment initially suggests that two positions are not strictly conserved in some bacterial type IIA topoisomerases (the aspartate in *E. coli* topo IV and one of the two arginines in *M. tuberculosis* gyrase), inspection of structural models available for these outliers shows that the salt bridge connection is actually maintained by compensatory mutations in nearby residues (shaded letters, see also panel **c**)
c) The salt-bridge networks in *E. coli* topo IV (ParC, *left*, salmon) and *M. tuberculosis* gyrase (GyrA, *right*, pale green).
d) Comparison of DNA-gate transitions in the principal DNA binding ("A´") region of type IIA topoisomerases. (*Left*) DNA-gate "closed." The present topo II cleavage complex is shown in cyan, with the TOPRIM domains removed for clarity. (*Right*) DNA-gate "open." An apo structure of yeast topo II (PDB ID 1BGW)(Berger et al., 1996) is shown with the TOPRIM domains removed for clarity. In both instances, the C-gate interface is closed, and constitutes the primary means through which the protein dimerizes.
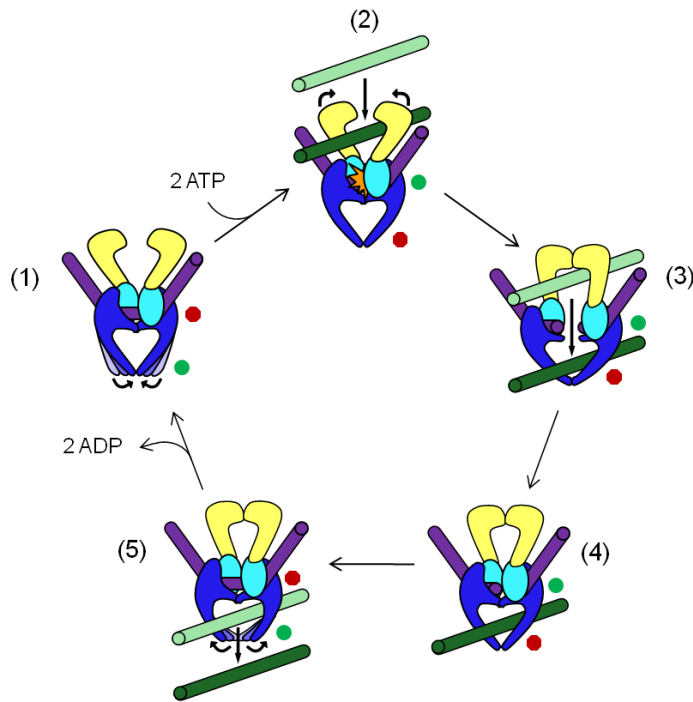
	(1) G-segment binding	(2) G-segment cleavage	(3) T-segment transport	(4) G-segment religation	(5) T-segment release
DNA gate	Closed	Closed	Open	Closed	Closed
C-gate	Open → Closed	Closed	Closed	Closed → Open	Open

Figure 2.10 – Model for the timing of type IIA topoisomerase gating motions

In all panels, a green circle denotes a cleaved G-segment or open C-gate, while a red octagon denotes a locked (closed) gate. Three dissociable interfaces – the N-gate (upper yellow domains), DNA-gate (middle blue/cyan region with purple cylinder) and C-gate (lower blue "tips") – control G-segment cleavage and T-segment transport in response to ATP binding and hydrolysis. Although the exact timing of gate opening and closure has not been determined experimentally, available structural information shows that the C-gate can spontaneously open upon G-segment binding, even when no T-segment is present(Dong and Berger, 2007). By contrast, the status of the C-gate appears closed when: 1) the enzyme is not bound to DNA and the DNA gate is shut(Morais Cabral et al., 1997; Tretter et al., 2010) 2) the enzyme is not bound to DNA and DNA gate is open(Berger et al., 1996; Corbett et al., 2005; Fass et al., 1999) or 3) the enzyme is bound to DNA, but the duplex is cleaved (as seen in the present study and elsewhere(Bax et al., 2010b; Laponogov et al., 2010; Laponogov et al., 2009; Wohlkonig et al., 2010; Wu et al., 2011).) These observations are consistent with a mechanism in which G-

segment binding allosterically destabilizes the C-gate, shifting the status of the interface from a predominantly associated form to one that can open and close with frequency. The likelihood of the C-gate opening would be adjusted (to a more or less favorable event) depending on the state of the topoisomerase reaction. (1) A G-segment DNA (purple) is bound and bent at the DNA gate. The C-gate is destabilized and now capable of opening, but trends toward a closed state. (2) ATP binding dimerizes the ATPase domains (the N-gate, yellow) capturing a T-segment (green). The G-segment DNA is cleaved, with the positioning of the active-site tyrosine ensuring that the C-gate is locked shut. (3) The DNA gate is opened, allowing T-segment passage. The C-gate remains closed. (4) The DNA-gate closes and configures the active site for G-segment religation. (5) Religation and loss of the tyrosine-DNA link allosterically frees the C-gate to open, an event that may be favored by the presence of the T-segment resident between the interfaces.
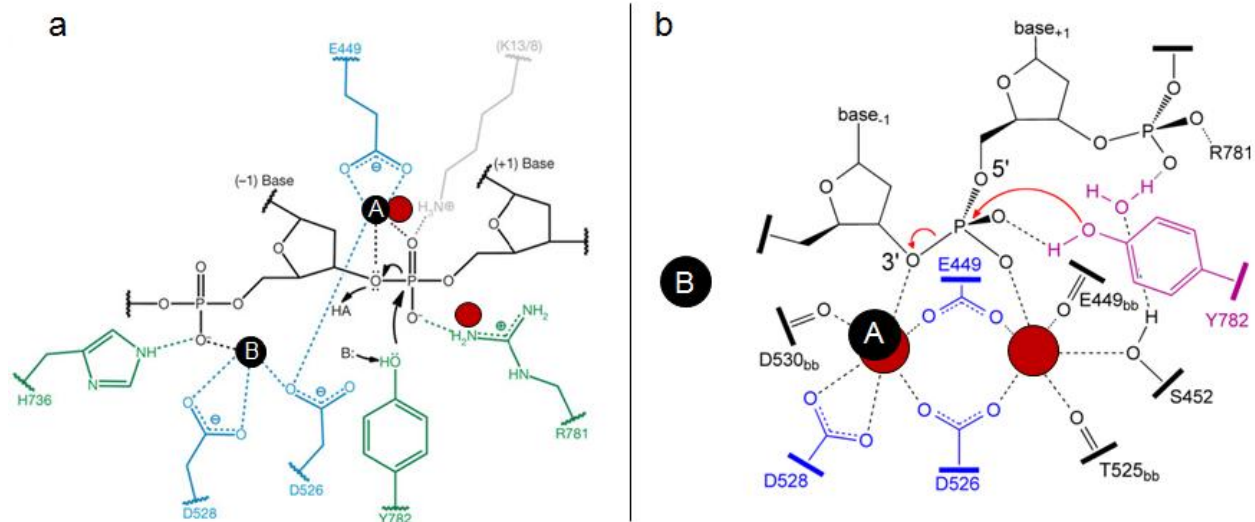
Figure 2.11 – Metal ion placement in my structural model vs. molecular dynamics simulations
a) In my model, zinc ions are indicated as black spheres. The approximate positions of magnesium ions in MD simulations are indicated in red.
b) In the model the de Vivo group proposes, their magnesium ions are indicated in red. The approximate positions of zinc ions from my model are indicated in black.
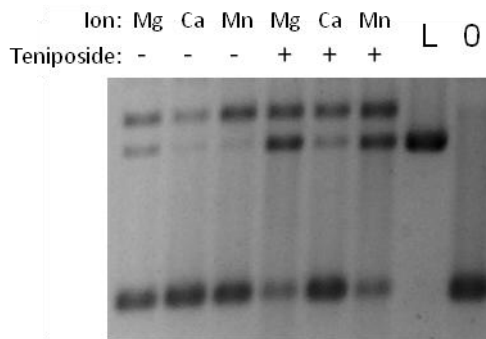
Figure 2.12 – S452 does not contact a metal ion

Cleavage assay. 0, negative control, no protein. L, plasmid linearized by BamHI. All lanes were incubated with 500 nM S452C mutant. Manganese does not increase or rescue cleavage levels, indicating the residue does not interact with a metal ion.

Chapter 3 - Structure of a functional topoisomerase II•DNA•nucleotide complex: DNA-dependent control of ATPase activity at a distance

(Portions of this chapter are adapted from: **Schmidt, B.H.**, Osheroff N. and Berger J.M. (2012), Nat Struct Mol Biol. *in press*.)

Introduction

Despite extensive study, a number of fundamental questions still persist regarding both the configuration of the type IIA topoisomerase holoenzyme and the coordination of the enzyme catalytic cycle by ATP. Although crystal structures of isolated ATPase and DNA-binding and cleavage regions of these enzymes have been reported (e.g., (Berger et al., 1996; Classen et al., 2003; Morais Cabral et al., 1997; Wigley et al., 1991)), how these elements are juxtaposed with respect to each other remains unknown. Mechanistically, how DNA binding stimulates ATP turnover(Lindsley and Wang, 1993a; Mizuuchi et al., 1978; Osheroff et al., 1983), or why ATP hydrolysis is sequential rather than synchronous (at least in yeast topo II)(Harkins et al., 1998), likewise has been difficult to explain at a structural or biochemical level. Given that type II topoisomerases are members of the broader pantheon of GHKL-family ATPases(Dutta and Inouye, 2000), a group that includes MutL-family DNA repair proteins and Hsp90-type chaperones, answers to these questions are likely to broadly resonate across diverse biochemical systems.

To define the global architecture of a type IIA topoisomerase holoenzyme, I determined the crystal structure of a fully-functional construct of *S. cerevisiae* topo II trapped in a covalent cleavage complex with a G-segment DNA and the non-hydrolyzable ATP analog, AMPPNP. The structure not only definitively establishes the relative juxtaposition between the ATPase regions and the DNA binding-and-cleavage core of the protein, but also reveals two unexpected, higher-order organizational features: a double domain-swapping event between ATPase subunits that forms a topological barrier to strand passage, and an interaction between the highly-bent G-segment and a lysine-rich loop in the ATPase domain. Biochemical studies validate the ATPase•DNA interaction, showing that it is not only critical for activity in both yeast and human topo IIα, but that it serves as a communication relay that couples DNA binding to the stimulation of ATP turnover. Together, these findings point to the existence of new and hitherto unsuspected intermediate states in the type IIA topoisomerase strand passage cycle, and highlight how discrete functional activities can be coordinated across long distances in a large macromolecular system.

Results

Structure of a functional topo II-DNA-AMPPNP complex

One impediment to imaging the ATPase and DNA-binding and cleavage elements of type IIA topoisomerases in conjunction with each other derives from the large size and dynamic nature of these enzymes. In particular, the three dimerization interfaces can each exist in an associated or dissociated state, giving rise to significant conformational variability within a population. To capture a minimally flexible state, we first used a nicked DNA oligonucleotide containing a single phosphorothiolate site as a suicide substrate to trap a covalent cleavage complex with a functional *S. cerevisiae* topo II construct comprising amino acids 1-1177 (**Fig. 1a, Supplementary Fig. 1**; **Methods**). Prior studies of covalent type IIA topoisomerase•DNA complexes using either this type of substrate or a drug-inhibited state have found that formation of the phosphotyrosyl linkage coincides with closure of the DNA-gate and C-gate of the enzyme(Bax et al., 2010b; Laponogov et al., 2010; Laponogov et al., 2009; Schmidt et al., 2010; Wohlkonig et al., 2010; Wu et al., 2011). We then added the non-hydrolyzable ATP analog, AMPPNP, which is known to lock the ATPase gate into its dimerized, clamped form(Roca and Wang, 1992; Wigley et al., 1991), as a means to promote association of all three interfaces. Crystals grown from this complex belonged to the space group $P2_12_12_1$ and permitted the collection of diffraction data to 4.4 Å resolution. Subsequent rounds of molecular replacement (MR) using single protomers of the isolated yeast topo II cleavage core and ATPase domain produced a solution that recapitulated a full topo II dimer in the asymmetric unit. Because of the moderate resolution of the data, side-chain positions were generally left in the position found in the original search model during refinement (**Methods**). Despite these relatively modest adjustments, the final structure was readily refined to an R_{work}/R_{free} of 24.0/27.7% with good stereochemistry (**Fig. 1b**, **Table 1, Methods**). Notably, the dimeric conformations of the ATPase domain and DNA binding and cleavage core in holoenzyme match those seen for the two regions observed in isolation, indicating that these structural states correspond to commonly-populated intermediates in the topo II reaction cycle (**Supplementary Fig. 2**).

Topo II ATPase elements domain-swap to contact DNA

Organizational models for full-length type IIA topoisomerases have generally speculated that the ATPase domains arch over the G-segment binding surface(Berger et al., 1996; Kampranis et al., 1999; Schultz et al., 1996). The actual orientation between the two regions has been the subject of speculation, however, both because the two functional elements are connected by a flexible and proteolytically-sensitive linker(Brown et al., 1979; Gellert et al., 1979; Lindsley and Wang, 1993b), and because structures of the isolated ATPase domains have exhibited a crossover at their extreme C-termini whose relevance has remained uncertain(Brino et al., 2000; Classen et al., 2003; Lamour et al., 2002; Wei et al., 2005; Wigley et al., 1991). Our model shows the ATPase domains do indeed sit atop the site of G-segment association and cleavage, but that the central cavity of the ATPase domain dimer is offset by approximately 45° from the hole that runs between the DNA- and C-gates (**Fig. 1b**). Interestingly, the juxtaposition of the domains

appears to give rise to a domain-swapping event, such that the ATPase region of one protomer contacts the TOPRIM fold of its associated partner subunit (**Supplementary Fig. 3**).

In addition to domain-swapping, the topo II configuration present in the crystal exhibits a second, distinctive feature: an apparent contact between the ATPase "transducer" subdomain and the backbone of the bent G-segment DNA (**Figs. 1, 2a**). A closer view of this region highlights a loop that emanates from the outer edge of the transducer domain to take up a position proximal to the DNA backbone. The amino acid sequence conservation of this region, hereafter termed the "K-loop," is somewhat variable among type IIA topoisomerases, but retains up to six consecutive lysines, several of which are well conserved among eukaryotic topo II homologs (**Fig. 2b**). In previous, higher-resolution structures of the isolated ATPase domains of yeast and human topo IIα, the K-loop has been disordered and unmodeled(Classen et al., 2003; Wei et al., 2005). By contrast, the peptide chain is readily visible in electron density for both protomers seen here (**Fig. 2a**). Although the resolution of our structure precludes precise modeling of side chain rotamers, the appearance of electron density for the K-loop main chain suggests that this region becomes ordered upon engaging DNA. Our structure also suggests that there may exist additional contacts between each transducer domain and both the TOPRIM and "tower" domains of its symmetry-related protomer; however, the resolution of our data does not permit us to definitively model specific interactions between these elements.

The K-loop is important for strand passage activities

To our knowledge, a functional role for the K-loop *per se* has not been established previously. A prior study had shown that deleting 57-residue region of the transducer region encompassing the K-loop eliminates DNA-stimulated ATPase activity(Bjergbaek et al., 2000), but the molecular basis for this effect was not determined. To test whether specific contacts between the K-loop and DNA might be important for topo II activity, we replaced various lysines in this stretch of the *S. cerevisiae* enzyme with either alanine or glutamate, and examined the ability of the mutant constructs to relax negatively-supercoiled DNA. In this assay, purified plasmid is incubated with a fixed starting level of ATP and increasing concentrations of topo II, after which the reaction products are analyzed by agarose gel electrophoresis (**Methods**). The appearance of discrete DNA topoisomers that migrate more slowly than the starting supercoiled substrate is a hallmark of the DNA relaxation reaction catalyzed by type II topoisomerases other than DNA gyrase(Goto and Wang, 1982; Liu et al., 1980).

We initially found that single K→A mutations at each of the six lysines in this region did not noticeably affect supercoil relaxation (not shown). However, stronger effects became apparent as individual mutations were combined, with a construct bearing a quadruple KKKK→AAAA mutation in the first four amino acids of the K-loop displaying an approximate 4-fold reduction in supercoil relaxation (**Fig. 3a**). Because any interaction between the K-loop and DNA is likely to rely on a significant electrostatic component, we reasoned that introducing negative charges at

the most highly conserved lysine positions might more significantly impact topo II activity. We therefore prepared a KKKK➔AEEA mutant, in which the two most highly-conserved lysines were replaced with glutamates. This mutant exhibits a level of specific activity reduced at least 15-fold from the wild-type enzyme (**Fig. 3a**). Importantly, both the AEEA protein and its AAAA counterpart could be expressed and purified under identical conditions compared to wild-type topo II, and showed no abnormal migration behavior by size-exclusion chromatography (**Supplementary Fig. 4**, **Methods**), indicating that the loss of activity displayed by the mutants is not due to folding or assembly defects. The relative distributions of topoisomer populations differ between the mutant and wild-type proteins, suggesting that K-loop integrity may play a role in enzyme processivity.

S. cerevisiae topo II is unusual among eukaryotic type IIA topoisomerases in that it bears six lysines in its K-loop; most other orthologs possess three, including the two that appear universally conserved from yeast to human (**Fig. 2b**). To determine whether the observed effects of K-loop substitutions on DNA supercoiling were generalizable, we cloned, expressed, and purified the KKK➔AAA and KKK➔EEE triple mutants of human topo IIα. Negative-supercoil relaxation assays were carried out and analyzed for the mutant and wild type topo IIα proteins as for yeast topo II. The resultant data show that both mutants impede the removal of supercoils, with the lysine-to-glutamate charge substitutions again exhibiting a more severe defect in activity compared to the alanine substitutions (**Supplementary Fig. 5**). Thus, the K-loop appears to play a part in strand passage across different topo II orthologs.

To more precisely define the action of the K-loop, we examined DNA decatenation by yeast topo II and the K-loop mutants. Decatenation can be assessed by incubating purified enzyme with kinetoplast DNA (kDNA) and ATP, and then resolving the products by agarose gel electrophoresis. kDNA normally comprises a large, catenated network of minicircles that cannot enter a standard agarose gel(Simpson and Da Silva, 1971); however, the unlinking action of a type II topoisomerase produces individual minicircles that migrate freely into the matrix(Marini et al., 1980). Using this assay, we found that the AAAA and AEEA mutants display reduced levels of activity comparable to those seen during supercoil relaxation (~4-fold and 15-fold, respectively) (**Fig 4a**). These results show that the role of the K-loop is not restricted to the type of DNA substrate encountered by topo II, but is instead necessary to support strand passage overall.

Because defects in strand passage could arise from an impaired ability to cleave DNA, we next set out to investigate the strand scission properties of the enzyme. Cleavage was examined by first incubating yeast topo II with negatively-supercoiled plasmid DNA in the presence of AMPPNP and either Mg^{2+} or Ca^{2+} ions, followed by rapid denaturation of the complex with SDS and resolution of the products on an agarose gel. Ca^{2+} is known to stimulate cleavage over background levels of cutting(Osheroff and Zechiedrich, 1987), resulting a species that

comigrates with linearized vector. Notably, both the AAAA and AEEA mutants produce similar amounts of linear DNA as the wild-type enzyme (**Fig. 4b**). These results support the position that topo II K-loop mutants are not generally compromised by a folding or assembly defect, and that the integrity of this region is necessary to support the strand passage reaction following G-segment binding and cleavage.

The K-loop couples DNA binding to ATPase activity
Loss of supercoil relaxation and decatenation activities can in principle arise from a deficiency in one of any number of steps in the type II topoisomerase catalytic cycle. Having established that DNA cleavage appears unperturbed in our K-loop mutants, we next examined the ATPase activity of enzyme. The transducer subdomain on which the K-loop resides is known to play a key role in ATP hydrolysis by providing an invariant amino acid (Lys367 in yeast topo II) that plugs into the GHKL nucleotide-binding pocket. Although the K-loop sits ~50 Å away from this active site residue, residing instead on the outer edge of the ATPase region (**Fig. 1b**), we reasoned that it might nonetheless indirectly influence nucleotide turnover at a distance. Using an established, coupled assay to report on ATPase function(Lindsley, 2001; Tamura and Gellert, 1990), we first assessed the basal ATPase rates between the WT, AAAA, and AEEA topo II constructs. The overall profiles of all three proteins are similar (**Fig. 5a**), with the AEEA actually exhibiting a slightly greater level of specific activity than the other two enzymes. The V_{max} and K_M values obtained from these curves also are similar (**Table 2**) and in line with values reported previously for the WT yeast enzyme(Lindsley and Wang, 1993a). Hence, the intrinsic ATPase activity of topo II does not appear to be compromised by K-loop alterations, again indicating that the substitutions do not directly impair the folding or function of the domain.

By contrast, the influence of DNA on the ATPase rate of mutant enzymes is striking. It has been well established that DNA stimulates ATP turnover by more than 10-fold in most type IIA topoisomerases studied to date(Lindsley and Wang, 1993a; Maxwell and Gellert, 1984; Mizuuchi et al., 1978; Osheroff et al., 1983). To assess this effect for our K-loop mutants, we measured ATPase rates at a single starting ATP concentration in the presence of increasing amounts of sheared salmon-sperm DNA. The ATPase activity of our wild-type topo II preparations is stimulated ~15 fold in this assay(**Fig. 5b**), a level consistent with prior measurements for this enzyme *in vitro* (Lindsley and Wang, 1993a). By contrast, both the AAAA and AEEA topo II mutants failed to exhibit stimulation upon the addition of DNA (**Fig. 5b**). To ensure that this effect was not limited to the yeast enzyme, we measured whether DNA could stimulate the activity of human topo IIα. Consistent with prior observations(Hammonds and Maxwell, 1997; West et al., 2002), the degree of enhancement observed for our wild-type topo IIα protein is ~20-fold; however, DNA increases the ATPase activity of the two topo IIα K-loop mutants by only 2-fold (**Supplementary Fig. 6**). Together, these data indicate that the K-loop plays an unexpected but direct role in coupling DNA binding with ATP turnover and strand passage.

Inspection of the crystal structure of our topo II•DNA complex shows that that the K-loop appears to interact with a DNA region that flanks the nucleolytic center and site of DNA bending (**Fig. 1c, 2a**). If the K-loop indeed allows the ATPase activity of topo II to sense whether DNA is stably associated with the enzyme, then the nature of this contact predicts that sensing should be dependent on the length of the G-segment associated with the primary DNA binding and cleavage center; i.e., oligos shorter than 30 bp should not be long enough to reach the K-loop and thus should stimulate ATPase rates only minimally, whereas longer oligos should extend past the ATPase domain and allow contact to occur. To test this assumption, we investigated the role of DNA oligonucleotide length on the stimulation of ATPase rate. A series of oligos, ranging from 20-70bp and each containing a centered, preferred site for topo II binding(Mueller-Planitz and Herschlag, 2007), were individually added to ATPase reactions containing WT topo II, and their effects monitored as a function of turnover rate. Notably, the intact 20mer substrate was unable to appreciably stimulate ATP turnover, even at a saturating molar ratio (250:1) of DNA:enzyme. By contrast, as the length of the intact oligos was increased at a constant DNA concentration, the ATPase activity of the enzyme also increased (**Fig. 6, Supplementary Fig. 7**). These findings are consistent with the concept that a bound G-segment DNA needs to be of a certain length to reach the ATPase domains and their associated K-loops.

Discussion

A complete topo II-DNA-nucleotide structure

Despite a general acceptance by the community, the structural organization of a fully-functional type IIA topoisomerase has not been established. The work described here fills this gap, resolving the question of how the ATPase domains connect with the rest of the enzyme (**Fig. 1**). The only part of the enzyme missing in our construct is a poorly-conserved C-terminal region (residues 1178-1428), which contains both phosphorylation and nuclear localization sites(Cardenas et al., 1992; Shiozaki and Yanagida, 1992). In human topo IIα, this element plays a role in the stimulating the relaxation of positive supercoils. However, this region is not required for negative-supercoil relaxation, nor are its stimulatory properties retained by its paralog, topo IIβ(McClendon et al., 2008). Moreover, deletion of the C-terminus of *S. cerevisiae* topo II has no effect on DNA strand passage compared to the full-length protein *in vitro*(Caron et al., 1994). Hence, our structure reflects a minimal type IIA topoisomerase variant that possesses all of the elements necessary to support normal strand passage activities.

One notable feature of our full-length model – which derives from a complete view of the topo II holoenzyme in the crystal – is that its two major functional parts, the ATPase domains and the DNA-binding and cleavage core, adopt dimeric conformational states that are essentially indistinguishable from structures of the same regions in isolation from each other (**Supplementary Fig. 2**)(Classen et al., 2003; Schmidt et al., 2010). This finding supports the

biological relevance of these and other fragment-derived models to understanding type IIA topoisomerase mechanism as a whole. In particular, we note the interior hole formed between the dimerized topo II ATPase domains remains much smaller than is seen for the equivalent regions of bacterial type IIA enzymes (**Supplementary Fig. 2**)(Brino et al., 2000; Classen et al., 2003; Lamour et al., 2002; Wei et al., 2005; Wigley et al., 1991). This finding is noteworthy because the size of this feature in topo II would appear to preclude the stable binding and trapping of DNA in its nucleotide-bound form. This observation likely accounts for the known inability of yeast topo II to accommodate a T-segment prior to DNA-gate opening(Roca, 2004).

Intriguingly, nearly all dimerized type IIA topoisomerase ATPase domain models visualized to date have displayed an intertwined structure that results from domain swapping events at both the N- and C-termini (**Supplementary Fig. 2**)(Brino et al., 2000; Classen et al., 2003; Lamour et al., 2002; Wei et al., 2005; Wigley et al., 1991). While the significance of this doubly-wrapped configuration has remained unclear, particularly insofar as the modest contact seen at the extreme C-terminus, we note that it is preserved in the DNA- and AMPPNP-bound topo II structure observed here (**Supplementary Fig. 3**). This consistency strongly argues that the reciprocal exchange of ATPase domain elements is a universal feature of type IIA topoisomerases that reflects a specific intermediate in the catalytic cycle. Interestingly, this domain-swapping event leads to the topological segregation of the upper ATPase domain hole from the G-segment binding surface. Taken together with the small interior hole manifest by the dimerized topo II ATPase domains, these physical features suggest that our model most likely corresponds to a state that follows both nucleotide binding and T-segment transport. Consistent with this proposal, biochemical studies of yeast topo II have shown that AMPPNP can support a single, complete round of DNA passage, but that the ATPase domains remain dimerized, preventing further rounds of activity(Baird et al., 1999; Osheroff, 1986; Roca and Wang, 1994).

A direct connection between the ATPase elements and DNA
The coupling between DNA binding and ATP turnover is of the most enigmatic aspects of type II topoisomerase function, and of many nucleic-acid dependent motors in general. A particularly unexpected feature of the ternary complex imaged here is the appearance of a direct connection between the ATPase "transducer" subdomain and the bound G-segment DNA (**Fig. 2**). Site-directed mutagenesis of conserved lysines in this region of both yeast topo II and human topo IIα did not appreciably affect DNA cleavage, but did adversely impact both DNA decatenation and supercoil relaxation activity (**Figs. 3, 4, Supplementary Fig. 5**). Moreover, the K-loop mutations resulted in essentially a complete loss of DNA-stimulated ATPase activity, without affecting basal ATP turnover rates (**Fig. 5, Supplementary Fig. 6**). These data indicate that the K-loop•DNA interaction we observe occurs in solution and that the K-loop itself is a hitherto unanticipated control element for coupling DNA binding with nucleotide hydrolysis at a distance. They also establish DNA as a conduit for linking the site of G-segment binding and bending with catalysis by the ATPase centers of the enzyme.

The dependence of DNA length in stimulating ATPase activity further corroborates the K-loop•G-segment interaction (**Fig. 6**). Whereas the stimulatory effect of a 20mer oligo substrate on hydrolysis rates is negligible, even when present in vast excess over enzyme, increasing DNA length results in progressively greater activity. Crystal structures have shown that 20mer duplexes can be bound and cleaved by the G-segment binding core(Bax et al., 2010b; Laponogov et al., 2010); however, these substrates do not extend far enough out of the active site to engage the K-loop. Notably, longer oligo substrates do not approach the stimulatory effect of sheared salmon-sperm DNA (**Figs. 5b, 6**), whose average length is on the order of hundreds of base pairs. This result suggests that while the K-loop•G-segment interaction directly contributes to ATPase stimulation, the interaction by itself is not sufficient to account for the full stimulation by DNA on ATPase rates. As previous work has implicated T-segment binding to the ATPase in stimulating ATPase activity(Hammonds and Maxwell, 1997; Tingey and Maxwell, 1996), it is possible that salmon sperm DNA is more greatly stimulatory because it is sufficiently long to serve as both a G- and T-segment. Alternatively (or in addition), there may exist additional contacts between G-segment DNA and the transducer or GHKL ATPase fold further up the domain that our structure does not reveal due to the short length (30 bp) of our DNA.

An inspection of the literature provides additional support for the K-loop•DNA contact that we observe. A prior protein "footprinting" study using *S. cerevisiae* topo II identified five lysines that become protected upon binding DNA(Li and Wang, 1997). Four of these residues lie in the major DNA binding groove of the catalytic core and are masked by the associated G-segment; however, the fifth lysine was found to reside on the K-loop. Although a role for this region was not known at the time of this effort, the authors speculated that protection within this region might have resulted from a conformational change or from direct DNA interactions – the present work indicates that it is both. In a second, more recent investigation, high-throughput mass spectrometry revealed that human topo IIβ is subject to acetylation(Choudhary et al., 2009). Interestingly, three acetylation sites were discovered, all of which either reside on or are proximal to the K-loop region (K365, K367, and K373 in hTop2β numbering). The biological significance of modifying these residues, if any, is not known, but based on the findings described here, might serve as a specific means for regulating topo IIβ activity inside the cell.

Complexities in type IIA topoisomerase strand-passage
If the structure reported here corresponds to a functional intermediate in the topo II strand passage cycle, then what might be purpose for the domain swapping we observe between ATPase domain elements? In the current, generalized version of the type IIA topoisomerase catalytic cycle, both a G- and a T-segment must be captured by the enzyme prior to ATP binding (**Fig. 7**)(Berger et al., 1996; Kampranis et al., 1999; Roca and Wang, 1992, 1994). Nucleotide association drives dimerization of the ATPase domains, along with the cleavage and opening of the G-segment, and passage of the T-segment through the break. During passage,

the T-segment DNA is generally considered to transit exclusively from the N-terminal portion of the protein to its C-terminal side(Roca et al., 1996; Williams and Maxwell, 1999b). Unidirectionality is thermodynamically aided by the consumption of ATP(Bates et al., 2011); however, the mechanical motions that enforce one-way movement have been ill-defined. The ability of the ATPase domains to wrap around themselves provides one possible solution to this problem, as a crossover of the protein chain would provide a physical impediment to movement of the T-segment back through the cleaved G-segment once passage has occurred. We note that this scheme would require the dimerized ATPase domains to twist about each other by perhaps as much as 180° before "locking" into place against the G-segment following transport (**Fig. 7**). Although extreme, an inspection of the ATP-dimerized Hsp90 chaperone, which employs the same family of ATPase fold as topo II, intertwines around itself to a similar extent (**Supplementary Fig. 8**)(Ali et al., 2006).

Our structure raises a second unanticipated issue involving type IIA topoisomerase mechanism, namely, why these enzymes might have evolved a contact that allows the ATPase domains to sense the presence of a properly bound and bent G-segment *after* strand passage has occurred. One possibility is that this contact affords an extra layer of control to more tightly couple ATP turnover with strand passage. Outside of gyrase, which uses the free energy of ATP to add negative supercoils to DNA(Gellert et al., 1976), the need for ATP in the type IIA topoisomerase reaction has remained enigmatic. One model is that ATP serves as a timing element, or "gatekeeper," that temporarily promotes the formation of a new dimer interface during DNA cleavage to secure the two DNA ends(Bates et al., 2011). Since establishment of the nucleolytic center appears to coincide with a very precisely phased DNA bend(Laponogov et al., 2010; Lee et al., 2012; Schmidt et al., 2010; Wohlkonig et al., 2010; Wu et al., 2011), having the ATPase domains touch the G-segment could help signal that the passage reaction is complete, and that ATP can be hydrolyzed to allow enzyme reset. Consistent with this idea, pre-steady state kinetic studies have shown that the ATPase elements of *S. cerevisiae* topo II fire asynchronously, with one ATP hydrolyzed prior to or concomitant with strand passage, and the other hydrolyzing later, likely after strand passage is complete(Harkins et al., 1998). These data suggest that the K-loop•DNA interaction we observe may predominantly affect the second ATPase event (**Fig. 7**). In accord with this reasoning, a human topo IIα heterodimer containing only a single functional ATP-binding site is weakly able to relax DNA supercoils, but shows no DNA-stimulated ATPase activity(Skouboe et al., 2003); our model would predict that this mutant enzyme can support only the first ATP turnover step that drives strand passage, but not the step required to stimulate enzyme turnover. Similarly, biochemical analyses have indicated that the ATPase activity of *B. subtilis* gyrase, which lacks the K-loop, is not asynchronous(Gottler and Klostermeier, 2007). Future studies will be needed to test these concepts further.

Concluding remarks

Type IIA topoisomerases are multisubunit DNA remodeling enzymes that undergo a series of highly-articulated movements to physically move one DNA through another. The structural and biochemical studies reported here definitively establish the higher-order structural organization of this class of enzymes, and further reveal new architectural linkages that help couple ATP turnover with strand passage. These findings highlight some of the unanticipated and sophisticated complexities that can be employed by molecular machines, particularly those that rely or act on nucleic acids, to coordinate disparate catalytic events in support of essential biochemical transactions.

Methods

Topo II expression and purification

Residues 1–1177 of *S. cerevisiae* topoisomerase II were expressed as a fusion with an amino-terminal tobacco etch virus (TEV) protease-cleavable hexahistidine (His$_6$) tag. Prior studies have shown that this construct retains the full catalytic activity of the wild-type protein *in vitro*, but lacks nuclear localization elements that would allow it to complement a *top2* ts allele *in vivo*(Caron et al., 1994). Overexpression was carried out in *S. cerevisiae* strain BCY123 grown in complete supplement mixture dropout medium lacking uracil (CSM-URA), supplemented with lactic acid (2%) and glycerol (1.5%) for a carbon source. Galactose was added at mid-log phase (20 g/L) for induction (6 h at 30 °C). Induced cells were collected by centrifugation, resuspended in Buffer A (300 mM KCl, 20 mM Tris-HCl (pH 8.5), 10% glycerol, 20 mM imidazole (pH 8.0), 1 mM phenylmethylsulphonyl fluoride), flash frozen in liquid nitrogen, and lysed by grinding under liquid nitrogen. Ground cell powder was resuspended in Buffer A and centrifuged (20 min, 16000 rpm) to clarify the lysate. Protein was purified by tandem nickel-affinity and ion-exchange chromatography (nickel-chelating Sepharose and HiTrap SP, GE), followed by removal of the His$_6$ tag with His$_6$-tagged TEV protease and passage over a second nickel affinity column to remove uncleaved protein and the protease. The protein was then run over a gel-filtration column (S-300, GE) equilibrated in 10% glycerol, 500 mM KCl and 20 mM Tris (pH 7.9). Peak fractions were assessed by SDS-PAGE, collected, and concentrated in Amicon 100 kDa cutoff concentrators (Millipore).

Human topo IIα was prepared similarly to the yeast enzyme, but was not tagged with a hexahistidine tag. As such, after resuspension in Buffer A (without imidazole), a 35% ammonium sulfate precipitation step, followed by centrifugation was performed. The resultant supernatant, which contains topo IIα, was subjected to an additional 65% ammonium sulfate cut, after which the protein was spun down in the precipitate. The precipitated protein was resuspended in 100 mM KCl, 20 mM Tris-HCl (pH 8.5), 10% glycerol, 1 mM phenylmethylsulphonyl fluoride, and flowed over an ion exchange column (HiTrap SP, GE). The protein was eluted with an increasing KCl salt gradient, and then collected and run over a

gel-filtration column (S-300, GE) equilibrated in 10% glycerol, 500 mM KCl and 20 mM Tris-Cl (pH 7.9). Peak fractions were assessed by SDS-PAGE, collected, and concentrated in Amicon 100 kDa cutoff concentrators (Millipore).

Covalent complex assembly and purification

Both standard and phosphorothiolate oligonucleotides were synthesized on an in-house ABI synthesizer. Phosphorothioamidite for producing the 3'-bridging phosphorothiolate was synthesized as reported(Deweese et al., 2008; Sabbagh et al., 2004). After synthesis, DNAs were purified by running on a 12% denaturing urea-formamide PAGE, illuminating by UV, excising the bands, crushing the gel matrix, and eluting overnight into 500 mM ammonium acetate and 10 mM magnesium acetate. The oligos were then cleaned with a C18 column (Waters), lyophilized overnight, and resuspended in 10 mM Tris-Cl (pH 7.9) and 200 mM KCl. The oligo containing the phosphorothiolated bond was mixed with the two shorter oligos to assemble a singly-nicked substrate (**Figure 3.2**), heated to 90°C in a water bath, and cooled to room temperature overnight to anneal. For producing the cleavage complex, annealed oligonucleotides were incubated for 45 min at room temperature at a 1.2:1 molar ratio of oligo:enzyme in 100 mM KCl, 10 mM Tris (pH 7.9) 5 mM $MnCl_2$, and 1 mM AMPPNP. Unreacted protein, DNA, and nucleotide were separated from the complex by passing the sample over a gel filtration column (S-300, GE) and cation exchange column (HiTrap SP, GE), connected in series and pre-equilibrated with 20 mM Tris (pH 7.9), 100 mM KCl, and 5 mM $MgCl_2$. The gel filtration column removed unbound DNA from the protein, whereas unbound protein and the DNA-cleavage complex were separated by the cation-exchange column. The protein–DNA complex was then concentrated to 5 mg ml^{-1} in the column buffer, with fresh AMPPNP added to 1 mM final concentration.

Crystallization and structure solution

Crystals were grown at 18°C in hanging drop format by mixing 1 μl protein solution with 1 μl well solution containing 23% PEG 300 and 100 mM Tris (pH 8.0). For harvesting, crystals were transferred for one minute to well solution containing 10% xylitol, and then looped and flash frozen in liquid nitrogen. Data were collected at Beamline 8.3.1 (wavelength 1.1159 Å) under a cryo-stream at the Advanced Light Source (ALS) at Lawrence Berkeley National Laboratory, and integrated using HKL2000(Otwinowski and Minor, 1997). Initial phases were calculated by molecular replacement (MR) using two independent search models for PHASER(McCoy et al., 2007). The first model corresponded to a single, DNA-free promoter from the cleavage complex of the *S. cerevisiae* topo II DNA binding and cleavage core (residues 421–1177 of PDB ID code 3L4J)(Schmidt et al., 2010), and the second to one protomer from the *S. cerevisiae* topo II ATPase domain dimer (residues 7-406 of PDB ID code 1PVG)(Classen et al., 2003). The final MR solution regenerated one intact holoenzyme dimer in the asymmetric unit and resulted in clear electron density for the duplex DNA substrate in difference maps. Building of the model was carried out in COOT(Emsley et al., 2010), followed by a refinement strategy using

PHENIX(Adams et al., 2010) that consisted of an initial round of rigid-body refinement, followed only by individual-atom and TLS refinement. For individual atom refinement, both secondary structure restraints and NCS restraints were employed, with refinement parameters weighted to highly favor geometry. This approach kept most side-chain rotamers in their original conformers, improved the model's geometry, better placed the peptide backbone into electron density maps, and markedly improved R_{free}. Structure validation was assisted by MolProbity(Chen et al., 2010), and figures were rendered using PYMOL. 97.7% of main-chain torsion angles fell within favored regions of Ramachandran space, as calculated by MolProbity, with only 2.3% in allowed regions, and 0% in disallowed.

Notes on structure modeling

As was the case in Chpater 2, a non-palindromic DNA sequence was used for co-crystallization (**Figure 3.2**); thus electron density for the DNA corresponded to an average of the two possible sequence orientations. As a result, I modeled the DNA density as two alternate oligonucleotide segments, each present at half-occupancy. This approach has been used in similar circumstances(Chen et al., 1998; Schmidt et al., 2010), and the DNA sequence orientation does not alter any subsequent analysis or conclusions in this chapter.

DNA supercoiling relaxation, decatenation, and cleavage assays

Wild-type or mutant topo II (or topo IIα) was incubated with 300 ng (7.5 μM) negatively-supercoiled pUC19 plasmid DNA or kDNA in 20 μL reactions for 30 min at either 30°C (for the yeast enzyme), or 37°C (human protein). The final reaction conditions included 10 mM Tris pH 7.9, 100 mM KCl, 5 mM $MgCl_2$, 2% glycerol, and 1 mM ATP. Reactions were stopped with the addition of 0.5% SDS and 12.5 mM EDTA (final concentrations), and then treated with proteinase K for 30 minutes at 42°C. Sucrose-based loading dye was added to samples, and samples were run on a 1.2% agarose (Invitrogen), 1X TAE gel at 1–1.5 V/cm for 16–18 h. Gels were stained with 0.5 μg/ml ethidium bromide (EtBr) for 20 min, followed by destaining for 30 min. Bands were visualized by UV transillumination.

ATPase assay

Wild-type and mutant topo II ATPase activities were measured using an established enzyme-coupled assay in which the hydrolysis of ATP to ADP is coupled to the oxidation of NADH to NAD^+(Lindsley, 2001; Tamura and Gellert, 1990). To determine standard kinetic parameters (K_M, V_{max}), 50 nM homodimeric enzyme was incubated with 0-4 mM ATP in 75 μl reactions. Reactions contained 50 mM Tris pH 7.9, 100 mM KCl, 8 mM $MgCl_2$, 5 mM β-mercaptoethanol, 0.2 mg/ml bovine serum albumin, 2 mM phosphoenol pyruvate (PEP), 0.2 mM β-nicotinamide adenine dinucleotide (NADH), and an excess of pyruvate kinase and lactate dehydrogenase (enzyme mix obtained from Sigma). Assays were performed at 30°C for yeast and 37°C for human enzymes, with the oxidation of NADH to NAD^+ monitored by measuring absorbance at 340 nm in a Perkin Elmer Victor ^{3}V 1420 multilabel plate reader. The rate of decrease in

absorbance was converted to μmol of ATP hydrolyzed to ADP using an NADH standard curve and the assumption that one ATP is hydrolyzed for every NADH oxidized. ATPase rate as a function of [ATP] was fit for K_M and V_{max} using Michaelis–Menten kinetics in KaleidaGraph (Synergy Software). DNA stimulation of ATPase activity was measured using assays performed as described, except that the starting concentration of ATP was held constant (0.25 mM for yeast and 1 mM for human), and reactions were supplemented either with varying amounts of sheared, purified sheared salmon-sperm DNA (Sigma), or with oligonucleotide substrates (IDT); in analyzing ATPase activity measured as a function of salmon-sperm DNA concentration, use of the Hill equation resulted in a much better fit to the observed data than did Michaelis–Menten treatment. In experiments of oligo-stimulated ATPase rates, oligos were titrated up to a 250:1 molar ratio of oligo:enzyme, where the stimulative effect of DNA was at a maximum.

Tables

Table 3.1 Data collection and refinement statistics

	Topo II•DNA•AMPPNP
Data collection	
Space group	$P2_12_12_1$
Cell dimensions	
a, b, c (Å)	169.14, 169.88, 169.21
α, β, γ (°)	90, 90, 90
Resolution (Å)	50 - 4.4 (4.57 - 4.41)
R_{sym}	7.6 (70.3)
$I / \sigma I$	15.5 (2.0)
Completeness (%)	91.7 (92.9)
Redundancy	4.3 (4.2)
Refinement	
Resolution (Å)	50 - 4.4
No. reflections	28660
R_{work} / R_{free}	23.9 / 27.5
No. atoms	
Protein	18054
DNA	2118
AMPPNP	62
Mg	2
B-factors	
Protein	244.3
DNA	288.1
AMPPNP	236.3
Mg	115.3
R.m.s. deviations	
Bond lengths (Å)	0.004
Bond angles (°)	0.842

*Values in parentheses are for highest-resolution shell.
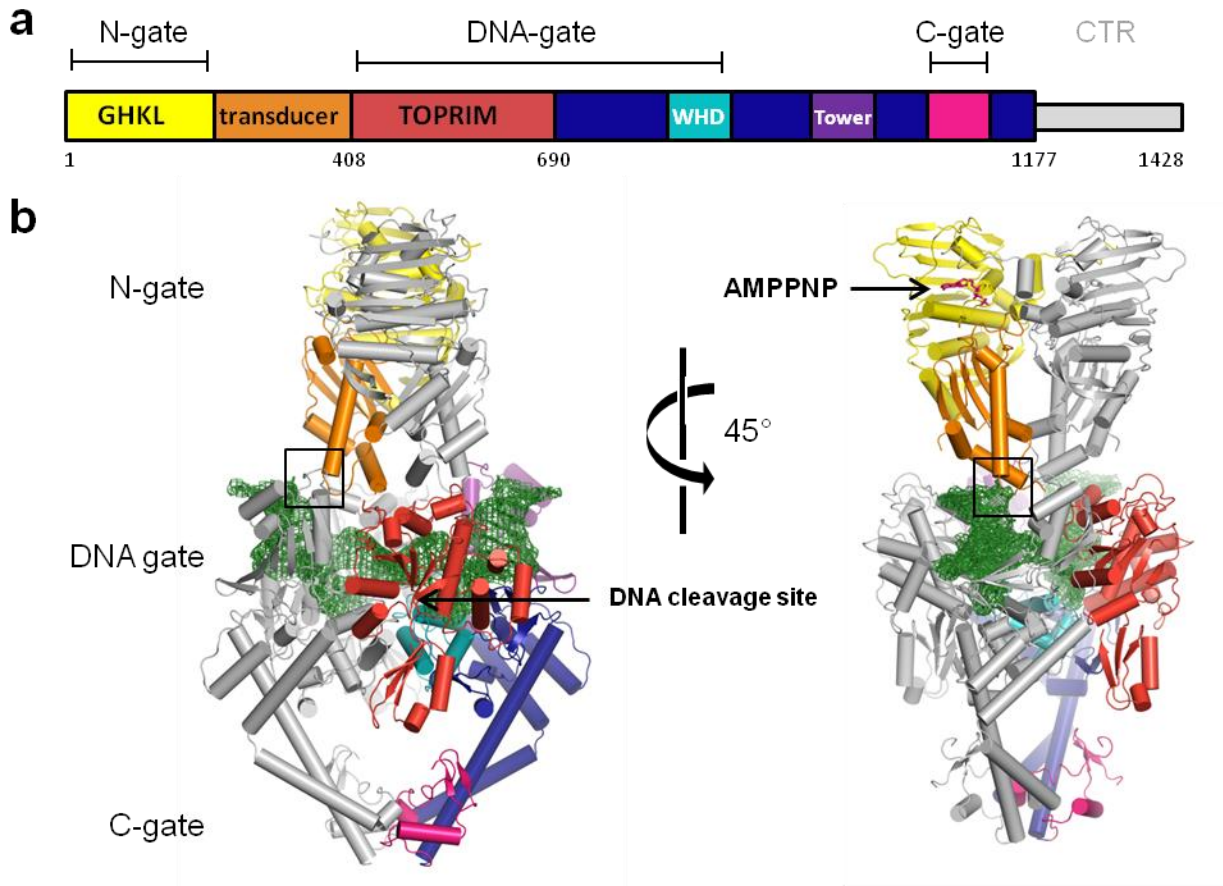
Figures

Figure 3.1 - Structure of topo II bound to DNA and AMPPNP
a) Domain arrangement of type IIA topoisomerases. Functional regions are colored and labeled.
b) Model of the ternary complex. One topo II protomer is shaded gray, the other colored as in
(**a**). $2F_o$-F_c density (1.5σ contour, green) is shown around the DNA (green sticks).
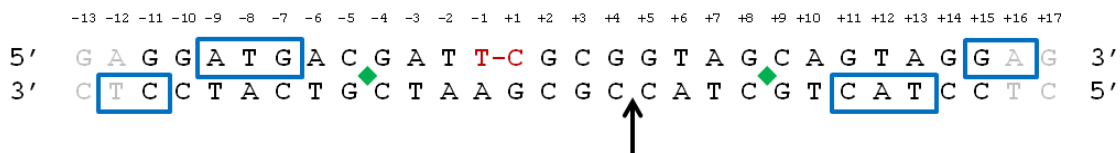
Figure 3.2 – DNA substrate

Sequence of the DNA oligo used in this study. The red dash indicates the position of the phosphorothiolate bond, the black arrow the site of the lone nick. Blue boxes demarcate bases whose phosphate groups are within the proximity of the K-loop. Green diamonds indicate intercalation sites that coincide with sharp DNA bends. Gray shaded bases were not visible in electron density maps and left unmodeled.
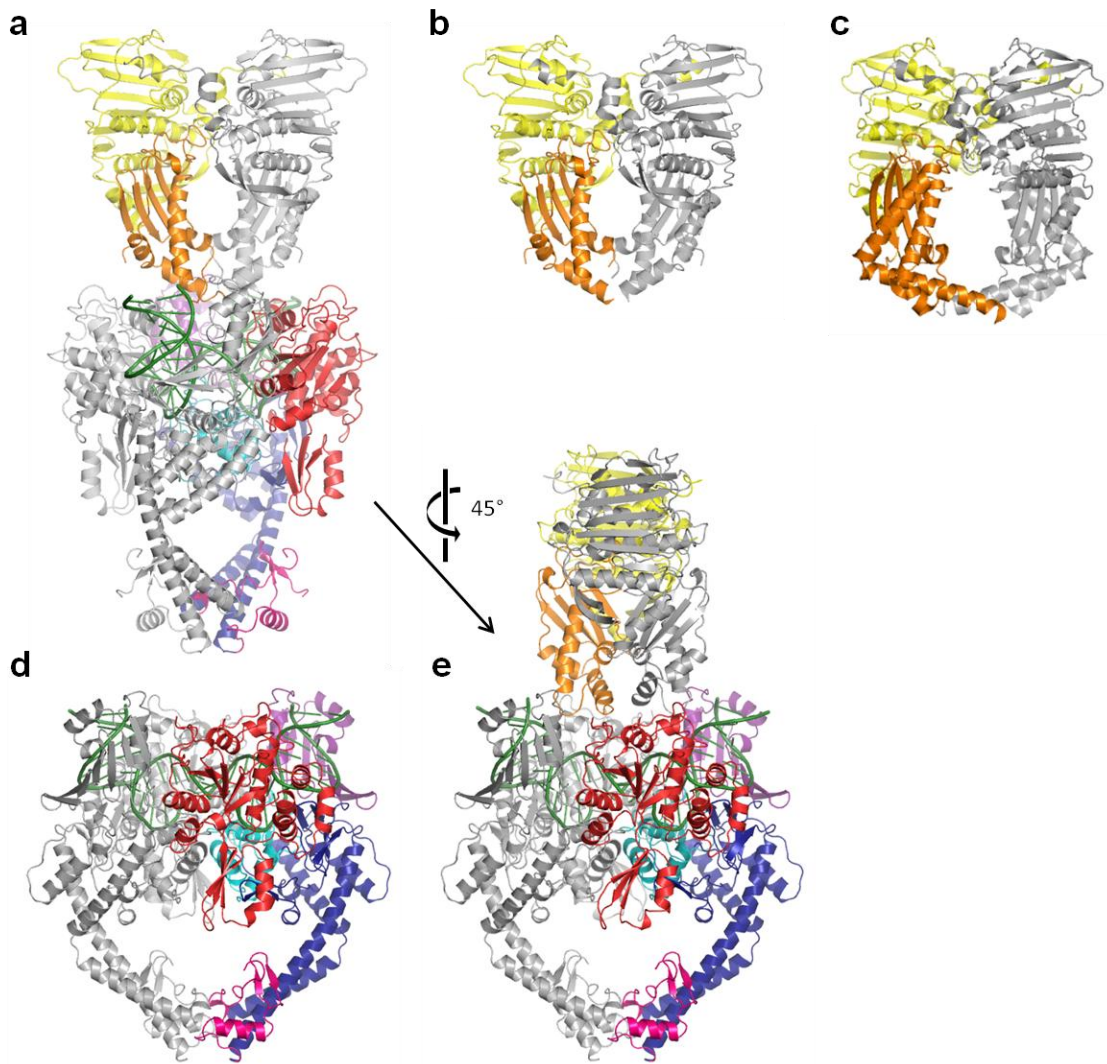
Figure 3.3 – Structures of topo II domains in isolation closely resemble their configurations within the fully-catalytic complex

a) Near full-length yeast topo II•DNA•AMAPPNP complex determined here. Domain colors as per **Fig. 1**; one subunit is colored gray for clarity.

b) *S. cerevisiae* topo II ATPase domain (PDB ID 1PVG)

c) *E. coli* GyrB ATPase domain (PDB ID 1EI1)

d) *S. cerevisiae* topo II DNA binding and cleavage core covalently bound to DNA (PDB ID 3L4K)

e) Same as panel (**a**), but rotated by 45°.
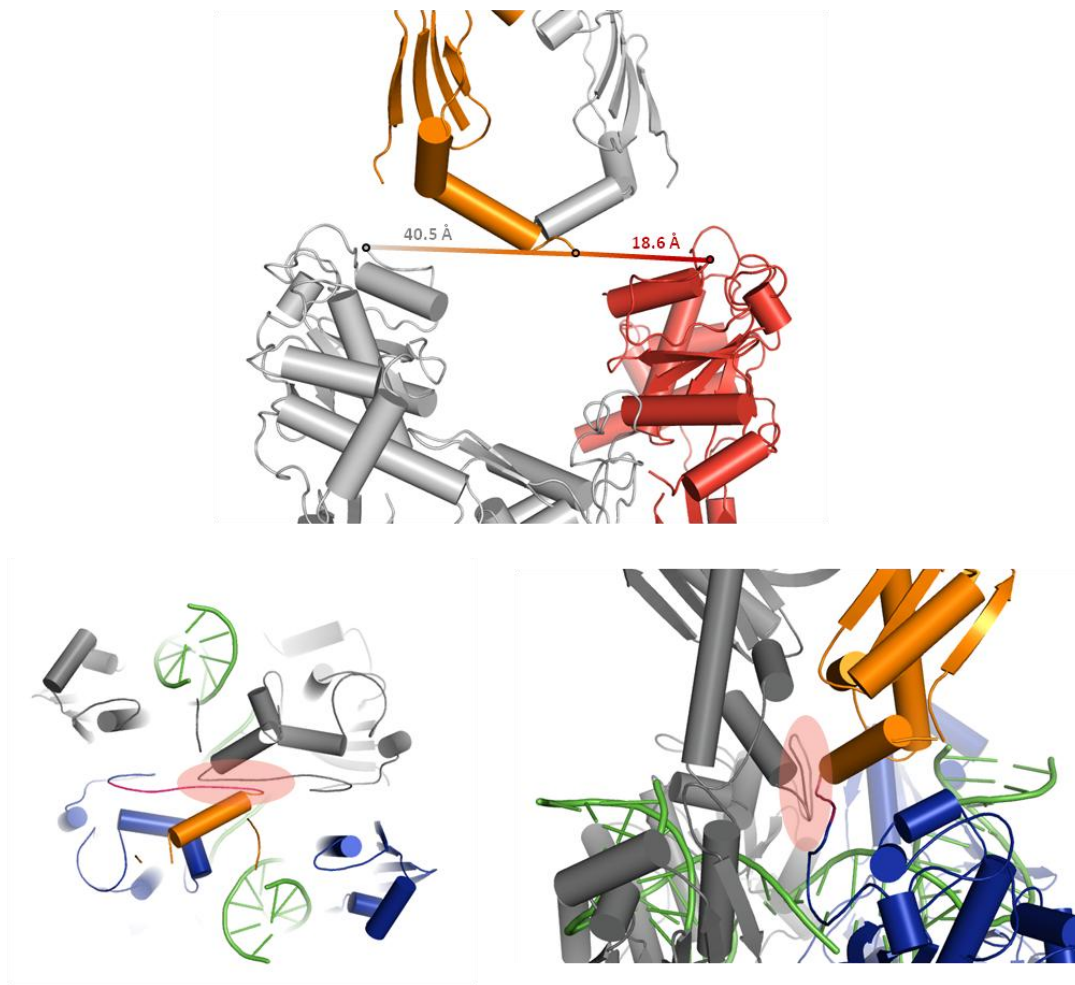
Figure 3.4 – ATPase-TOPRIM connectivity

(*Top*) Distance between the C-terminus of one ATPase domain (orange) and the N-termini of both TOPRIM folds. One TOPRIM N-terminus (gray) is 40.5 Å away, while the other (red) is 18.6 Å away. The bound DNA is not shown for clarity. Although electron density for the 12 amino acids that connect these ATPase and TOPRIM regions is disordered, and hence unbuildable, the relative positions of the C- and N-termini of the two domains are only close enough to support connectivity if the ATPase domains connect to the closer of the two TOPRIM folds, a link that leads to domain swapping.

(*Bottom*) Connecting the ATPase domains to their more distal TOPRIM counterparts requires a fully extended, strained linker (magenta) that sharply doubles back on itself and clashes with its symmetry mate. Top-down (left) and side (right) views of a modeled, non-swapped linker using a fully-extended non-crossover configuration. The region where clashes occur is denoted by a shaded oval.
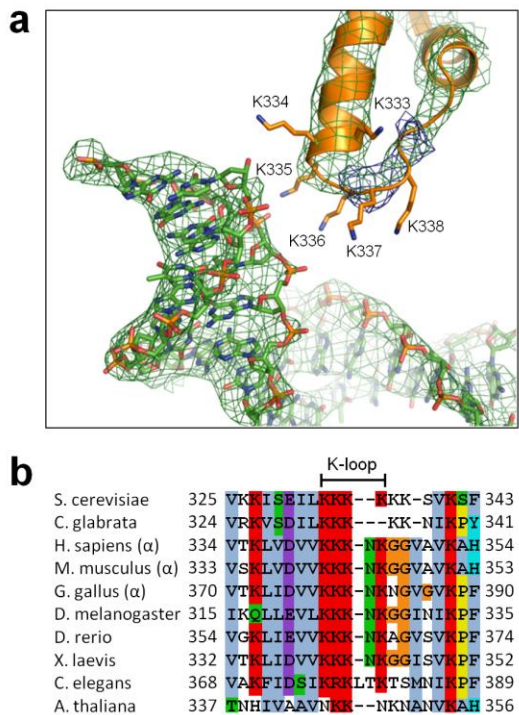
Figure 3.5 – The topo II ATPase domain appears to engage bound DNA

a) Close-up of the K-loop interaction with DNA . View corresponds to the boxed region in Fig. 1b. DNA is surrounded by 2*Fo-Fc* density contoured to 1.5σ. The K-loop is surrounded by 2*Fo-Fc* density, contoured to 1.0σ (green), as well as original *Fo-Fc* density from the initial MR solution contoured to 2.5σ (blue). The original search model had a gap spanning residues 335-339.

b) Sequence alignment of eukaryotic type IIA topoisomerases. The K-loop lysines are boxed. The human, mouse, and chicken sequences correspond to the alpha isoforms; topo IIβ isoforms also bear K-loop lysines.
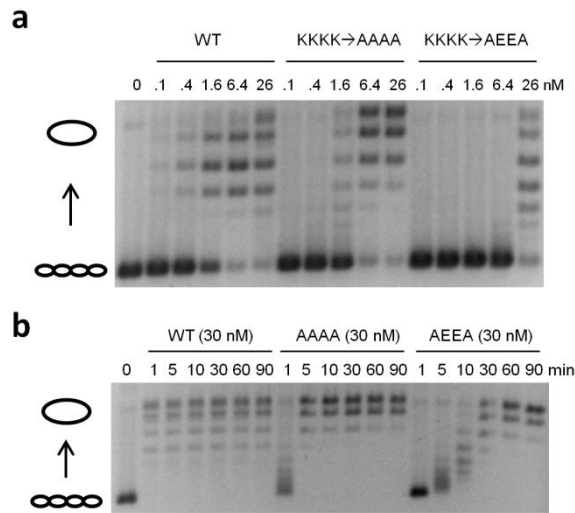
Figure 3.6 – K-loop mutants are deficient at relaxing negatively-supercoiled DNA
a) Concentration-dependent relaxation of negatively-supercoiled DNA. Supercoiled and relaxed topoisomers are denoted with coiled and open circles, respectively.
b) Timecourse-dependent negative supercoil relaxation. 7.5 nM DNA is present in both sets of reactions.
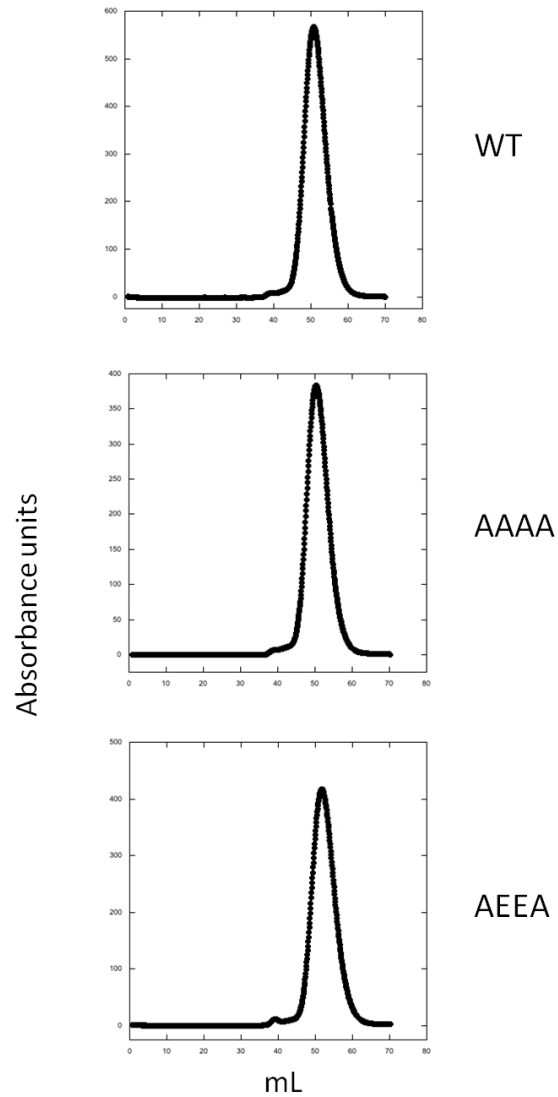
Figure 3.7 – K-loop mutants show similarly solution properties to wild-type topo II
Size exclusion chromatography column traces for WT, AAAA, and AEEA topo II mutants.
Each protein preparation gives rise to a single monodisperse peak eluting at the same expected
volume.
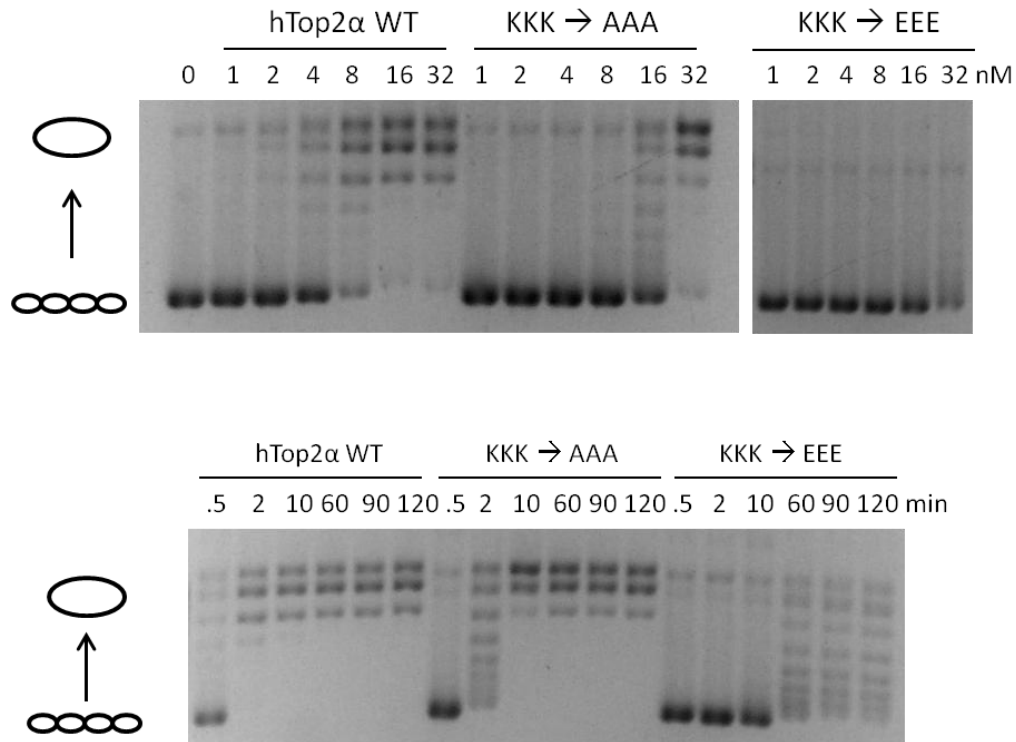
Figure 3.8 – The K-loop of human topo IIα is required for function

(*Top*) Enzyme titration for wild-type and selected K-loop mutants for human topo IIα. The AAA mutant is knocked down about 3-fold, while the EEE mutant barely shows activity at 32 nM (4-fold excess over DNA).

(*Bottom*) Time-course for all three proteins at 40 nM enzyme concentration. The AAA mutant is slower than WT but can still relax DNA to completion. The EEE mutant proceeds so slowly that it does not finish after 120 minutes, and shows only minimal progress between 60 and 120 minutes.
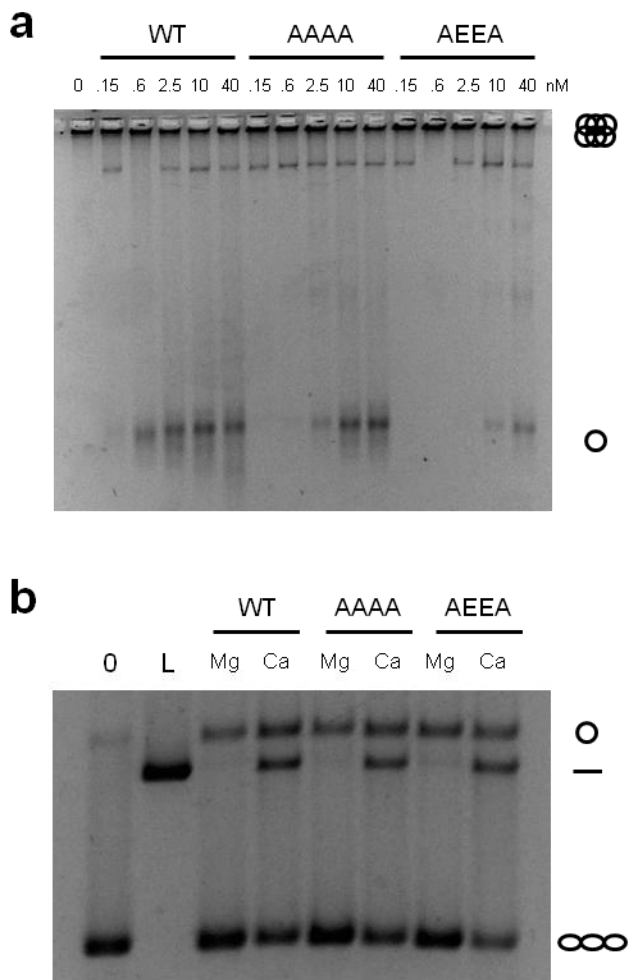
Figure 3.9 – K-loop mutants are defective for decatenation but not DNA cleavage
a) Decatenation assay. The degree to which the AAAA and AEEA mutants are impaired in decatenation activity follows the trend seen for the relaxation of negatively-supercoiled DNA.
b) Cleavage assay. Left lane, negative control, no protein. L, plasmid linearized by BamHI. The WT and K-loop mutants show similar propensities to cleave DNA in a calcium-dependent manner.
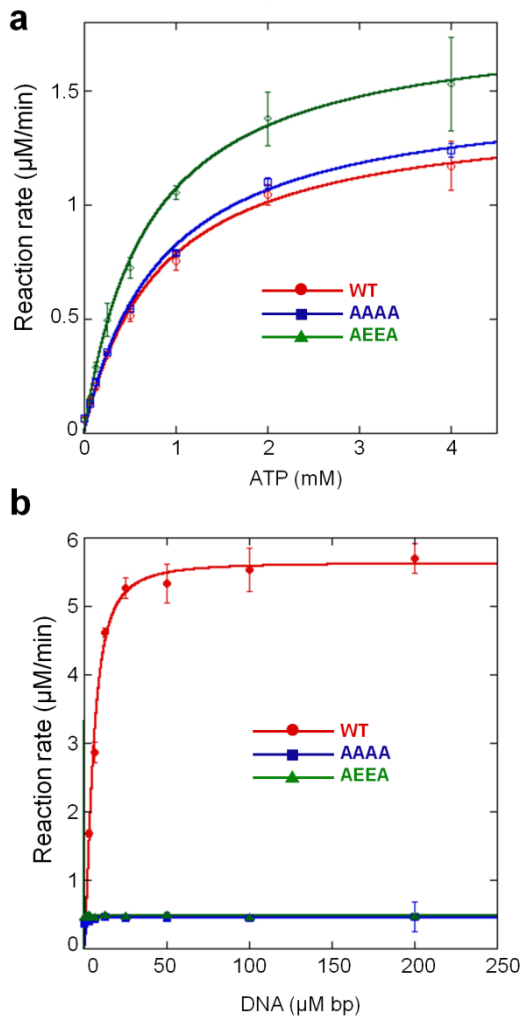
Figure 3.10 – K-loop mutants maintain basal ATPase rates but lose DNA-stimulation of ATP hydrolysis

a) Basal ATPase activity. Wild-type and K-loop mutant activities are plotted as a function of ATP concentration and fit to a standard Michaelis–Menten kinetic model. Apparent V_{max} values of 1.42 ± 0.06, 1.51 ± 0.06, and 1.82 ± 0.05 μM/min were calculated for WT, AAAA, and AEEA topo II constructs, respectively. Calculated K_M values are 0.82 ± 0.09, 0.84 ± 0.09, and 0.70 ± 0.05 mM ATP.

b) DNA-stimulated ATPase activity. Wild-type and K-loop mutant activities are monitored at a constant starting concentration of ATP, and are plotted as a function of sheared salmon-sperm DNA concentration.
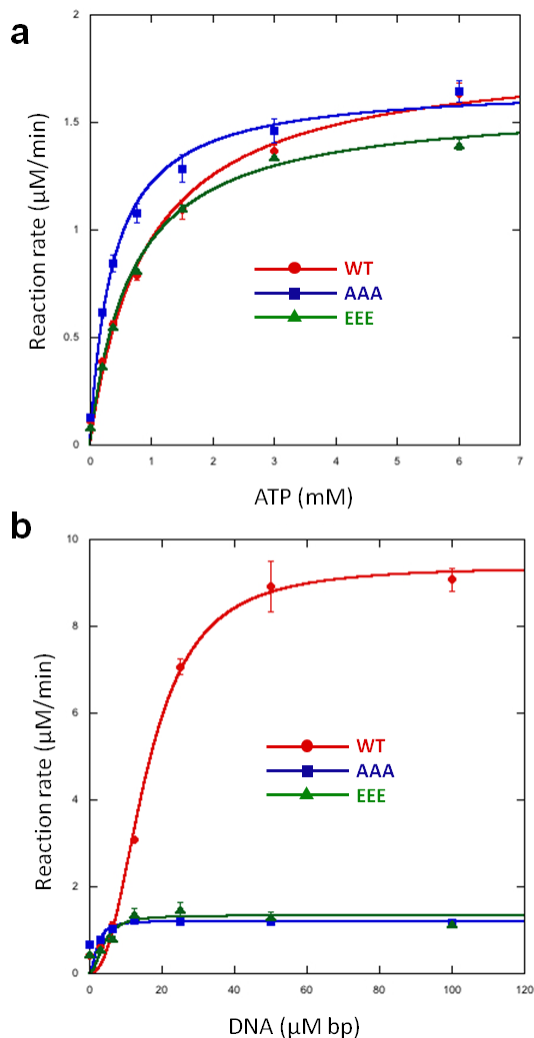
Figure 3.11 – The K-loop of human topo IIα is required for DNA-stimulated, but not basal, ATPase activity

a) Basal ATPase profiles. Wild-type and K-loop mutant activities are plotted as a function of ATP concentration and fit to a standard Michaelis–Menten kinetic model. Apparent V_{max} values of 1.83 ± .10, 1.67 ± .07, and 1.59 ± .05 μM/min were calculated for WT, AAA, and EEE topo IIα constructs, respectively. Calculated K_M values are 0.92 ± 0.15, 0.38 ± .06, and 0.68 ± 0.07 mM ATP.

b) DNA-stimulated ATPase activity. Wild-type and K-loop mutant activities were measured at a constant starting ATP concentration, and plotted as a function of sheared salmon sperm DNA concentration. Fit is to the Hill equation (Methods).
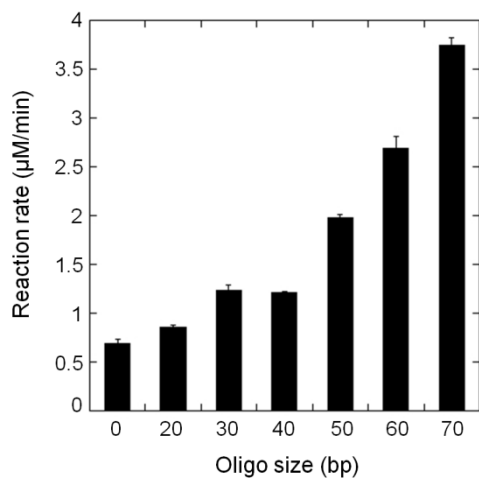
Figure 3.12 – Oligos stimulate ATP hydrolysis in a length-dependent manner
A 20mer oligo fails to stimulate ATP hydrolysis beyond the basal rate. As length increases, ATPase stimulation increases. The ratio of DNA:protein is the same in all instances, and error bars derive from an average of three independent experiments.
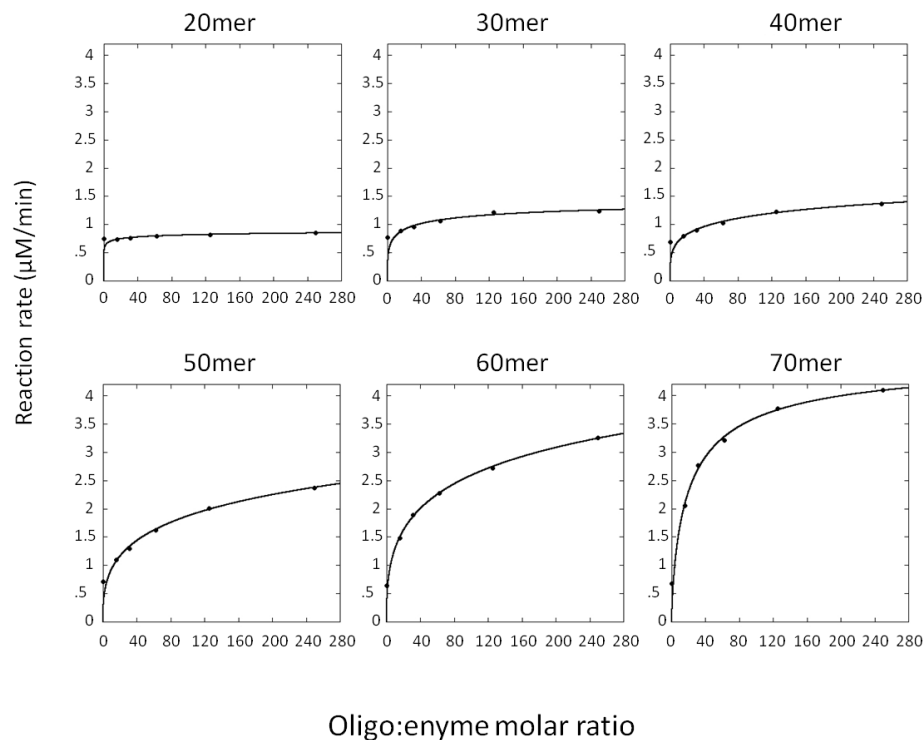
Figure 3.13 – Representative traces of oligo-stimulated ATP hydrolysis
For all oligo-stimulated ATPase assays, yeast WT topo II was incubated with 0.25 mM ATP and increasing concentrations of oligo substrate. Representative curves for the 20mer through 70mer substrates are shown here. The data demonstrate that the 20mer fails to stimulate ATP hydrolysis, but that the stimulative effect of oligos increases as their length increases.
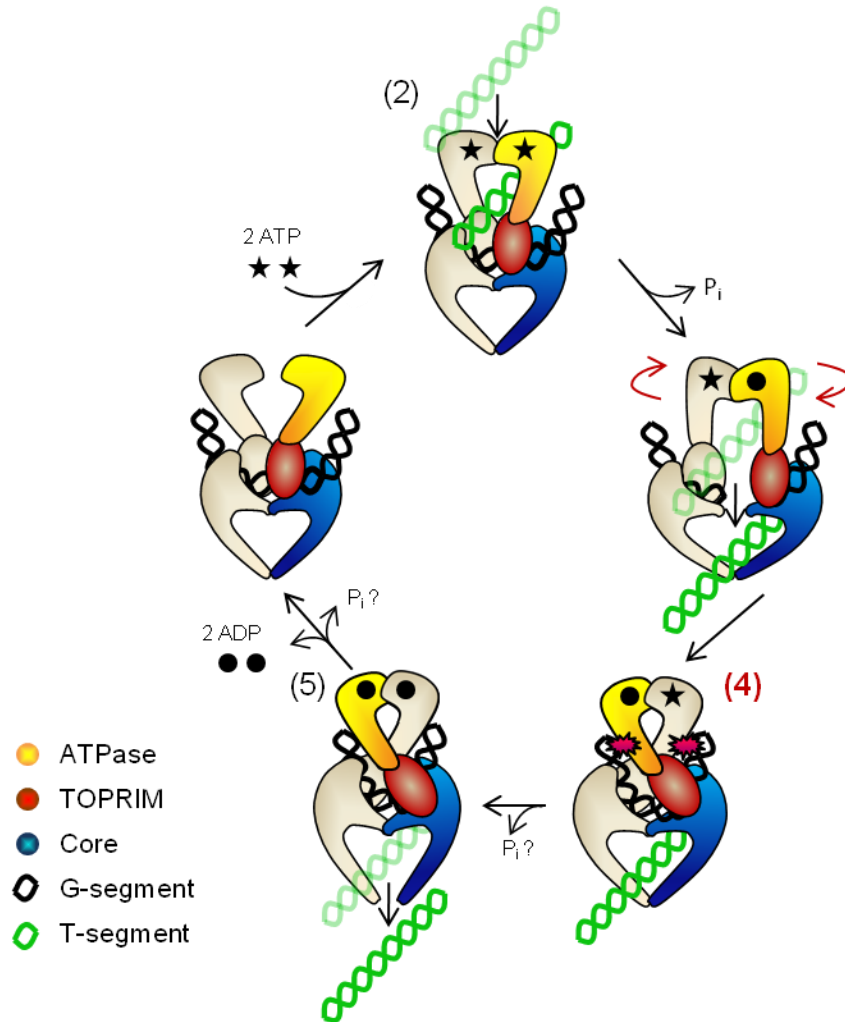
Figure 3.14 – Unexpected complexities in the type IIA topoisomerase catalytic cycle
(1) Homodimer at the beginning of cycle. One monomer is shaded gray and the other is colored as indicated in the key. The enzyme binds and bends a G-segment (black). (2) The binding of two ATP (stars) promotes T-segment capture (green). (3) Hydrolysis of one ATP to ADP (circle) leads to G-segment cleavage and T-segment transport through the break. Following strand transport the ATPase domains swivel about each other to impede backward translocation of the T-segment. (4) G-segment ends are brought back together for religation. K-loop contacts are proposed to trigger hydrolysis of the second ATP. (5) T-segment escape, followed by ADP release, resets the enzyme. Steps (3) and (4) are highlighted in red to denote the new findings from this work. As many prokaryotic type IIA topoisomerases appear to lack a K-loop (**Figure 3.16**), interactions between this region and G-segment DNA (step 4) may be limited to eukaryotic topo II homologs. The precise point of P_i release following the second hydrolysis step is not known (question marks)
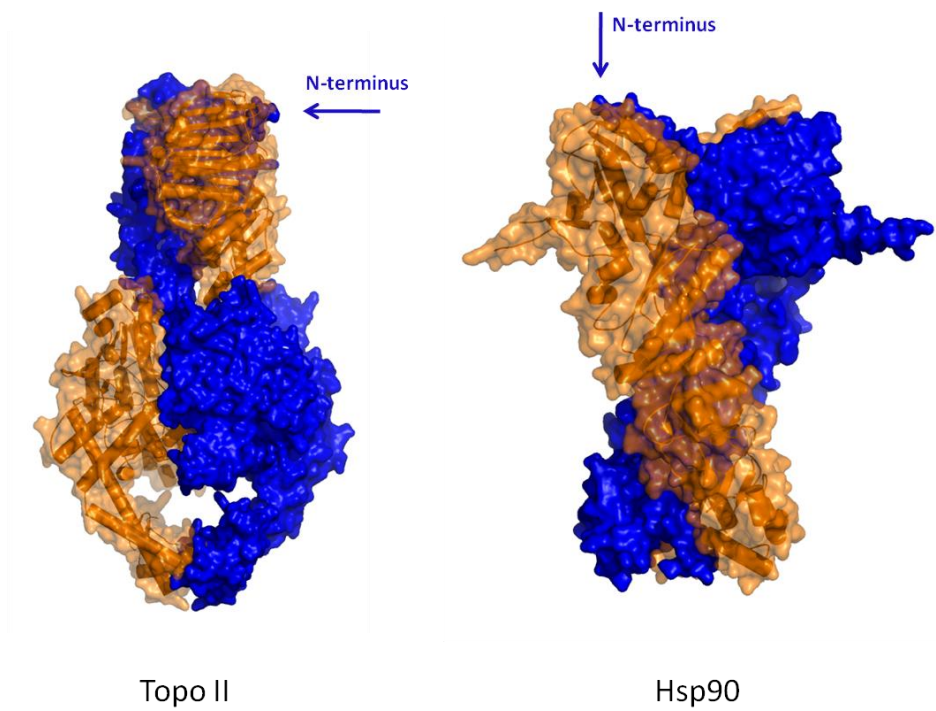
Topo II   Hsp90

Figure 3.15 – Domain-swapping in different GHKL ATPase assemblies
The topo II and Hsp90 holoenzymes share a common ATPase domain and form intertwined dimers. One protomer of each protein is colored blue and the other orange.
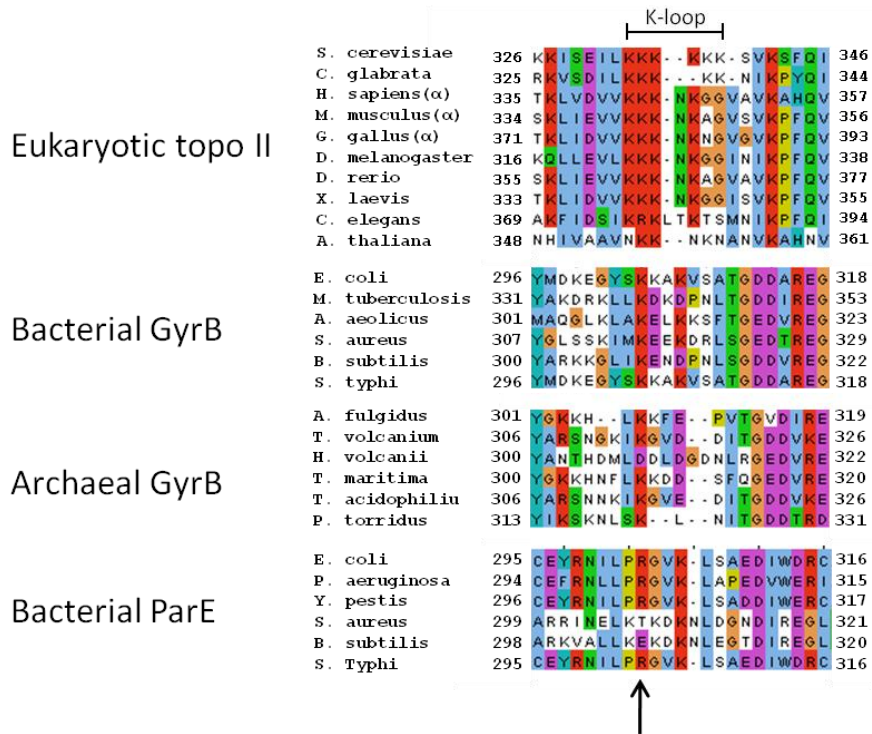
Figure 3.16 – Alignment of K-loop regions among prokaryotic and eukaryotic type IIA topoisomerases
Two lysines are essentially invariant among eukaryotic homologs. One or two lysines are frequently found in the analogous region of prokaryotic type IIA topoisomerases, but are less well conserved and often accompanied by acidic residues, which are not found in eukaryotes. Arrow denotes the single most conserved basic position.

Chapter 4 – The structure of a DNA-bound human topoisomerase IIα: conformational mechanisms for coordinating inter-subunit interactions with DNA cleavage

(Portions of this chapter are adapted from: Wendorff, T.J., **Schmidt, B.H.**, Heslop, P., Austin, C.A., and Berger J.M. (2012), J Mol Biol, 2012 Jul 25. [Epub ahead of print].)

Introduction

The work described in the previous two chapters examined a topoisomerase II•DNA cleavage complex, the architecture of a full-catalytic enzyme•DNA•nucleotide complex, and the ways in which domains interacted with and influenced one another by long-rang communications and allostery. Chapter 2 in particular focused on how topoisomerase II ordinarily cleaves DNA. As discussed in Chapter 1, cleavage activity may be corrupted by a number of agents that have been exploited for therapeutic gain. One longstanding goal of my thesis research was to determine the structure of a ternary complex of topoisomerase II•DNA•poison. Such a complex would help elucidate the means by which these drugs stabilize the cleaved state and/or prevent religation. Additionally, it would serve as a platform for the design of future inhibitors. I adopted several strategies to pursue this goal: drug soaks of my pre-existing crystal form, co-crystallization with a covalent cleavage complex, and identification of oligonucleotide substrates and conditions that display drug-dependent cleavage. I began these strategies with the yeast topo II DNA-binding and cleavage core, but later explored more biomedically relevant human topo II constructs.

Although I did not obtain a drug-bound complex, in the course of working toward these goals I helped to determine the structure of a binary complex of human topoisomerase IIα bound to DNA. The structure, along with a careful comparative structural analysis of 21 other type IIA topoisomerase structures, reveals that the type IIA topoisomerase nucleolytic center undergoes highly quantized conformational transitions between distinct DNA binding, cleavage, and drug-inhibited states that correlate with both the control of subunit-subunit interactions and metal ion occupancy (see: Chapter 2). Additional consideration of the human topo IIα model compared with an etoposide-inhibited complex of human topo IIβ suggests possible avenues for the development of isoform-specific inhibitors that could address the tendency of topo II-targeting chemotherapeutics to generate secondary malignancies.

Results and Discussion
Soaks of pre-existing crystals
The most straightforward strategy to obtain a ternary complex was to take the crystals of the covalent cleavage complex I grew in Chapter 2 and soak them with drugs. After scaling up crystal production, I prepared solutions containing crystallization well solution plus 1 mM of one of each of the following anticancer drugs: etoposide, teniposide, mAMSA, doxorubicin, and vosaroxin. Doxorubicin rapidly dissolved the crystals, whereas the other three drugs showed no visual effects on crystal morphology. Nonetheless, after collecting diffraction data from the soaked crystals, no difference density could be observed at or near the active site that might correspond to a bound drug molecule. Evaluation of the structures of drug-bound complexes that were determined subsequent to my early efforts(Bax et al., 2010b; Laponogov et al., 2010; Laponogov et al., 2009; Wohlkonig et al., 2010; Wu et al., 2011), revealed that the drug-bound state requires significant structural rearrangements. Thus, this soaking strategy was never going to work because drug binding would have perturbed the crystal lattice of my crystal form

Co-crystallization of the covalent cleavage complex
The next strategy I pursued was to co-crystallize various drugs with the trapped, phosphorothiolate covalent cleavage complex described earlier (Chapters 2 and 3). In this scheme, drug was added directly to a 5 mg/mL solution of complex to a final concentration of 1 mM prior setting sparse matrix screens. Screening did reveal a new crystal form that grew in a new condition when vosaroxin was present. I collected diffraction data from these crystals and used molecular replacement to obtain a solution. However, as before the resultant electron density (both F_o-F_c and $2F_o$-F_c maps) revealed no evidence for drug binding. No other promising hits emerged from this co-crystallization approach.

Attempts to establish drug-dependent DNA cleavage
The previous two strategies both depended on assembling a covalent cleavage complex with phosphorothiolated DNA and then using either drug soaks or co-crystallization on an already assembled covalent cleavage complex. As an alternative strategy, I sought to make different oligonucleotide substrates that would not be cleaved in the absence of drug (as the suicide substrate is), but that could be analyzed biochemically for drug-dependent cleavage. The rationale for this approach was that drug-dependent cleavage would highlight the existence of a ternary complex between enzyme•DNA•drug. If the ternary complex were the major species in solution, then it would be more likely for any new crystal forms to be of the ternary complex itself instead of a binary complex as had been imaged previously.

A variety of substrates were surveyed by this approach including drug identity (doxorubicin, etoposide, teniposide, mAMSA, and vosaroxin), oligo length (20-34 bp), nicking of the complementary strand, and incorporation of mismatches(Bigioni et al., 1996). In every instance, the oligonucleotide substrates proved refractory towards cleavage by the yeast topoisomerase II

DNA-binding and cleavage core. This result raised the question whether the truncated yeast construct might itself be a problem, so I also tried using the fully-catalytic yeast topo II construct, and tested it for cleavage with either ATP or AMPPNP present. In all cases cleavage levels never exceeded 10% of the total material (**Figure 4.1**).

Adopting human topoisomerase II as a new crystallographic target
Despite the many variables I tested, a possible limitation of the drug-inhibited structural studies is that they were all performed with yeast topo II. This constraint is potentially significant because the clinical target of anticancer agents such as etoposide and doxorubicin is human topo II, and there is strong interest in understanding how the human enzymes are inhibited by such agents. Although genomes of lower eukaryotes such as yeast typically encode only a single topo II homolog, higher eukaryotes, including humans, possess two isoforms, termed topo IIα and topo IIβ(Austin and Fisher, 1990; Chung et al., 1989; Tsai-Pflugfelder et al., 1988). During my doctoral research, the Chan group published a paper showing the structure of human topo IIβ captured in a cleavage complex with DNA and the anticancer drug etoposide(Wu et al., 2011). This paper accelerated my thinking that I should focus efforts on the two human enzymes instead of the yeast construct.

Type IIA topoisomerases share significant amino acid sequence homology between species, with the human type II topoisomerases ~40% identical to yeast topoisomerase II. Overall, the two human enzymes are 68% identical to each other(Austin et al., 1993), with the catalytic portions of the proteins sharing ~78% identity. Topo IIα and topo IIβ have different expression patterns in mice(Capranico et al., 1992), with topoisomerase IIα produced in proliferating tissues and topoisomerase IIβ expressed more systemically. Expression of both isoforms are cell cycle dependent; levels for both are highest in dividing cells, but topo IIβ is the predominant isoform in non-dividing and post-mitotic cells(Lyu and Wang, 2003; Tsutsui et al., 1993; Tsutsui et al., 2001). In general, topo IIα plays a more central role in chromosome segregation and DNA replication(Grue et al., 1998; Niimi et al., 2001), whereas topo IIβ seems to be involved primarily in transcriptional regulation(Ju et al., 2006; McNamara et al., 2008; Perillo et al., 2008).

Due to its role in cell proliferation, topo IIα expression has been used as a cancer cell marker(Dingemans et al., 1998; Fry et al., 1991; Kasahara et al., 1992). Both human type II topoisomerases are targets of highly effective anticancer drugs such as epipodophyllotoxins (e.g., etoposide); however, in some human patients these agents also increase the likelihood of therapy-related malignancies, such as acute myeloid leukemia(Felix, 1998, 2001; Pedersen-Bjergaard et al., 2002). Several studies have suggested these secondary cancers may be linked to the undesired action of such drugs on topo IIβ(Azarova et al., 2007; Cowell et al.; Haffner et al.; Lyu et al., 2007), raising the possibility that topo IIα-specific inhibitors (e.g., NK314(Toyoda et al., 2008)) might be useful for improving therapeutic outcomes. One challenge to identifying

such compounds arises from the fact that the principal drug-binding locus, the DNA-gate, is one of the most highly-conserved regions between the two enzymes. Structural insights from both drug-bound and drug-free states of DNA-bound topo IIα and topo IIβ complexes are ultimately needed to aid efforts aimed at improving specificity; currently, only an etoposide-inhibited form of the human topo IIβ DNA cleavage core has been imaged crystallographically(Wu et al., 2011).

The work described in the remainder of this chapter was undertaken with a rotation student I was mentoring, Timothy Wendorff, who subsequently joined the lab and helped complete the study. To better understand both type IIA topoisomerase mechanism and identify features that can distinguish between closely related epipodophyllotoxin-binding sites, we crystallized and solved the structure of the central catalytic region of human topo IIα bound non-covalently to a doubly-nicked DNA substrate. The complex exhibits the now-canonical DNA bend exemplified by the type IIA topoisomerase family(Charvin et al., 2005; Dong and Berger, 2007; Hardin et al., 2011; Laponogov et al., 2009; Schmidt et al., 2010; Wohlkonig et al., 2010; Wu et al., 2011), and allows for comparative studies that provide new insights into how the relative configuration of the active site for DNA cleavage correlates with both metal-ion occupancy and the opening and closing of the distal C-terminal dimer interface. Analysis of the topoisomerase IIα structure in light of the etoposide-inhibited state of human topo IIβ confirms the close relationship between the two isoforms that fosters inhibitor cross-reactivity, while also highlighting two amino acid differences in the drug-binding pocket that could serve as differentiating features for developing more selective anti-topoisomerase agents.

Overview of the human topoisomerase IIα-DNA complex

As no structure of the human topo IIα DNA binding and cleavage core had been determined previously, we used sequence homology and existing type IIA topoisomerase structures as a guide for constructing a minimal, crystallizable fragment (residues 431-1193, **Figure 4.2a**). This protein was expressed and purified (**Methods**), and subsequently co-crystallized with a duplex DNA 13mer containing complementary 4-base, 5' overhangs (**Figure 4.2b**). Following data collection and phasing by molecular replacement (**Methods**), the resultant electron density maps readily permitted modeling of the entire DNA substrate and essentially all of the protein. The final model was refined to 2.9Å resolution with an R_{work}/R_{free} of 23.2/27.5% and excellent stereochemistry (**Table 4.1**).

The topo IIα•DNA complex forms a homodimer (**Figure 4.3**), in which the two protomers derive from a pair of asymmetric units related by crystal symmetry. Two DNA oligos associate with the dimer, forming a doubly-nicked, pseudo-continuous duplex in which the complementary overhangs pair with one another across the molecular dyad. A single isoleucine on each protomer (Ile856) intercalates into the minor groove of DNA, together bending the duplex by 130°; additional DNA contacts are manifest by numerous non-specific, electrostatic

interactions within the large (~3130 Å²), positively-charged DNA-binding surface of the protein. The degree of bending seen in the structure coincides with that reported for topo IIα by FRET (136±17°)(Hardin et al., 2011), and with structures of other type IIA topoisomerase•DNA complexes(Dong and Berger, 2007; Laponogov et al., 2010; Schmidt et al., 2010; Wohlkonig et al., 2010). The catalytic tyrosine (Tyr805), responsible for nucleophilic attack on the DNA, resides ~6 Å from the backbone, opposite the nick; the two aspartates (Asp541, Asp543) that form the conserved DxD motif of the TOPRIM region sit nearby, coordinating a single Mg^{2+} ion. A third acidic moiety of the TOPRIM domain, Glu461, hydrogen bonds to the 3' OH of the DNA strand, while His759 rests ~3.5 Å away from the phosphate of the -1 base. Arg804, which ligands the scissile phosphate in covalent cleavage complexes determined for type IIA topoisomerases, coordinates the -1 phosphate in this structure. In general, these contacts comport with the active-site environments seen in other structures of type IIA topoisomerases complexed with DNA(Bax et al., 2010b; Dong and Berger, 2007; Laponogov et al., 2010; Laponogov et al., 2009; Schmidt et al., 2010; Wohlkonig et al., 2010; Wu et al., 2011)

Implications for inhibition of topo IIα by etoposide

Our topo IIα model provides valuable insights for efforts aimed at engineering compounds that discriminate between the two isoforms in humans. A recent structure of human topo IIβ in complex with etoposide establishes the binding pocket and modality for this class of topoisomerase II poisons(Wu et al., 2011). This pocket is solvent accessible in our topoisomerase IIα structure, but insufficiently large to accommodate drug. In topoisomerase IIβ the expanded pocket derives from changes in global protein conformation; association of the relatively non-planar compound alters the disposition of the two WHDs in the dimer interface with respect to each other, deforming the DNA and pushing each TOPRIM domain away from the WHD of its partner protomer. These structural changes derive from rigid-body, *en bloc* movements between the WHDs and TOPRIM domains in the dimer, suggesting that drug binding occurs during transient opening or breathing of the DNA-gate following DNA cleavage.

To investigate how etoposide might interact with human topo IIα, we individually superposed both the WHD and TOPRIM domain from our structure onto that of topo IIβ. A single superposition using both domains simultaneously was not feasible due to the aforementioned conformational changes in the region (**Figure 4.4a**); however, upon superposition, the backbones of both domains individually align well with those of topo IIβ (WHD Cα RMSD =0.70Å, TOPRIM Cα RMSD = 0.51Å). Of the four topo IIβ residues that make side chain contacts with the drug, the only residue that is different in the corresponding topo IIα binding site is the substitution of a methionine (Met762) for glutamine (Gln778 in topo IIβ) (**Figure 4.4b-c**). The sulfur atom in methionine is unlikely to substitute for the hydrogen-bonding interaction that is seen to occur between the glutamine amide and O12 on the "D" ring of etoposide. Nevertheless, etoposide is known to act *in vitro* against both human paralogs(Gentry et al., 2011), and targets both isoforms in cells(Bandele and Osheroff, 2008; Willmore et al.,

1998). Since Gln778 adopts two conformations in the topo IIβ structure(Wu et al., 2011), its observed contacts with etoposide likely are not crucial for inhibitor activity.

A comparison of the two structures suggests a few possible avenues by which etoposide might be modified to better discriminate between topo IIα and topo IIβ. One approach could include adding different substituents to the lactone group of etoposide to take advantage of the different chemistries, steric bulk and rotamer preferences of glutamine vs. methionine. The reactivity of methionine might also be exploited, for instance through platinum conjugates(Dedon and Borch, 1987), to select for topo IIα reactivity. Our modeling suggests that the glycosidic moiety on the etoposide "C" ring is another possible candidate for modification (**Figure 4.4b-c**). In the topo IIβ model, this group resides within a large binding pocket on the enzyme, but makes few contacts with the protein surface. NMR studies have corroborated this paucity of contacts(Bender et al., 2008), and removal of the sugar is known to cause little change in drug activity *in vitro*(Bender et al., 2008; Wilstermann et al., 2007). Comparison of this region between human topo IIα and topo IIβ reveals a single point difference between the two isoforms, with Ser800 of topo IIα replacing Ala816 of topo IIβ (**Figure 4.4c**). This substitution suggests that the addition of a hydrogen-bonding or serine-reactive partner to the 8″ carbon position of the glycosidic group of etoposide might be useful for increasing topo IIα selectivity. Interestingly, teniposide, an etoposide analog that shows a 4-fold greater inhibitor effect against topo IIα as compared with topo IIβ *in vitro*(Drake et al., 1989), may already employ such an approach: teniposide possesses a thienyl sulfur in lieu of the methyl group found on etoposide's glycosidic C-ring, which modeling suggests could make van der Waals contacts with Ser800.

Inter-subunit conformational states correlate with DNA cleavage status
The topo IIα •DNA complex presented here joins a growing number of structures for the DNA binding and cleavage core of type IIA topoisomerases. This collection in turn provides a wealth of data for comparative analyses. While considering our topo IIα model in light of these related systems, we noted that the majority of structures (22 out of 25) retained an associated, or "closed", C-gate(Bax et al., 2010b; Berger et al., 1996; Corbett et al., 2005; Fass et al., 1999; Laponogov et al., 2010; Laponogov et al., 2009; Laponogov et al., 2007; Morais Cabral et al., 1997; Schmidt et al., 2010; Schoeffler et al., 2010; Tretter et al., 2010; Wohlkonig et al., 2010; Wu et al., 2011). However, three completely distinct complexes – *S. cerevisiae* topo II(Dong and Berger, 2007), *A. baumannii* topoisomerase IV(Wohlkonig et al., 2010), and our human topo IIα – also have been obtained in which this C-gate interface is dissociated, or "open". The existence of multiple models that derive from different topoisomerase homologs and crystal packing environments, yet still exhibit an open C-gate, strongly argues against suggestions that this conformation represents a non-physiologic state(Laponogov et al., 2010; Laponogov et al., 2009).

The factors that control C-gate status have been the subject of debate. One suggested proposal was made by me, as discussed in Chapter 2, which posited that the formation of a covalent protein•DNA cleavage complex favors C-gate association, whereas G-segment binding alone promotes (but does not strictly enforce) C-gate opening(Schmidt et al., 2010). Support for this argument centers on the existence of a physical linkage between the active-site tyrosine and the α-helical arms that extend into the C-terminal interface (α14 and α18 in human topo IIα); this connection would appear to allow DNA-gate movements, triggered by entry into a cleavage-competent conformational state, to lever the arms toward each other and shut the gate. By contrast, the imaging of certain non-covalent, DNA-bound type IIA topoisomerases with a closed C-gate has raised the possibility that an alternative mechanism may account for the opening of this region(Bax et al., 2010b; Laponogov et al., 2010). Entrapment of the T-segment in the cavity between the DNA-gate and C-gate could constitute one such approach(Roca, 2004).

A close inspection between all 22 published type IIA topoisomerase structures bearing a closed DNA-gate helps resolve this question(Bax et al., 2010b; Dong and Berger, 2007; Laponogov et al., 2010; Laponogov et al., 2009; Laponogov et al., 2007; Morais Cabral et al., 1997; Schmidt et al., 2010; Schoeffler et al., 2010; Tretter et al., 2010; Wohlkonig et al., 2010; Wu et al., 2011). In particular, superpositions between the WHDs of these models reveal that the DNA-gate samples only a limited number of conformational states as the region engages a duplex substrate (**Figure 4.5a**). For example, in comparing apo and substrate-bound forms, the presence of DNA correlates with a single, quantized sliding motion of the WHDs with respect to each other, along a vector that is both perpendicular to the dyad axis of the topoisomerase dimer, and roughly parallel with the axes of the two α-helices that abut each other at the domain interface (α3 in bacterial GyrA, and A'α3 in eukaryotic topo II) (**Figure 4.5a-b**). This movement corresponds to a translational shift of the helix-turn-helix (HTH) motif of each WHD past each other by a distance corresponding to single helical turn, which causes the TOPRIM and tower domains to clamp around the G-segment DNA. Interestingly, the etoposide-bound topo IIβ •DNA structure exhibits an analogous shift of two helical turns, along with a rotational reorientation of the TOPRIM domain (**Figure 4.5b**), as its DNA-gate cracks open.

The relative rotational status of the two WHDs and their associated active-site tyrosines is similarly quantized, and correlates with both DNA cleavage status and the dimerization state of the C-gate (**Figures 4.5a,c**). An open C-gate is observed only at one end of the rotational range, which is populated by two non-covalent topoisomerase•DNA complexes, as well as one apo-enzyme structure(Dong and Berger, 2007; Wohlkonig et al., 2010). By contrast, all other apo and DNA-bound complexes occupy a distinct set of alternate WHD•WHD juxtapositions that coincide with C-gate closure. For instance, all DNA-cleavage complexes stabilized by small-molecule poisons not only have an associated C-gate, but also exhibit a consistent

counterclockwise rotation of the two WHDs with respect to each other(Bax et al., 2010b; Laponogov et al., 2010; Laponogov et al., 2009; Wohlkonig et al., 2010). This conformational change is preserved in the etoposide-inhibited structure between DNA and human topo IIβ(Wu et al., 2011), where an extra translational shift between WHDs also has occurred (**Figure 4.5b**). A less-extreme, but still evident, counterclockwise movement is seen in every DNA-free structure that displays a closed C-gate(Morais Cabral et al., 1997; Schoeffler et al., 2010; Tretter et al., 2010), as well as in the yeast topo II cleavage complex I obtained using a phosphorothiolate substrate(Schmidt et al., 2010).

Overall, in instances where DNA is present, these comparisons reveal a tight correlation between a relative movement on the part of WHDs to elicit DNA cleavage, and the predisposition of the C-gate to be closed. Indeed, out of the 15 topoisomerase II•DNA co-crystal structures in the database, only two appear to violate this correspondence. However, a closer consideration of these outliers (which represent non-covalent, DNA-bound states), suggests that they may actually be exceptions that prove the rule: in particular, both structures derive from topoisomerase/DNA complexes that were exposed to a small-molecule agent that interferes with the normal cleavage cycle of the enzyme. In one example, the cleavage core of *S. aureus* gyrase was co-crystallized with an intact DNA duplex and a non-intercalative inhibitor of strand scission (GSK299943). Interestingly, this inhibitor binds at the interface between the two apposed WHDs, in a pocket that materializes when the domains adopt a cleavage-like orientation relative to each other(Bax et al., 2010b). This concurrence suggests that GSK299943 traps the DNA-gate of bacterial type IIA topoisomerases in a conformation similar to that adopted after the action of fluoroquinolone poisons, which are known to impede normal phosphotransfer chemistry(Bax et al., 2010b; Laponogov et al., 2010; Laponogov et al., 2009; Wohlkonig et al., 2010). In the other instance, the core region of *S. pneumoniae* topo IV was first crystallized with the dione PD 0305970 to stabilize a cleavage complex, after which religation was promoted *in situ* by first soaking out the drug in the presence of EDTA, and then re-soaking the crystals with Mg^{2+} ions to foster religation. Thus, this latter structure derives from a state in which the topoisomerase•DNA complex had already been captured with a rotated WHD configuration and closed C-gate. An inspection of the contacts arising from the crystal lattice indicates that molecular packing interactions would prevent subsequent WHD/WHD rearrangements or C-gate opening upon removal of the drug.

Resolving metal ion occupancy in the DNA cleavage mechanism
In Chapter 2, I outlined a debate that has emerged regarding the positioning and occupancy of metal ions in the topo II nucleolytic center. I predominantly focused on metal positioning in Chapter 2; the human topo IIα structure discussed here, along with a systematic comparative analysis of related topoisomerases, allows us to address the occupancy issue. Based on biochemical data, there is a general consensus that type IIA topoisomerases rely on two metal ions for DNA cleavage(Deweese et al., 2009; Noble and Maxwell, 2002; West et al., 2000).

Crystallographic efforts have refined this picture to suggest that only one metal ion (metal A) actively assists with the chemistry of strand scission and religation, whereas the other (metal B) serves a more structural role, anchoring the DNA at the -1 phosphate position(Bax et al., 2010b; Dong and Berger, 2007; Laponogov et al., 2010; Laponogov et al., 2009; Schmidt et al., 2010; Wohlkonig et al., 2010; Wu et al., 2011). The use of a single metal for phosphodiester bond breakage and reformation parallels the mechanism of strand cleavage employed by $\beta\beta\alpha$-Me and HUH nucleases(Yang, 2008). However, debate remains as to whether the two metals found in the type II topoisomerase active site bind simultaneously during DNA breakage and religation, or if a single "dynamic" ion hops between the two coordination sites at different stages of the reaction.

Support for the simultaneous two-metal mechanism has derived from thiol-rescue studies(Deweese et al., 2009; Noble and Maxwell, 2002; West et al., 2000), and from the structure of *S. cerevisiae* topo II captured in a covalent product complex with a phosphorothiolated DNA and zinc ions described in Chapter 2(Schmidt et al., 2010)(**Figure 4.6a**). By comparison, the dynamic metal concept derives from topo II•DNA complex structures that exhibit only a single metal in either one position or the other(Bax et al., 2010b; Dong and Berger, 2007; Laponogov et al., 2010; Laponogov et al., 2009; Wohlkonig et al., 2010; Wu et al., 2011). However, all one-metal structures correspond to, or derive from, either drug-inhibited states of the enzyme, or complexes in which the DNA substrate is not competent to support cleavage. For instance, in all structures where topo II is bound to an intercalative poison, or where the DNA is nicked at the scissile position (as in our topo IIα model), only metal B is visible (**Figures 4.6b-c**). The inability of poisoned or nicked DNAs to support metal binding at the A-position is readily understandable, as the phosphate which coordinates this metal ion is either shifted out of the active site pocket (in drug-bound states), or missing altogether (as in our human topo IIα model). Alternatively, in the two examples where a topoisomerase II poison is not present, either because the protein is bound to a non-intercalative drug (e.g., GSK29994), or because the enzyme was first co-crystallized with a poison before removal of the drug, only site A is filled (**Figure 4.6d**). The physical impediment to metal binding at site B in the GSK29994-associated, or dione-pretreated complexes arises from a misalignment of the coordinating residues in the DxD motif. This misalignment is likely coupled to the more extreme WHD juxtaposition exhibited by these structures, which matches that of other cleavage-impaired drug-bound complexes (**Fig. 6a**). These shifts may also explain why metal A remains present in the active site of the dione-inhibited state even during EDTA treatment, and why no other divalent species appear following Mg^{2+} addition: this behavior suggests that drug reconfigures the active site to tightly bind only a single cofactor, which is capable of slowly promoting religation in a non-ideal crystalline environment once drug is removed. Overall, the most parsimonious interpretation of these data is that under normal circumstances, two metals are present in the active site during strand scission, whereas inhibitor binding introduces new conformational constraints that allow for occupancy of only a single

metal ion. Put another way, these drugs function as inhibitors precisely because they perturb the DNA cleavage/religation equilibrium by altering when and how specific metal ions are coordinated by the enzyme.

Concluding remarks

In summary, this work presents the first structure of the DNA binding and cleavage core of human topoisomerase IIα bound to DNA. Consideration of the model in light of existing structures of homologous enzymes has enabled us to better understand several important facets of type IIA topoisomerase mechanism and inhibition. In particular, we find that the two winged-helix domains of a topoisomerase dimer, which form part of the region responsible for cleaving and opening DNA (the DNA-gate), adopt only a small set of positional configurations with respect to each other. These quantized conformations appear to couple DNA cleavage status with the allosteric control of interactions at a distal subunit interface, the C-gate, which sits more than 50 Å away from the enzyme active site. Anti-topoisomerase agents that bind within the DNA-gate appear to subvert these movements, altering the position and occupancy of reactive elements to either impede or stabilize cleavage and religation events. Comparisons of our model with an etoposide-inhibited state of the second human type IIA topoisomerase, topo IIβ, highlight the similarities between the two isoforms, but also suggest avenues for improving epipodophyllotoxin selectivity that may be used to counter secondary malignancies. Future efforts aimed at imaging additional functional intermediates and drug-bound states will be needed to test these ideas and improve ongoing antibiotic and anticancer therapies.

Methods

Topo IIα expression and purification

A truncation of the DNA binding and cleavage core from the human gene topo IIα (Tsai-Pflugfelder et al. 1988) (residues 431-1193, **Figure 4.2a**) was cloned into a GAL1-based yeast shuttle vector, in frame with an N-terminal tobacco etch virus (TEV) protease-cleavable His_6-MBP tag. Protein was expressed by transforming the plasmid into *Saccharomyces cerevisiae* strain BCY123 (*MATa pep3::HIS3 prb1::LEU2 bar1::HISG lys2::GAL1/10-GAL4 can1 ade2 trp1 ura3 his3 leu2-3,112,* (Wasserman and J C Wang 1994) originally from the laboratory of R. Kornberg), which was grown in CSM-Ura⁻ media with a lactic acid and glycerol carbon source at 30°C, and inducing by the addition of 2% galactose at A_{600}=0.9. Six hours after induction, cells were centrifuged (4500 rpm, 4°C, 15 min), and flash frozen drop-wise in liquid nitrogen following the addition of 1mL of 1mM EDTA and 250mM NaCl per liter liquid culture to the cell pellets. Frozen cells were lysed under liquid nitrogen by grinding with a mortar and pestle, and resultant powder was both thawed and re-suspended in a 20 mM Tris 8.5, 300 mM KCl, 20 mM imidazole, 10% glycerol buffer supplemented with protease inhibitors (1 mM PMSF, 2.34 µM leupeptin, and 1.45 µM pepstatin). Lysate was clarified by centrifugation (15000 rpm, 4°C, 20 min) and run over a nickel-chelating sepharose column (GE) at 4°C. Following a column wash in resuspension buffer, tagged topo IIα was eluted in resuspension buffer plus 200 mM imidazole. Eluted protein was concentrated using a 100kDa cutoff centrifugal filter (Amicon), buffer exchanged with resuspension buffer, and then incubated overnight with TEV protease at 4°C (Tropea, Cherry, and Waugh 2009). Protease and uncleaved protein were removed by running over a second nickel column, and the eluted cleaved protein was run over a gel filtration column (S300, GE) equilibrated in 500 mM KCl, 20 mM Tris 7.9 and 10% glycerol. Fraction purity was determined by SDS-PAGE, and peak fractions were combined and concentrated to ~15.8 mg/ml protein using a 100 kDa cutoff filter.

Complex assembly and crystal growth

Oligonucleotides were ordered from Integrated DNA Technologies. After receiving them, DNAs were purified by urea-formamide PAGE and annealed to form a 13bp duplex with a complementary 4 base 5'overhang, resulting in a doubly nicked 30 base pair DNA substrate (**Figure 4.2b**) when bound to a topo IIα dimer. DNA and protein were combined in a ratio of 1.1:1 30bp DNA substrate: topo IIα dimer and dialyzed stepwise against 20 mM Tris 7.9, 10 mM $MgCl_2$ and decreasing concentrations of KCl (500 mM, 250 mM, 100 mM). Dialysis ran over the course of 16 hrs at 4°C to a final condition of 20 mM Tris 7.9, 10 mM $MgCl_2$ and 100 mM KCl using a 1000 kDa cut-off mini-capillary dialyzer (Harvard Apparatus). Crystals were grown within a day of setting hanging drops by mixing 150 nL of a 5 mg/mL protein sample with 150 nL 10% (w/v) PEG 3000, 100 mM cacodylate pH 6.5 and 200 mM $MgCl_2$ solution at 18°C. Crystals were looped and cryoprotected with well solution plus 29% glycerol before being flash frozen in liquid nitrogen.

Structure determination and refinement

Diffraction experiments were performed at the 8.3.1 beamline of the Advanced Light Source at Lawrence Berkeley National Laboratory. Data were collected on an ADSC Q210 CCD detector using a wavelength of 1.1159Å beam, and crystals maintained at 100 Kelvin. Data were integrated and scaled using HKL2000(Otwinowski and Minor, 1997). A molecular replacement search model was prepared from the DNA-gate of the crystal structure of yeast topoisomerase II bound to DNA (residues 419-989 and 1153-1177, PDB accession No. 2RGR) with side chain length reduced to the last common atom using CHAINSAW. From this model PHASER determined initial phases(McCoy et al., 2007). The asymmetric unit consisted of a single protomer and half the DNA substrate. Crystallographic base stacking interactions formed long range "sinusoidal" duplexes which traverse the crystal lattice. After a round of rigid body refinement using PHENIX(Adams et al., 2010), the model was improved by building in COOT(Emsley et al., 2010) and refinement in PHENIX using individual site refinement, individual ADP refinement, and TLS. The final model included the entire DNA substrate and the entire protein construct, excluding residues 1092-1124, the N-terminus (residues 431-2) and the C-terminus (residues 1190-1193). Model validation was performed by Molprobity(Chen et al., 2010).

Tables

Table 4.1 Data collection and refinement statistics

	Human topo IIα•DNA
Data collection	
Space group	$C222_1$
Cell dimensions	
a, *b*, *c* (Å)	85.91, 215.08, 128.65
α, β, γ (°)	90, 90, 90
Resolution (Å)	50 - 2.9 (3.00 - 2.90)
R_{sym}	7.6 (70.3)
$I / \sigma I$	15.4 (2.0)
Completeness (%)	95.3 (91.6)
Redundancy	7.2 (4.5)
Refinement	
Resolution (Å)	50 - 2.9
No. reflections	25373
R_{work} / R_{free}	23.2 / 27.5
No. atoms	
Protein/DNA	6527
Solvent	46
B-factors	
Protein/DNA	73.8
Solvent	41.2
R.m.s. deviations	
Bond lengths (Å)	0.005
Bond angles (°)	0.833
Ramachandran favored	96.3%
Ramachandran outliers	0.0%

*Values in parentheses are for highest-resolution shell.
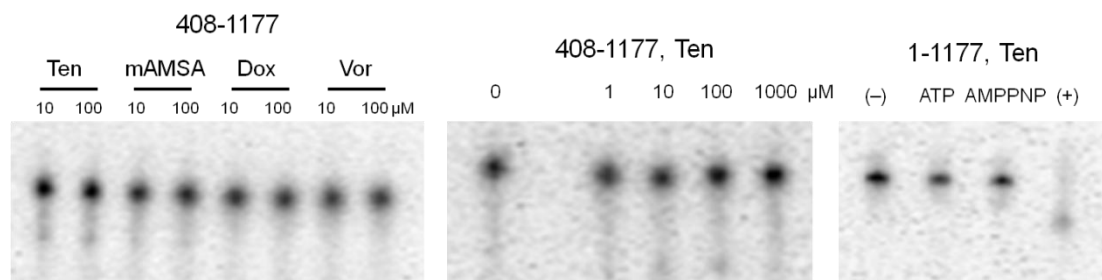
Figures

Figure 4.1 – Oligonucleotides make poor substrates for DNA cleavage
(Left) An initial screen of drug-induced cleavage against a nicked 30mer oligonucleotide substrate showed only teniposide to have any appreciable cleavage. (Middle) Increasing teniposide concentration up to 1 mM does not increase cleavage levels. (Right) Testing the fully-catalytic construct with nucleotides does not improve cleavage; in fact, cleavage levels are lower in this case. Ten; teniposide, Dox; doxorubicin, Vor; vosaroxin
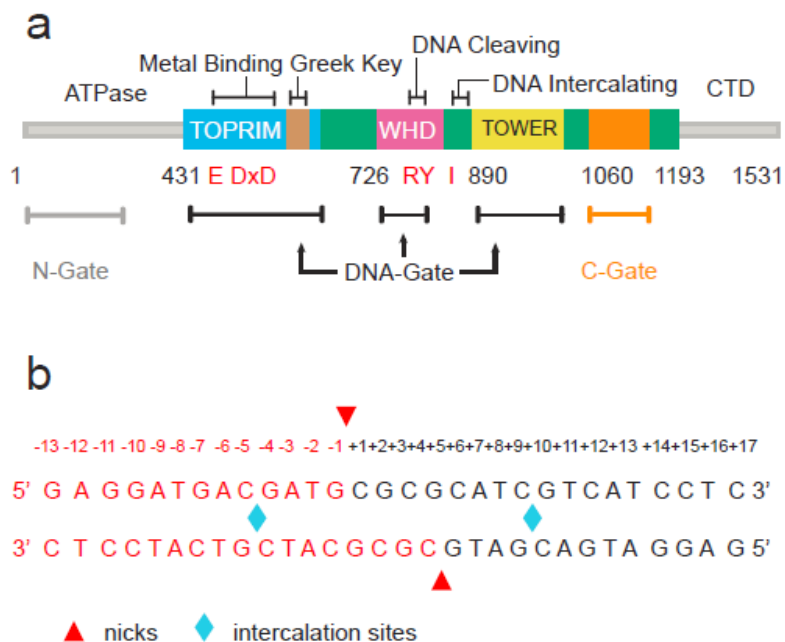
Figure 4.2 – Crystallization constructs

a. Primary structure of human topoisomerase IIα. The fragment crystallized (residues 431-1193) is shown in color. Domains (TOPRIM, WHD, tower) and dimerization gates are shown with important residues and features highlighted: catalytic tyrosine and associated arginine – RY, intercalating isoleucine – I, metal binding motif – DxD, the 3'-OH coordinating glutamate – E. **b**. Schematic of the doubly-nicked, 30 basepair DNA substrate. Nicks and intercalation sites are highlighted.
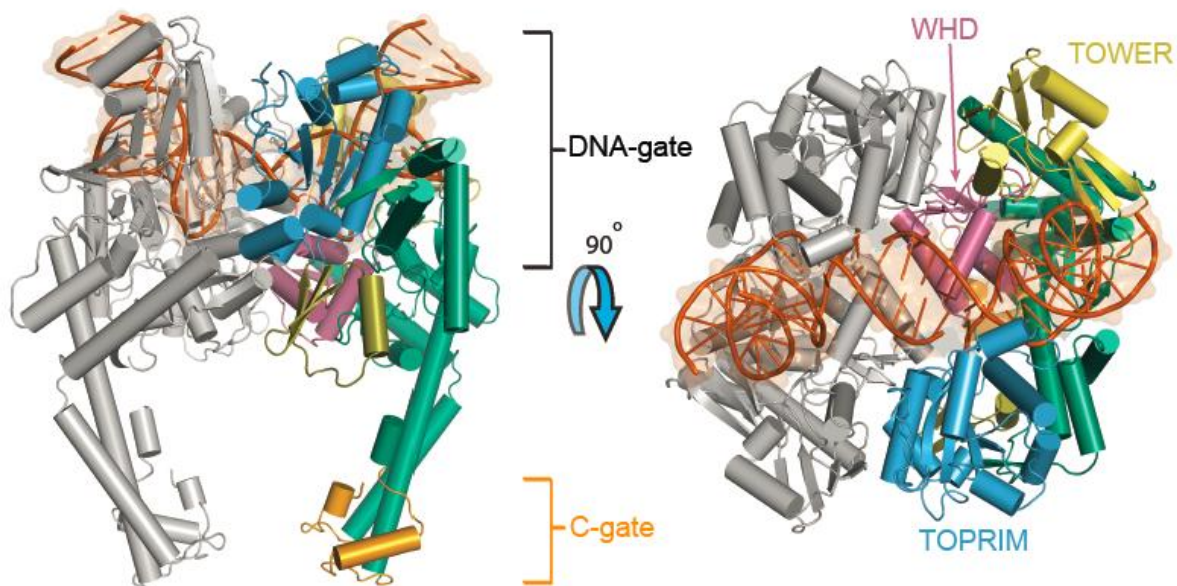
Figure 4.3 – Structure of human topo IIα DNA cleavage core bound to DNA
The human topoisomerase IIα•DNA complex as viewed from the front (*left*) and above (*right*).
Domains are colored as in **Figure 4.2a**, with DNA in dark orange. The G-segment is bound at
the DNA gate, and the C-gate dimerization interface is dissociated.
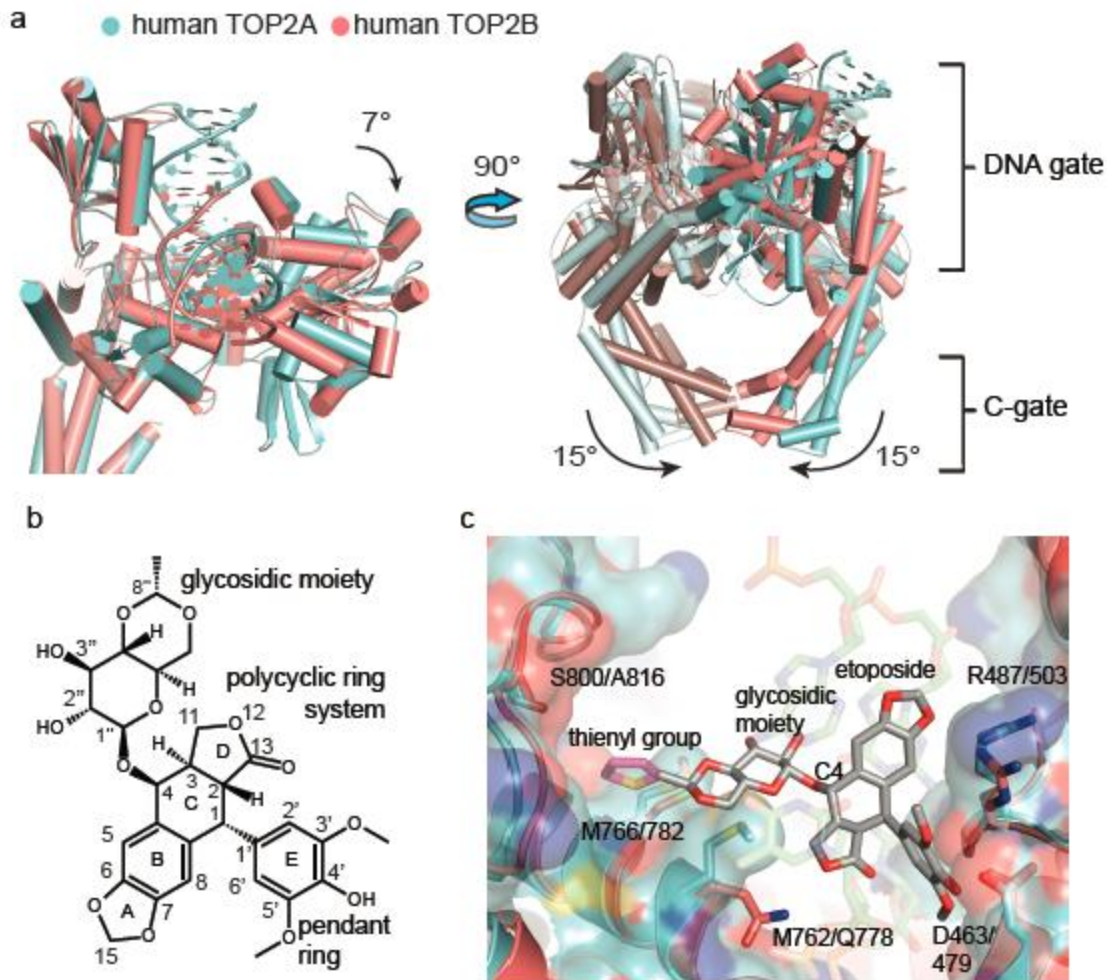
Figure 4.4 – Comparison of topo IIα and etoposide-bound topo IIβ

a. The global conformation of TOP2A and TOP2B differs. Superposition of the two human isoforms shows that the TOPRIM domain in the etoposide-bound TOP2B cleavage complex (PDB ID 3QX3) is rotated relative to the WHD and tower domain in the TOP2A structure (*left panel*). The TOP2B cleavage complex also has a closed C-gate compared to TOP2A (*right panel*).
b. Structure and ring numbering of etoposide.
c. Only two amino acids differ in the etoposide-binding pocket of TOP2A and TOP2B. The WHD and TOPRIM of TOP2A are shown individually superposed on the TOP2B drug-binding site. The residues that differ – Met762 in TOP2A *vs*. Gln778 in TOP2B, and Ser800 *vs*. Ala816 – are labeled. Etoposide is shown as cyan sticks with transparent spheres.
d. The glycosidic moiety off the C4 carbon of etoposide only partially fills a larger, solvent accessible binding pocket. Synthesis of derivatives with additions off the glycosidic methyl group could take advantage of this remaining binding interface. Serine (S800) in TOP2A is substituted by alanine in the TOP2B. The surface representation highlights how this difference could be used to increase drug specificity for TOP2A. The thienyl group of the related anticancer drug teniposide is modeled in magenta.

79
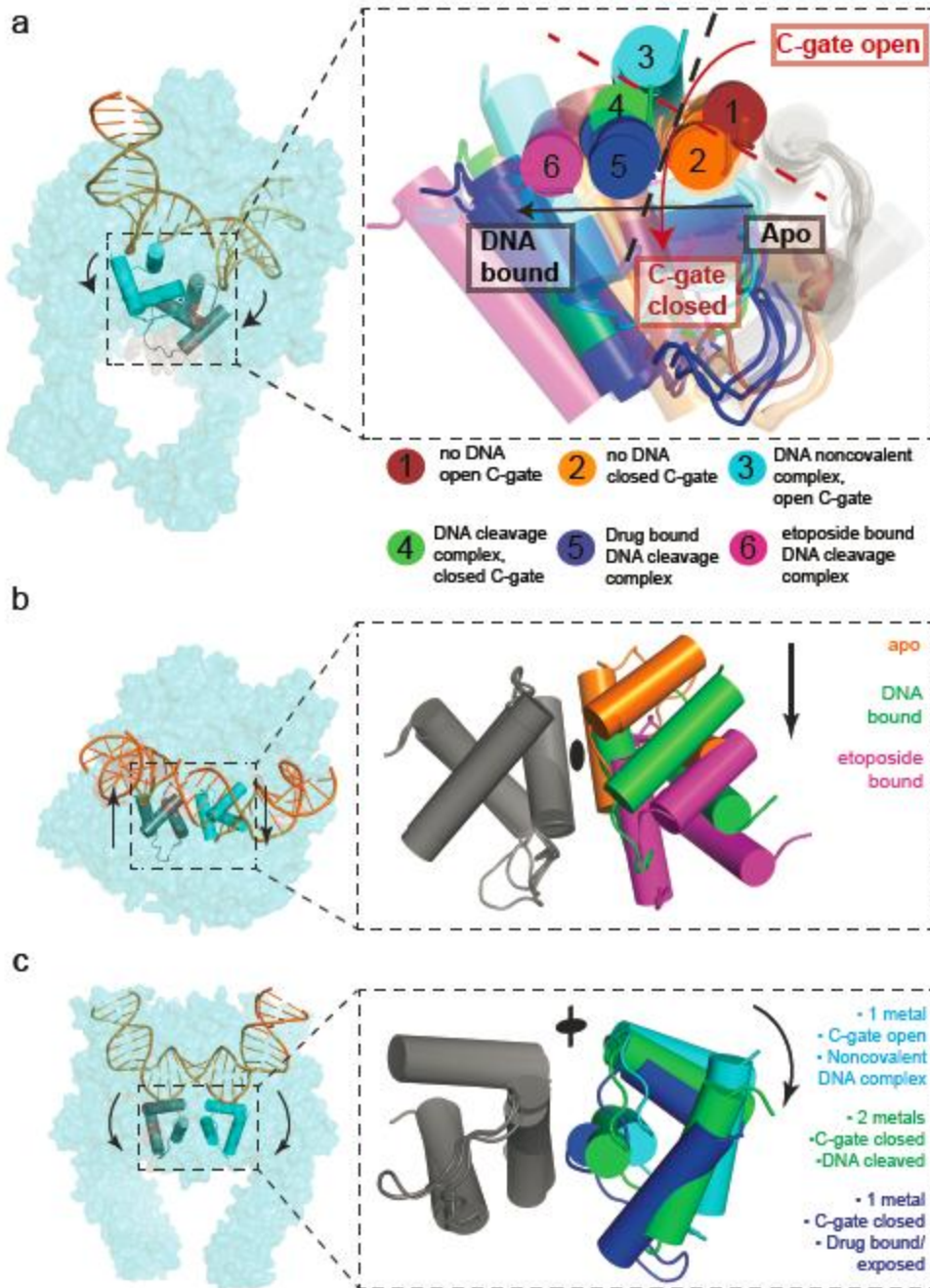
Figure 4.5 – Alignment of topoisomerase IIA structures with respect to the WHD
22 type IIA topoisomerase structures aligned using the WHD in one protomer reveal six juxtapositions taken at the dimer interface. These juxtapositions are best observed in the free WHD, surface representations are provided for orientation:
a. The 22 structures take on just six juxtapositions: 1) no DNA bound, C-gate open (A. baumanni topo IV(2XKJ)); 2) no DNA bound, C-gate closed (E. coli gyrase (3NUH) also: E. coli gyrase(1AB4), M. tuburculosis gyrase (3ILW)); 3) DNA noncovalently bound, C-gate open (human TOP2A, also yeast Top2(2RGR)); 4) DNA cleavage complex, C-gate closed (yeast Top2

cleavage complex (3L4K)); 5) DNA cleavage complex, C-gate closed, initial crystallization with drug bound (A. baumanni topo IV bound to moxifloxacin (2XKK), also: S. pneumoniae topo IV cleavage complex bound to moxifoxacin(3FOF), clinafloxacin(3FOE), levofloxacin(3K9F) a dione inhibitor (3LTN), the dione complex back soaked with EDTA(3KSA) and the EDTA soaked complex resealed by a $MgCl_2$ soak(3KSB), S. aureus gyrase noncovalent complex bound to GSK299943(2XCR, 2XCS) and cleavage complex bound to ciprofloxacin(2XCT)); 6) DNA cleavage complex, C-gate closed, etoposide bound (human TOP2B (3QX3)).

b. Binding of DNA causes the WHDs in opposing protomers to slide past each other by one helical turn along the A'α4 helix. This sliding can be quantized into juxtapositions taken by the apo-enzyme (conformations 1 and 2 in **5a**) and juxtapositions taken by DNA bound enzymes (conformations 3-5 in **5a**). A more extreme lateral shift is seen in the etoposide bound TOP2B complex where the DNA-gate interface has been disrupted (conformation 6 in **5a**).

c. DNA cleavage and C-gate dimerization are correlated to the rotation of the WHD away from the ATP-gate. This rotation is quantized into juxtapositions with an open C-gate and non-covalently bound DNA (conformation 1, 3 in **5a**), a closed C-gate and covalently bound DNA (conformation 2, 4 in **5a**), and a closed C-gate, covalently bound DNA, and drug binding (conformation 5, 6 in **5a**).
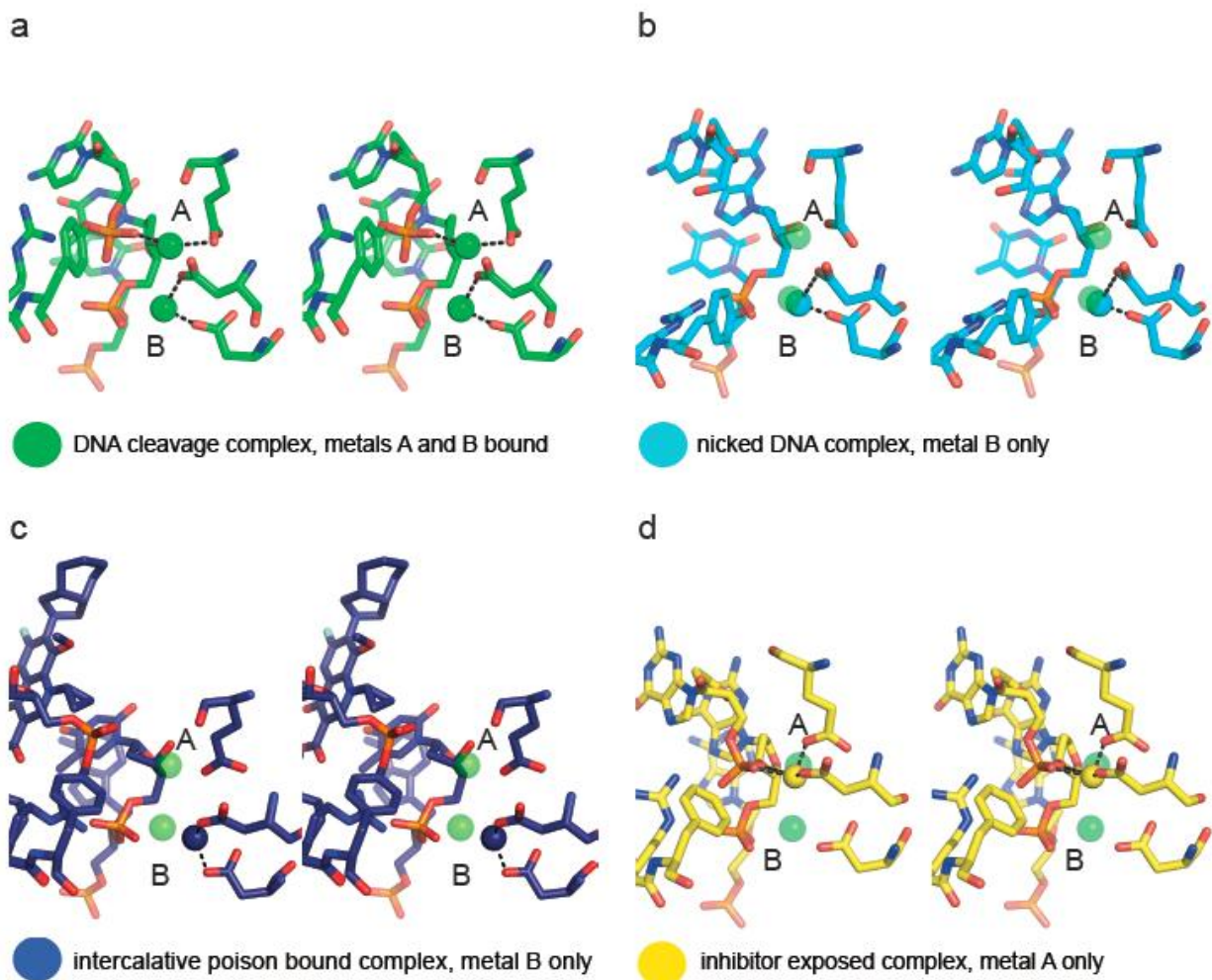
Figure 4.6 – Comparison of metal occupancy between topo II structures

a. The structure of *Sc*Top2 trapped in a cleavage intermediate by a phosphorothiolate suicide substrate has two metals, A and B, bound in the active site.

b. In structures solved with nicked substrates, only metal B is present, as metal A binding requires coordination by the missing scissile phosphate.

c: Structures bound to a topoisomerase II poison bind only metal B, due to poisons shifting the phosphotyrosine required to coordinate metal A out of the active site.

d: In structures bound to a non-intercalative drug (e.g., GSK29994), or where poison has been removed following co-crystallization, only metal A is present. In these structures, residues in the DxD motif do not form appropriate geometry for metal B coordination. This may be due to deformation of the DNA gate retained in these structures.

Chapter 5 – Concluding Remarks

Conclusions

Type IIA topoisomerases are molecular machines that act as Nature's magicians, capable of passing one segment of DNA through another much like the old magic trick of connecting and separating linked rings. To achieve this feat, topoisomerases carry out a complex mechanistic cycle involving four catalytic centers and three dissociable interfaces in which the "trick" relies on the transient cleavage of one DNA segment. In Chapter 2 of this dissertation I present the first crystal structure of a DNA cleavage complex for a type IIA topoisomerase. These results indicate that type IIA topoisomerases, and the related type IA family, catalyze DNA cleavage by a novel variation of the classic two-metal approach to phosphoryl transfer chemistry. Additionally, the structure displays a structural rearrangement revealing how DNA cleavage is coupled with the dimerization of the C-gate interface over 50 Å away. This connection illustrates how an indispensable chromosome-disentangling machine auto-regulates DNA breakage to prevent the aberrant formation of mutagenic and cytotoxic genomic lesions.

The theme of long-range allostery was continued in Chapter 3, where I described the first crystal structure of a fully-catalytic type IIA topoisomerase bound to both DNA and nucleotide. The enzyme adopts a doubly domain-swapped configuration that produces an unexpected interaction between a conformational transducing element in the ATPase domain and the bound DNA. Biochemical studies reveal this contact is critical for both DNA-stimulated ATP hydrolysis and global topoisomerase function. These data indicate that the ATPases pivot about each other to ensure unidirectional movement of DNA through the enzyme and that this "twist-lock" state relies on a nucleic-acid conduit to promote ATP turnover and enzyme reset. These findings illustrate how a large-scale, DNA-remodeling enzyme can systematically couple disparate and spatially segregated functional activities to carry out a physically elaborate event.

In Chapter 4 I describe the first structure of human topo IIα bound to DNA. It further develops the concept, initially introduced in Chapter 2, that the relative configuration of the DNA cleavage active site is coupled with both the opening and closing of the distal C-terminal dimer interface, as well as metal-ion occupancy. This latter point, along with recent biochemical studies(Pitts et al., 2011), helps to address the controversy over metal-ion placement and occupancy by supporting the model that two metal ions may bind at the same time, and one of them is directly catalytic. Additional analysis of the topo IIα structure in light of the etoposide-inhibited state of human topo IIβ(Wu et al., 2011) confirms the close relationship between the two isoforms that fosters inhibitor cross-reactivity, while also highlighting amino acid differences in the drug-binding pocket that could serve as differentiating features for developing more selective anti-topoisomerase agents.

Future Directions

While this dissertation provides a structural framework for understanding type IIA topoisomerase-mediated DNA cleavage, much remains to be learned about how this chemical reaction is corrupted by small-molecule inhibitors. Recent reports from several independent groups have begun to describe in molecular detail the structural basis for inhibition(Bax et al., 2010b; Laponogov et al., 2010; Laponogov et al., 2009; Wohlkonig et al., 2010; Wu et al., 2011). All but one of these reports describe structures of prokaryotic type IIA topoisomerase•DNA complexes bound to antibacterial quinolones, diones, or, in one case, a novel catalytic inhibitor. The one exception describes human topo IIβ bound to etoposide, an agent that belongs to the epipodophyllotoxin class of anticancer therapeutics. Despite these breakthroughs, a thorough understanding of specificity between classes of drugs and families of enzymes remains lacking. For example, nearly all quinolones in clinical use against prokaryotic type IIA topos have limited action against eukaryotic type IIA topos, in particular the two human isoforms. Likewise, certain anticancer compounds targeting the human topos (e.g., vosaroxin) are not effective as antibiotics. This is surprising, given the high degree of conservation at the active sites across all topoisomerases. One way to shed light on this mystery is to take advantage of one of the few quinolones that works as an anticancer agent. I possess several grams of one such agent, vosaroxin, which is currently in Phase 3 clinical trials for treatment of acute myeloid leukemia. A structure of a topo II•DNA•vosaroxin complex and subsequent comparative analyses may reveal the molecular basis by which most quinolones – but not vosaroxin – are effective against prokaryotic topoisomerases without targeting human topo II isoforms. Understanding this important medical distinction has direct implications for developing better, targeted therapeutics. Additionally, while the structural events corresponding to gate opening and closing in type IIA topoisomerases are now much better understood, the precise timing and triggers of these and other key events in the mechanistic cycle remain open questions. Structural and biophysical studies will be required to better understand these key events, and, as Chapter 3 indicates, will undoubtedly continue to yield surprises.

Final Remarks

The first topoisomerase was discovered serendipitously at UC Berkeley and reported by Jim Wang in 1971(Wang, 1971). Over 40 years later, the topoisomerase field is still very much alive and filled with important, outstanding questions. The structural biology of topoisomerases has evolved from crystallizing any possible fragment of the protein alone, to capturing ever more sophisticated complexes of the protein bound to DNA, nucleotides, metal ions, and drugs. Many of these complexes have captured the enzyme in different states of its catalytic cycle, giving significant insights into the complex mechanism topoisomerases must carry out with fidelity, and how this fidelity can be corrupted for clinical benefit. This dissertation adds to the large body of knowledge about topoisomerase structure and function by presenting discoveries concerning the control of DNA cleavage and its associated structural movements. New

questions will undoubtedly continue to arise as we learn more about these remarkable molecular machines and how they manage the topological challenges inherent to the double helix.

References

The PyMOL Molecular Graphics System, Version 1.5.0.1 Schrödinger, LLC.

Adams, P.D., Afonine, P.V., Bunkoczi, G., Chen, V.B., Davis, I.W., Echols, N., Headd, J.J., Hung, L.W., Kapral, G.J., Grosse-Kunstleve, R.W*., et al.* (2010). PHENIX: a comprehensive Python-based system for macromolecular structure solution. Acta Crystallogr D Biol Crystallogr *66*, 213-221.

Ali, M.M., Roe, S.M., Vaughan, C.K., Meyer, P., Panaretou, B., Piper, P.W., Prodromou, C., and Pearl, L.H. (2006). Crystal structure of an Hsp90-nucleotide-p23/Sba1 closed chaperone complex. Nature *440*, 1013-1017.

Aravind, L., Leipe, D.D., and Koonin, E.V. (1998). Toprim--a conserved catalytic domain in type IA and II topoisomerases, DnaG-type primases, OLD family nucleases and RecR proteins. Nucleic Acids Res *26*, 4205-4213.

Austin, C.A., and Fisher, L.M. (1990). Isolation and characterization of a human cDNA clone encoding a novel DNA topoisomerase II homologue from HeLa cells. FEBS Lett *266*, 115-117.

Austin, C.A., Sng, J.H., Patel, S., and Fisher, L.M. (1993). Novel HeLa topoisomerase II is the II beta isoform: complete coding sequence and homology with other type II topoisomerases. Biochim Biophys Acta *1172*, 283-291.

Azarova, A.M., Lyu, Y.L., Lin, C.P., Tsai, Y.C., Lau, J.Y., Wang, J.C., and Liu, L.F. (2007). Roles of DNA topoisomerase II isozymes in chemotherapy and secondary malignancies. Proc Natl Acad Sci U S A *104*, 11014-11019.

Baird, C.L., Harkins, T.T., Morris, S.K., and Lindsley, J.E. (1999). Topoisomerase II drives DNA transport by hydrolyzing one ATP. Proc Natl Acad Sci U S A *96*, 13685-13690.

Bandele, O.J., and Osheroff, N. (2008). The efficacy of topoisomerase II-targeted anticancer agents reflects the persistence of drug-induced cleavage complexes in cells. Biochemistry *47*, 11900-11908.

Bates, A.D., Berger, J.M., and Maxwell, A. (2011). The ancestral role of ATP hydrolysis in type II topoisomerases: prevention of DNA double-strand breaks. Nucleic Acids Res *39*, 6327-6339.

Bax, B.D., Chan, P.F., Eggleston, D.S., Fosberry, A., Gentry, D.R., Gorrec, F., Giordano, I., Hann, M.M., Hennessy, A., Hibbs, M*., et al.* (2010a). Type IIA topoisomerase inhibition by a new class of antibacterial agents. Nature, 1-9.

Bax, B.D., Chan, P.F., Eggleston, D.S., Fosberry, A., Gentry, D.R., Gorrec, F., Giordano, I., Hann, M.M., Hennessy, A., Hibbs, M*., et al.* (2010b). Type IIA topoisomerase inhibition by a new class of antibacterial agents. Nature *466*, 935-940.

Bender, R.P., Jablonksy, M.J., Shadid, M., Romaine, I., Dunlap, N., Anklin, C., Graves, D.E., and Osheroff, N. (2008). Substituents on etoposide that interact with human topoisomerase IIalpha in the binary enzyme-drug complex: contributions to etoposide binding and activity. Biochemistry *47*, 4501-4509.

Berger, J.M., Fass, D., Wang, J.C., and Harrison, S.C. (1998). Structural similarities between topoisomerases that cleave one or both DNA strands. Proc Natl Acad Sci U S A *95*, 7876-7881.

Berger, J.M., Gamblin, S.J., Harrison, S.C., and Wang, J.C. (1996). Structure and mechanism of DNA topoisomerase II. Nature *379*, 225-232.

Bernard, P., and Couturier, M. (1992). Cell killing by the F plasmid CcdB protein involves poisoning of DNA-topoisomerase II complexes. J Mol Biol *226*, 735-745.

Bigioni, M., Zunino, F., Tinelli, S., Austin, C.A., Willmore, E., and Capranico, G. (1996). Position-specific effects of base mismatch on mammalian topoisomerase II DNA cleaving activity. Biochemistry *35*, 153-159.

Bjergbaek, L., Kingma, P., Nielsen, I.S., Wang, Y., Westergaard, O., Osheroff, N., and Andersen, A.H. (2000). Communication between the ATPase and cleavage/religation domains of human topoisomerase IIalpha. J Biol Chem *275*, 13041-13048.

Brino, L., Urzhumtsev, A., Mousli, M., Bronner, C., Mitschler, A., Oudet, P., and Moras, D. (2000). Dimerization of Escherichia coli DNA-gyrase B provides a structural mechanism for activating the ATPase catalytic center. J Biol Chem *275*, 9468-9475.

Brown, P.O., Peebles, C.L., and Cozzarelli, N.R. (1979). A topoisomerase from Escherichia coli related to DNA gyrase. Proc Natl Acad Sci U S A *76*, 6110-6114.

Burgin, A.B., Jr., Huizenga, B.N., and Nash, H.A. (1995). A novel suicide substrate for DNA topoisomerases and site-specific recombinases. Nucleic Acids Res *23*, 2973-2979.

Capranico, G., Tinelli, S., Austin, C.A., Fisher, M.L., and Zunino, F. (1992). Different patterns of gene expression of topoisomerase II isoforms in differentiated tissues during murine development. Biochim Biophys Acta *1132*, 43-48.

Cardenas, M.E., Dang, Q., Glover, C.V., and Gasser, S.M. (1992). Casein kinase II phosphorylates the eukaryote-specific C-terminal domain of topoisomerase II in vivo. EMBO J *11*, 1785-1796.

Caron, P.R., Watt, P., and Wang, J.C. (1994). The C-terminal domain of Saccharomyces cerevisiae DNA topoisomerase II. Mol Cell Biol *14*, 3197-3207.

Changela, A., DiGate, R.J., and Mondragon, A. (2001). Crystal structure of a complex of a type IA DNA topoisomerase with a single-stranded DNA molecule. Nature *411*, 1077-1081.

Charvin, G., Strick, T.R., Bensimon, D., and Croquette, V. (2005). Topoisomerase IV bends and overtwists DNA upon binding. Biophys J *89*, 384-392.

Chen, V.B., Arendall, W.B., 3rd, Headd, J.J., Keedy, D.A., Immormino, R.M., Kapral, G.J., Murray, L.W., Richardson, J.S., and Richardson, D.C. (2010). MolProbity: all-atom structure validation for macromolecular crystallography. Acta Crystallogr D Biol Crystallogr *66*, 12-21.

Chen, X., Vinkemeier, U., Zhao, Y., Jeruzalmi, D., Darnell, J.E., Jr., and Kuriyan, J. (1998). Crystal structure of a tyrosine phosphorylated STAT-1 dimer bound to DNA. Cell *93*, 827-839.

Cheng, B., Annamalai, T., Sorokin, E., Abrenica, M., Aedo, S., and Tse-Dinh, Y.C. (2009). Asp-to-Asn substitution at the first position of the DxD TOPRIM motif of recombinant bacterial topoisomerase I is extremely lethal to E. coli. J Mol Biol *385*, 558-567.

Choudhary, C., Kumar, C., Gnad, F., Nielsen, M.L., Rehman, M., Walther, T.C., Olsen, J.V., and Mann, M. (2009). Lysine acetylation targets protein complexes and co-regulates major cellular functions. Science *325*, 834-840.

Chung, T.D., Drake, F.H., Tan, K.B., Per, S.R., Crooke, S.T., and Mirabelli, C.K. (1989). Characterization and immunological identification of cDNA clones encoding two human DNA topoisomerase II isozymes. Proc Natl Acad Sci U S A *86*, 9431-9435.

Classen, S., Olland, S., and Berger, J.M. (2003). Structure of the topoisomerase II ATPase region and its mechanism of inhibition by the chemotherapeutic agent ICRF-187. Proc Natl Acad Sci U S A *100*, 10629-10634.

Corbett, K.D., and Berger, J.M. (2006). Structural basis for topoisomerase VI inhibition by the anti-Hsp90 drug radicicol. Nucleic Acids Res *34*, 4269-4277.

Corbett, K.D., Schoeffler, A.J., Thomsen, N.D., and Berger, J.M. (2005). The structural basis for substrate specificity in DNA topoisomerase IV. J Mol Biol *351*, 545-561.

Cortes Ledesma, F., El Khamisy, S.F., Zuma, M.C., Osborn, K., and Caldecott, K.W. (2009). A human 5'-tyrosyl DNA phosphodiesterase that repairs topoisomerase-mediated DNA damage. Nature *461*, 674-678.

Cowell, I.G., Sondka, Z., Smith, K., Lee, K.C., Manville, C.M., Sidorczuk-Lesthuruge, M., Rance, H.A., Padget, K., Jackson, G.H., Adachi, N*., et al.* Model for MLL translocations in therapy-related leukemia involving topoisomerase IIbeta-mediated DNA strand breaks and gene proximity. Proc Natl Acad Sci U S A *109*, 8989-8994.

Dedon, P.C., and Borch, R.F. (1987). Characterization of the reactions of platinum antitumor agents with biologic and nonbiologic sulfur-containing nucleophiles. Biochem Pharmacol *36*, 1955-1964.

Deweese, J.E., Burgin, A.B., and Osheroff, N. (2008). Using 3'-bridging phosphorothiolates to isolate the forward DNA cleavage reaction of human topoisomerase IIalpha. Biochemistry *47*, 4129-4140.

Deweese, J.E., Guengerich, F.P., Burgin, A.B., and Osheroff, N. (2009). Metal ion interactions in the DNA cleavage/ligation active site of human topoisomerase IIalpha. Biochemistry *48*, 8940-8947.

Dingemans, A.M., Pinedo, H.M., and Giaccone, G. (1998). Clinical resistance to topoisomerase-targeted drugs. Biochim Biophys Acta *1400*, 275-288.

Domanico, P.L., and Tse-Dinh, Y.C. (1991). Mechanistic studies on E. coli DNA topoisomerase I: divalent ion effects. J Inorg Biochem *42*, 87-96.

Dong, K.C., and Berger, J.M. (2007). Structural basis for gate-DNA recognition and bending by type IIA topoisomerases. Nature *450*, 1201-1205.

Drake, F.H., Hofmann, G.A., Bartus, H.F., Mattern, M.R., Crooke, S.T., and Mirabelli, C.K. (1989). Biochemical and pharmacological properties of p170 and p180 forms of topoisomerase II. Biochemistry *28*, 8154-8160.

Dutta, R., and Inouye, M. (2000). GHKL, an emergent ATPase/kinase superfamily. Trends Biochem Sci *25*, 24-28.

Edwards, M.J., Flatman, R.H., Mitchenall, L.A., Stevenson, C.E., Le, T.B., Clarke, T.A., McKay, A.R., Fiedler, H.P., Buttner, M.J., Lawson, D.M.*, et al*. (2009). A crystal structure of the bifunctional antibiotic simocyclinone D8, bound to DNA gyrase. Science *326*, 1415-1418.

Elsea, S.H., Osheroff, N., and Nitiss, J.L. (1992). Cytotoxicity of quinolones toward eukaryotic cells. Identification of topoisomerase II as the primary cellular target for the quinolone CP-115,953 in yeast. J Biol Chem *267*, 13150-13153.

Emsley, P., Lohkamp, B., Scott, W.G., and Cowtan, K. (2010). Features and development of Coot. Acta Crystallogr D Biol Crystallogr *66*, 486-501.

Fass, D., Bogden, C.E., and Berger, J.M. (1999). Quaternary changes in topoisomerase II may direct orthogonal movement of two DNA strands. Nat Struct Biol *6*, 322-326.

Felix, C.A. (1998). Secondary leukemias induced by topoisomerase-targeted drugs. Biochim Biophys Acta *1400*, 233-255.

Felix, C.A. (2001). Leukemias related to treatment with DNA topoisomerase II inhibitors. Med Pediatr Oncol *36*, 525-535.

Forterre, P., Gribaldo, S., Gadelle, D., and Serre, M.C. (2007). Origin and evolution of DNA topoisomerases. Biochimie *89*, 427-446.

Fry, A.M., Chresta, C.M., Davies, S.M., Walker, M.C., Harris, A.L., Hartley, J.A., Masters, J.R., and Hickson, I.D. (1991). Relationship between topoisomerase II level and chemosensitivity in human tumor cell lines. Cancer Res *51*, 6592-6595.

Gellert, M., Fisher, L.M., and O'Dea, M.H. (1979). DNA gyrase: purification and catalytic properties of a fragment of gyrase B protein. Proc Natl Acad Sci U S A *76*, 6289-6293.

Gellert, M., Mizuuchi, K., O'Dea, M.H., and Nash, H.A. (1976). DNA gyrase: an enzyme that introduces superhelical turns into DNA. Proc Natl Acad Sci U S A *73*, 3872-3876.

Gentry, A.C., Pitts, S.L., Jablonsky, M.J., Bailly, C., Graves, D.E., and Osheroff, N. (2011). Interactions between the etoposide derivative F14512 and human type II topoisomerases: implications for the C4 spermine moiety in promoting enzyme-mediated DNA cleavage. Biochemistry *50*, 3240-3249.

Goto, T., Laipis, P., and Wang, J.C. (1984). The purification and characterization of DNA topoisomerases I and II of the yeast Saccharomyces cerevisiae. J Biol Chem *259*, 10422-10429.

Goto, T., and Wang, J.C. (1982). Yeast DNA topoisomerase II. An ATP-dependent type II topoisomerase that catalyzes the catenation, decatenation, unknotting, and relaxation of double-stranded DNA rings. J Biol Chem *257*, 5866-5872.

Gottler, T., and Klostermeier, D. (2007). Dissection of the nucleotide cycle of B. subtilis DNA gyrase and its modulation by DNA. J Mol Biol *367*, 1392-1404.

Grue, P., Grasser, A., Sehested, M., Jensen, P.B., Uhse, A., Straub, T., Ness, W., and Boege, F. (1998). Essential mitotic functions of DNA topoisomerase IIalpha are not adopted by topoisomerase IIbeta in human H69 cells. J Biol Chem *273*, 33660-33666.

Haffner, M.C., Aryee, M.J., Toubaji, A., Esopi, D.M., Albadine, R., Gurel, B., Isaacs, W.B., Bova, G.S., Liu, W., Xu, J.*, et al.* Androgen-induced TOP2B-mediated double-strand breaks and prostate cancer gene rearrangements. Nat Genet *42*, 668-675.

Hammonds, T.R., and Maxwell, A. (1997). The DNA dependence of the ATPase activity of human DNA topoisomerase IIalpha. J Biol Chem *272*, 32696-32703.

Hardin, A.H., Sarkar, S.K., Seol, Y., Liou, G.F., Osheroff, N., and Neuman, K.C. (2011). Direct measurement of DNA bending by type IIA topoisomerases: implications for non-equilibrium topology simplification. Nucleic Acids Res *39*, 5729-5743.

Harkins, T.T., Lewis, T.J., and Lindsley, J.E. (1998). Pre-steady-state analysis of ATP hydrolysis by Saccharomyces cerevisiae DNA topoisomerase II. 2. Kinetic mechanism for the sequential hydrolysis of two ATP. Biochemistry *37*, 7299-7312.

Hegde, S., Vetting, M., Roderick, S., Mitchenall, L., Maxwell, A., Takiff, H., and Blanchard, J. (2005). A fluoroquinolone resistance protein from Mycobacterium tuberculosis that mimics DNA. Science *308*, 1480.

Hoch, U., Lynch, J., Sato, Y., Kashimoto, S., Kajikawa, F., Furutani, Y., and Silverman, J.A. (2009). Voreloxin, formerly SNS-595, has potent activity against a broad panel of cancer cell lines and in vivo tumor models. Cancer Chemother Pharmacol *64*, 53-65.

Ju, B.G., Lunyak, V.V., Perissi, V., Garcia-Bassets, I., Rose, D.W., Glass, C.K., and Rosenfeld, M.G. (2006). A topoisomerase IIbeta-mediated dsDNA break required for regulated transcription. Science *312*, 1798-1802.

Kampranis, S.C., Bates, A.D., and Maxwell, A. (1999). A model for the mechanism of strand passage by DNA gyrase. Proc Natl Acad Sci U S A *96*, 8414-8419.

Kasahara, K., Fujiwara, Y., Sugimoto, Y., Nishio, K., Tamura, T., Matsuda, T., and Saijo, N. (1992). Determinants of response to the DNA topoisomerase II inhibitors doxorubicin and etoposide in human lung cancer cell lines. J Natl Cancer Inst *84*, 113-118.

Lamour, V., Hoermann, L., Jeltsch, J.M., Oudet, P., and Moras, D. (2002). An open conformation of the Thermus thermophilus gyrase B ATP-binding domain. J Biol Chem *277*, 18947-18953.

Laponogov, I., Pan, X.S., Veselkov, D.A., McAuley, K.E., Fisher, L.M., and Sanderson, M.R. (2010). Structural basis of gate-DNA breakage and resealing by type II topoisomerases. PLoS One *5*, e11338.

Laponogov, I., Sohi, M.K., Veselkov, D.A., Pan, X.S., Sawhney, R., Thompson, A.W., McAuley, K.E., Fisher, L.M., and Sanderson, M.R. (2009). Structural insight into the quinolone-DNA cleavage complex of type IIA topoisomerases. Nat Struct Mol Biol *16*, 667-669.

Laponogov, I., Veselkov, D.A., Sohi, M.K., Pan, X.S., Achari, A., Yang, C., Ferrara, J.D., Fisher, L.M., and Sanderson, M.R. (2007). Breakage-reunion domain of Streptococcus pneumoniae topoisomerase IV: crystal structure of a gram-positive quinolone target. PLoS One *2*, e301.

Lee, S., Jung, S.R., Heo, K., Byl, J.A., Deweese, J.E., Osheroff, N., and Hohng, S. (2012). DNA cleavage and opening reactions of human topoisomerase IIalpha are regulated via Mg2+-mediated dynamic bending of gate-DNA. Proc Natl Acad Sci U S A *109*, 2925-2930.

Lewis, R.J., Singh, O.M., Smith, C.V., Skarzynski, T., Maxwell, A., Wonacott, A.J., and Wigley, D.B. (1996). The nature of inhibition of DNA gyrase by the coumarins and the cyclothialidines revealed by X-ray crystallography. EMBO J *15*, 1412-1420.

Li, W., and Wang, J.C. (1997). Footprinting of yeast DNA topoisomerase II lysyl side chains involved in substrate binding and interdomainal interactions. J Biol Chem *272*, 31190-31195.

Lindsley, J.E. (2001). Use of a real-time, coupled assay to measure the ATPase activity of DNA topoisomerase II. Methods Mol Biol *95*, 57-64.

Lindsley, J.E., and Wang, J.C. (1993a). On the coupling between ATP usage and DNA transport by yeast DNA topoisomerase II. J Biol Chem *268*, 8096-8104.

Lindsley, J.E., and Wang, J.C. (1993b). Study of allosteric communication between protomers by immunotagging. Nature *361*, 749-750.

Liu, L.F., Liu, C.C., and Alberts, B.M. (1980). Type II DNA topoisomerases: enzymes that can unknot a topologically knotted DNA molecule via a reversible double-strand break. Cell *19*, 697-707.

Liu, Q., and Wang, J.C. (1998). Identification of active site residues in the "GyrA" half of yeast DNA topoisomerase II. J Biol Chem *273*, 20252-20260.

Lyu, Y.L., Kerrigan, J.E., Lin, C.P., Azarova, A.M., Tsai, Y.C., Ban, Y., and Liu, L.F. (2007). Topoisomerase IIbeta mediated DNA double-strand breaks: implications in doxorubicin cardiotoxicity and prevention by dexrazoxane. Cancer Res *67*, 8839-8846.

Lyu, Y.L., and Wang, J.C. (2003). Aberrant lamination in the cerebral cortex of mouse embryos lacking DNA topoisomerase IIbeta. Proc Natl Acad Sci U S A *100*, 7123-7128.

MacDowell, A.A., Celestre, R.S., Howells, M., McKinney, W., Krupnick, J., Cambie, D., Domning, E.E., Duarte, R.M., Kelez, N., Plate, D.W.*, et al.* (2004). Suite of three protein crystallography beamlines with single superconducting bend magnet as the source. J Synchrotron Radiat *11*, 447-455.

Marini, J.C., Miller, K.G., and Englund, P.T. (1980). Decatenation of kinetoplast DNA by topoisomerases. J Biol Chem *255*, 4976-4979.

Maxwell, A., and Gellert, M. (1984). The DNA dependence of the ATPase activity of DNA gyrase. J Biol Chem *259*, 14472-14480.

McClendon, A.K., Gentry, A.C., Dickey, J.S., Brinch, M., Bendsen, S., Andersen, A.H., and Osheroff, N. (2008). Bimodal recognition of DNA geometry by human topoisomerase II alpha: preferential relaxation of positively supercoiled DNA requires elements in the C-terminal domain. Biochemistry *47*, 13169-13178.

McCoy, A.J., Grosse-Kunstleve, R.W., Adams, P.D., Winn, M.D., Storoni, L.C., and Read, R.J. (2007). Phaser crystallographic software. J Appl Crystallogr *40*, 658-674.

McNamara, S., Wang, H., Hanna, N., and Miller, W.H., Jr. (2008). Topoisomerase IIbeta negatively modulates retinoic acid receptor alpha function: a novel mechanism of retinoic acid resistance. Mol Cell Biol *28*, 2066-2077.

Mizuuchi, K., Fisher, L.M., O'Dea, M.H., and Gellert, M. (1980). DNA gyrase action involves the introduction of transient double-strand breaks into DNA. Proc Natl Acad Sci USA *77*, 1847-1851.

Mizuuchi, K., O'Dea, M.H., and Gellert, M. (1978). DNA gyrase: subunit structure and ATPase activity of the purified enzyme. Proc Natl Acad Sci U S A *75*, 5960-5963.

Morais Cabral, J.H., Jackson, A.P., Smith, C.V., Shikotra, N., Maxwell, A., and Liddington, R.C. (1997). Crystal structure of the breakage-reunion domain of DNA gyrase. Nature *388*, 903-906.

Mueller-Planitz, F., and Herschlag, D. (2007). DNA topoisomerase II selects DNA cleavage sites based on reactivity rather than binding affinity. Nucleic Acids Res *35*, 3764-3773.

Nichols, M.D., DeAngelis, K., Keck, J.L., and Berger, J.M. (1999). Structure and function of an archaeal topoisomerase VI subunit with homology to the meiotic recombination factor Spo11. EMBO J *18*, 6177-6188.

Niimi, A., Suka, N., Harata, M., Kikuchi, A., and Mizuno, S. (2001). Co-localization of chicken DNA topoisomerase IIalpha, but not beta, with sites of DNA replication and possible involvement of a C-terminal region of alpha through its binding to PCNA. Chromosoma *110*, 102-114.

Nitiss, K.C., Malik, M., He, X., White, S.W., and Nitiss, J.L. (2006). Tyrosyl-DNA phosphodiesterase (Tdp1) participates in the repair of Top2-mediated DNA damage. Proc Natl Acad Sci U S A *103*, 8953-8958.

Noble, C.G., and Maxwell, A. (2002). The role of GyrB in the DNA cleavage-religation reaction of DNA gyrase: a proposed two metal-ion mechanism. J Mol Biol *318*, 361-371.

Nowotny, M., Gaidamakov, S.A., Crouch, R.J., and Yang, W. (2005). Crystal structures of RNase H bound to an RNA/DNA hybrid: substrate specificity and metal-dependent catalysis. Cell *121*, 1005-1016.

Nowotny, M., and Yang, W. (2006). Stepwise analyses of metal ions in RNase H catalysis from substrate destabilization to product release. EMBO J *25*, 1924-1933.

Okada, Y., Ito, Y., Kikuchi, A., Nimura, Y., Yoshida, S., and Suzuki, M. (2000). Assignment of functional amino acids around the active site of human DNA topoisomerase IIalpha. J Biol Chem *275*, 24630-24638.

Osheroff, N. (1986). Eukaryotic topoisomerase II. Characterization of enzyme turnover. J Biol Chem *261*, 9944-9950.

Osheroff, N., Shelton, E.R., and Brutlag, D.L. (1983). DNA topoisomerase II from Drosophila melanogaster. Relaxation of supercoiled DNA. J Biol Chem *258*, 9536-9543.

Osheroff, N., and Zechiedrich, E.L. (1987). Calcium-promoted DNA cleavage by eukaryotic topoisomerase II: trapping the covalent enzyme-DNA complex in an active form. Biochemistry *26*, 4303-4309.

Otwinowski, Z., and Minor, W. (1997). Processing of X-ray diffraction data collected in oscillation mode. Methods Enzymol *276*, 307-326.

Pedersen-Bjergaard, J., Andersen, M.K., Christiansen, D.H., and Nerlov, C. (2002). Genetic pathways in therapy-related myelodysplasia and acute myeloid leukemia. Blood *99*, 1909-1912.

Perillo, B., Ombra, M.N., Bertoni, A., Cuozzo, C., Sacchetti, S., Sasso, A., Chiariotti, L., Malorni, A., Abbondanza, C., and Avvedimento, E.V. (2008). DNA oxidation as triggered by H3K9me2 demethylation drives estrogen-induced gene expression. Science *319*, 202-206.

Pitts, S.L., Liou, G.F., Mitchenall, L.A., Burgin, A.B., Maxwell, A., Neuman, K.C., and Osheroff, N. (2011). Use of divalent metal ions in the DNA cleavage reaction of topoisomerase IV. Nucleic Acids Res *39*, 4808-4817.

Pouliot, J.J., Yao, K.C., Robertson, C.A., and Nash, H.A. (1999). Yeast gene for a Tyr-DNA phosphodiesterase that repairs topoisomerase I complexes. Science *286*, 552-555.

Redinbo, M.R., Stewart, L., Kuhn, P., Champoux, J.J., and Hol, W.G. (1998). Crystal structures of human topoisomerase I in covalent and noncovalent complexes with DNA. Science *279*, 1504-1513.

Roca, J. (2004). The path of the DNA along the dimer interface of topoisomerase II. J Biol Chem *279*, 25783-25788.

Roca, J., Berger, J.M., Harrison, S.C., and Wang, J.C. (1996). DNA transport by a type II topoisomerase: direct evidence for a two-gate mechanism. Proc Natl Acad Sci U S A *93*, 4057-4062.

Roca, J., and Wang, J.C. (1992). The capture of a DNA double helix by an ATP-dependent protein clamp: a key step in DNA transport by type II DNA topoisomerases. Cell *71*, 833-840.

Roca, J., and Wang, J.C. (1994). DNA transport by a type II DNA topoisomerase: evidence in favor of a two-gate mechanism. Cell *77*, 609-616.

Sabbagh, G., Fettes, K.J., Gosain, R., O'Neil, I.A., and Cosstick, R. (2004). Synthesis of phosphorothioamidites derived from 3'-thio-3'-deoxythymidine and 3'-thio-2',3'-dideoxycytidine and the automated synthesis of oligodeoxynucleotides containing a 3'-S-phosphorothiolate linkage. Nucleic Acids Res *32*, 495-501.

Schmidt, B.H., Burgin, A.B., Deweese, J.E., Osheroff, N., and Berger, J.M. (2010). A novel and unified two-metal mechanism for DNA cleavage by type II and IA topoisomerases. Nature *465*, 641-644.

Schoeffler, A.J., and Berger, J.M. (2008). DNA topoisomerases: harnessing and constraining energy to govern chromosome topology. Q Rev Biophys *41*, 41-101.

Schoeffler, A.J., May, A.P., and Berger, J.M. (2010). A domain insertion in Escherichia coli GyrB adopts a novel fold that plays a critical role in gyrase function. Nucleic Acids Res *38*, 7830-7844.

Schultz, P., Olland, S., Oudet, P., and Hancock, R. (1996). Structure and conformational changes of DNA topoisomerase II visualized by electron microscopy. Proc Natl Acad Sci U S A *93*, 5936-5940.

Shiozaki, K., and Yanagida, M. (1992). Functional dissection of the phosphorylated termini of fission yeast DNA topoisomerase II. J Cell Biol *119*, 1023-1036.

Simpson, L., and Da Silva, A. (1971). Isolation and characterization of kinetoplast DNA from Leishmania tarentolae. J Mol Biol *56*, 443-473.

Skouboe, C., Bjergbaek, L., Oestergaard, V.H., Larsen, M.K., Knudsen, B.R., and Andersen, A.H. (2003). A human topoisomerase II alpha heterodimer with only one ATP binding site can go through successive catalytic cycles. J Biol Chem *278*, 5768-5774.

Smith, A.B., and Maxwell, A. (2006). A strand-passage conformation of DNA gyrase is required to allow the bacterial toxin, CcdB, to access its binding site. Nucleic Acids Res *34*, 4667-4676.

Staker, B.L., Hjerrild, K., Feese, M.D., Behnke, C.A., Burgin, A.B., Jr., and Stewart, L. (2002). The mechanism of topoisomerase I poisoning by a camptothecin analog. Proc Natl Acad Sci U S A *99*, 15387-15392.

Steitz, T.A., and Steitz, J.A. (1993). A general two-metal-ion mechanism for catalytic RNA. Proc Natl Acad Sci U S A *90*, 6498-6502.

Strahs, D., Zhu, C.X., Cheng, B., Chen, J., and Tse-Dinh, Y.C. (2006). Experimental and computational investigations of Ser10 and Lys13 in the binding and cleavage of DNA substrates by Escherichia coli DNA topoisomerase I. Nucleic Acids Res *34*, 1785-1797.

Tamura, J.K., and Gellert, M. (1990). Characterization of the ATP binding site on Escherichia coli DNA gyrase. Affinity labeling of Lys-103 and Lys-110 of the B subunit by pyridoxal 5'-diphospho-5'-adenosine. J Biol Chem *265*, 21342-21349.

Tingey, A.P., and Maxwell, A. (1996). Probing the role of the ATP-operated clamp in the strand-passage reaction of DNA gyrase. Nucleic Acids Res *24*, 4868-4873.

Toyoda, E., Kagaya, S., Cowell, I.G., Kurosawa, A., Kamoshita, K., Nishikawa, K., Iiizumi, S., Koyama, H., Austin, C.A., and Adachi, N. (2008). NK314, a topoisomerase II inhibitor that specifically targets the alpha isoform. J Biol Chem *283*, 23711-23720.

Tretter, E.M., Schoeffler, A.J., Weisfield, S.R., and Berger, J.M. (2010). Crystal structure of the DNA gyrase GyrA N-terminal domain from Mycobacterium tuberculosis. Proteins *78*, 492-495.

Tropea, J.E., Cherry, S., and Waugh, D.S. (2009). Expression and purification of soluble His(6)-tagged TEV protease. Methods Mol Biol *498*, 297-307.

Tsai-Pflugfelder, M., Liu, L.F., Liu, A.A., Tewey, K.M., Whang-Peng, J., Knutsen, T., Huebner, K., Croce, C.M., and Wang, J.C. (1988). Cloning and sequencing of cDNA encoding human DNA topoisomerase II and localization of the gene to chromosome region 17q21-22. Proc Natl Acad Sci U S A *85*, 7177-7181.

Tsai, F.T., Singh, O.M., Skarzynski, T., Wonacott, A.J., Weston, S., Tucker, A., Pauptit, R.A., Breeze, A.L., Poyser, J.P., O'Brien, R., *et al.* (1997). The high-resolution crystal structure of a 24-kDa gyrase B fragment from E. coli complexed with one of the most potent coumarin inhibitors, clorobiocin. Proteins *28*, 41-52.

Tse, Y.C., Kirkegaard, K., and Wang, J.C. (1980). Covalent bonds between protein and DNA. Formation of phosphotyrosine linkage between certain DNA topoisomerases and DNA. J Biol Chem *255*, 5560-5565.

Tsutsui, K., Okada, S., Watanabe, M., Shohmori, T., Seki, S., and Inoue, Y. (1993). Molecular cloning of partial cDNAs for rat DNA topoisomerase II isoforms and their differential expression in brain development. J Biol Chem *268*, 19076-19083.

Tsutsui, K., Sano, K., Kikuchi, A., and Tokunaga, A. (2001). Involvement of DNA topoisomerase IIbeta in neuronal differentiation. J Biol Chem *276*, 5769-5778.

Viadiu, H., and Aggarwal, A.K. (1998). The role of metals in catalysis by the restriction endonuclease BamHI. Nat Struct Biol *5*, 910-916.

Vizán, J., Hernández-Chico, C., del Castillo, I., and Moreno, F. (1991). The peptide antibiotic microcin B17 induces double-strand cleavage of DNA mediated by E. coli DNA gyrase. EMBO J *10*, 467.

Wang, J., Yu, P., Lin, T.C., Konigsberg, W.H., and Steitz, T.A. (1996). Crystal structures of an NH2-terminal fragment of T4 DNA polymerase and its complexes with single-stranded DNA and with divalent metal ions. Biochemistry *35*, 8110-8119.

Wang, J.C. (1971). Interaction between DNA and an Escherichia coli protein omega. J Mol Biol *55*, 523-533.

Wei, H., Ruthenburg, A.J., Bechis, S.K., and Verdine, G.L. (2005). Nucleotide-dependent domain movement in the ATPase domain of a human type IIA DNA topoisomerase. J Biol Chem *280*, 37041-37047.

West, K.L., Meczes, E.L., Thorn, R., Turnbull, R.M., Marshall, R., and Austin, C.A. (2000). Mutagenesis of E477 or K505 in the B' domain of human topoisomerase II beta increases the requirement for magnesium ions during strand passage. Biochemistry *39*, 1223-1233.

West, K.L., Turnbull, R.M., Willmore, E., Lakey, J.H., and Austin, C.A. (2002). Characterisation of the DNA-dependent ATPase activity of human DNA topoisomerase IIbeta: mutation of Ser165 in the ATPase domain reduces the ATPase activity and abolishes the in vivo complementation ability. Nucleic Acids Res *30*, 5416-5424.

Wigley, D.B., Davies, G.J., Dodson, E.J., Maxwell, A., and Dodson, G. (1991). Crystal structure of an N-terminal fragment of the DNA gyrase B protein. Nature *351*, 624-629.

Williams, N.L., and Maxwell, A. (1999a). Locking the DNA gate of DNA gyrase: investigating the effects on DNA cleavage and ATP hydrolysis. Biochemistry *38*, 14157-14164.

Williams, N.L., and Maxwell, A. (1999b). Probing the two-gate mechanism of DNA gyrase using cysteine cross-linking. Biochemistry *38*, 13502-13511.

Willmore, E., Frank, A.J., Padget, K., Tilby, M.J., and Austin, C.A. (1998). Etoposide targets topoisomerase IIalpha and IIbeta in leukemic cells: isoform-specific cleavable complexes visualized and quantified in situ by a novel immunofluorescence technique. Mol Pharmacol *54*, 78-85.

Wilstermann, A.M., Bender, R.P., Godfrey, M., Choi, S., Anklin, C., Berkowitz, D.B., Osheroff, N., and Graves, D.E. (2007). Topoisomerase II - drug interaction domains: identification of substituents on etoposide that interact with the enzyme. Biochemistry *46*, 8217-8225.

Wohlkonig, A., Chan, P.F., Fosberry, A.P., Homes, P., Huang, J., Kranz, M., Leydon, V.R., Miles, T.J., Pearson, N.D., Perera, R.L., *et al.* (2010). Structural basis of quinolone inhibition of type IIA topoisomerases and target-mediated resistance. Nat Struct Mol Biol *17*, 1152-1153.

Worland, S.T., and Wang, J.C. (1989). Inducible overexpression, purification, and active site mapping of DNA topoisomerase II from the yeast Saccharomyces cerevisiae. J Biol Chem *264*, 4412-4416.

Wu, C.C., Li, T.K., Farh, L., Lin, L.Y., Lin, T.S., Yu, Y.J., Yen, T.J., Chiang, C.W., and Chan, N.L. (2011). Structural basis of type II topoisomerase inhibition by the anticancer drug etoposide. Science *333*, 459-462.

Yang, W. (2008). An equivalent metal ion in one- and two-metal-ion catalysis. Nat Struct Mol Biol *15*, 1228-1231.

Yang, W., Lee, J.Y., and Nowotny, M. (2006). Making and breaking nucleic acids: two-$Mg2+$-ion catalysis and substrate specificity. Mol Cell *22*, 5-13.

Zechiedrich, E.L., Christiansen, K., Andersen, A.H., Westergaard, O., and Osheroff, N. (1989). Double-stranded DNA cleavage/religation reaction of eukaryotic topoisomerase II: evidence for a nicked DNA intermediate. Biochemistry *28*, 6229-6236.

Zeng, Z., Cortes-Ledesma, F., El Khamisy, S.F., and Caldecott, K.W. TDP2/TTRAP is the major 5'-tyrosyl DNA phosphodiesterase activity in vertebrate cells and is critical for cellular resistance to topoisomerase II-induced DNA Damage. J Biol Chem *286*, 403-409.

Appendix

Making competent BCY123 yeast cells

<u>Solutions required</u>:

YPD media (per 1 L):
   10 g yeast extract
   20 g peptone
   20 g dextrose (D-glucose)

sterile 10x TE: 100 mM Tris pH 7.5, 10 mM EDTA
sterile 10x LiOAc: 1 M LiOAc pH 7.5 (pH adjusted with acetic acid)
sterile 50 % PEG-3350

TEL solution (need 15 mL if preparing 200 mL of cells):
   1.5 mL of 10x TE
   1.5 mL 10x LiOAc
   12 mL water

PEG/TEL (make 1 mL per transformation):
   100 μL 10x TE
   100 μL 10x LiOAc
   800 μL of 50 % PEG-3350

<u>Making competent cells</u>:

Innoculate 5 mL of YPD with BCY123 yeast stock. Grow overnight at 180 rpm at 30°C (OD600 should be around 2 in the morning). Innoculate 200 mL of YPD with 2 mL overnight culture and grow 10-12 hours until OD600 = 0.6-1 (Best to start this first thing in the morning). Divide into 4, sterile 50 mL tubes and spin 2500 rpm for 5 min. Remove supernatant and resuspend cells in 20 mL of sterile water. Respin at 2500 rpm for 5 min. Resuspend in 10 mL TEL solution (see above), then spin 5 min. Respuspend in 2 mL TEL solution, with glycerol to 15% final concentration. Aliquot 100 μL cells per 1.5 mL eppendorf tube. Store aliquots at -80°C (no need to quick freeze).

Yeast transformation

Add 10 μL of 10 mg/mL sheared salmon sperm DNA (this should be heated to 95°C and then quickly frozen) and 0.5-1 μg of yeast vector to the 100 μL cells. Add 800 μL of PEG/TEL solution, mix by pipeting up and down. Incubate 30 min at 30°C, no shaking. Heat shock 15 min at 42°C. Spin cells 5 sec on high. Respuspend in 200 μL water and then plate 50 μL on SM+G plates (see below). Place plates in incubator at 30°C (colonies will start to appear in 2

days). Note: the sheared salmon sperm is key to the transformation. I get at least 100 colonies per plate. Competent yeast cells seem to last for years at -80°C.

Expressing and purifying topo II in yeast

Yeast Media:

Synthetic Media (SM) per 1 L:
    5 g ammonium sulfate
    1.7 g yeast nitrogen base (with no ammonium sulfate, Sunrise Science Products)
    0.81 CSM –URA+ADE (Sunrise Science Products)
fill to 950 mL with water and autoclave 45 minutes.
When solution is cool, add 50 mL of a sterile filtered solution of 30% glycerol/40% lactic acid.

SM+G (1L) synthetic media with glucose:
    same as SM, except add 20 g of D-glucose before autoclaving

SM+G plates:
    use SM+G but don't add lactic acid or glycerol
    add 20 g of bacto-agar before autoclaving.

To prepare 6 L of SM media, I prepare 600 mL of 10X solution of ammonium sulfate, YNB, and CSM-URA+ADE and add 100 mL of it into 850 mL water and autoclave.

When solution is cool, I add 50 mL of a 20X sterile filtered solution of 30% glycerol/40% lactic acid (i.e. final concentrations of 1.5% glycerol and 2% lactic acid.)

Protein purification buffers:

Buffer A: Ni loading buffer
        300 mM KCl
        20 mM Tris pH 7.9
        20 mM imidazole pH 8.0
        10% glycerol

Buffer B: bumping from Ni column to HiTrap SP column
        100 mM KCl
        20 mM Tris pH 7.9
        200 mM imidazole pH 8.5
        10 % glycerol

Buffer C: eluting from the SP column
    500 mM KCl
    20 mM Tris 7.9
    10% glycerol

Buffer D: ortho Ni loading
    500 mM KCl
    20 mM Tris 7.9
    20 mM imidazole 8.0
    10% glycerol

Buffer E: ortho Ni bump
    500 mM KCl
    20 mM Tris 7.9
    200 mM imidazole 8.0
    10% glycerol

Buffer F: Gel filtration S300 column
    20 mM Tris 7.9
    500 mM KCl
    10% glycerol

<u>Expression (I usually do 6 L of cells, but I might do as little as 1 L for biochemistry purposes):</u>
Day 1: At ~4:00 PM, I use a pipet tip to scrape cells from a colony and add to 5 mL SM+G media. (Alternatively, I can scrape a visible amount of cells from a -80°C clone glycerol stock.) Shake overnight at 30°C at 180 rpm.
Day 2: At ~4:00 PM, add the 5 mL to 100 mL SM+G and shake overnight as before.
Day 3: At ~4:00 PM, add 10 mL media (OD is roughly 1.8) per 1 L flask, each containing 1 L SM media (**not** SM+G). Shake as before.
Day 4: At about 8:00 AM, the cells are usually at OD = 0.90, which is when I aim to induce. The latest I aim to induce is at OD = 1.0 (and the earliest is 0.80). As such, it's worth getting in earlier the first time you do this to avoid missing the time.
To induce, add 20 g galactose per L and let shake for 6 hours. Spin down cells at 4500 rpm for 15 minutes. Pour off the supernatant, and resuspend the cells by adding 2 mL Buffer A per 1 L cells. Use a pipet to drip the cells, one drop at a time, into a bowl with liquid nitrogen. Collect the cells into two 50 mL conical tubes (using a funnel) and store the cells indefinitely at -80°C.

Purification:

Day 1: In-series Ni^{2+} and cation exchange column

Add 10 mL 100 mM PMSF, 1 mL 1mg/mL leupeptin, and 1 mL 1mg/mL pepstatin per 1 L buffer for buffers A, B, and C. Begin by grinding the cells in a mortar with pestle for 15 minutes while under liquid nitrogen. This requires several refillings of the mortar with liquid nitrogen. The cells should resemble a very fine powder. For a good yield, and with 6 L cells it is worth doing this for the full 15 minutes. Once crushed, add the cells from the mortar to a pre-chilled conical tube or small bottle. I use a funnel to do this, and then wait to allow the liquid nitrogen to evaporate. Then, resuspend crushed yeast pellets in 20 mL Buffer A per L cells (i.e add 120 mL for 6 L prep).

Spin down at 17k rpm, 4°C for 20 minutes. Collect supernatant from spin, and load onto a superloop. Load onto a 5 mL Ni Sepharose high performing column (HisTrap HP, GE) column loaded with 0.2 M NiSO4 and equilibrated into buffer A. Wash the column with at least 100 mL buffer A or until flow-through shows protein has stopped coming off (by UV trace). Put a cation-exchange HS column (GE) in line with the chelating column. Elute protein from the chelating column directly onto the HS column with 50 mL buffer B. (**Note**: sometimes some of the protein elutes at this phase, so this is where I start collecting fractions, but most of the topo should stick to the column. Make sure the SP column is equilibrated in 100 mM KCl and no higher. Some people add an A2 buffer wash step in which buffer A2 is just like A but with 100 mM salt, but I do not do this.) Take the chelating column off line and keep the HS column in line. Elute protein with a 0-100% gradient of buffer A/buffer C over the course of 75 mL and collect fractions. Run on a gel to identify correct fractions, combine and concentrate using Amicon 100 kDa cutoff spin columns until the volume is reduced to ~1 mL or less.

Add His-TEV protease (1:10 ratio TEV to protein, or one full tube from MacroLab) to the sample and let it sit overnight at 4°C.

Day 2: ortho Ni and S300 gel filtration column

Equilibrate a Ni column with buffer D. Load sample onto the Ni column and collect the flow through. The flow-through will contain the topo with the His-tag removed. Identify the fractions to pool and save by either testing 50 μL Coomassie stain with 5 μL of each 1 mL fraction or by UV trace if using an FPLC. (If you wish, you can bump with Buffer E. These fractions should contain some uncleaved His-tagged topo II and the His-tagged TEV protease, but I typically don't collect these fractions and just wash with buffer E straight into waste.) Concentrate the flow through down to ~1 mL. Onto a preequilibrated S300 gel filtration column (buffer F), load the sample and collect fractions. Collect appropriate fractions, run on gel to test purity, and then concentrate using Amicon 100 kDa until the concentration of the protein is ~ 10 mg/mL (again, for me this is mostly for crystallography, and I usually spin it down to under 500 μL). Typical yield is 1-2 mg per L cells.

Clean up of DNA from DNA synthesizer

These protocols are for DNAs that I use in crystallography. For oligos synthesized in-house on our DNA synthesizer, including phosphorothiolated DNA, they must be deprotected and cleaned up. The next two steps address this need. For oligos that are ordered directly from a company, one can skip ahead to the gel-purification step (Day 3).

Day 1: Oligo Deprotection:
Uncap synthesis column and pour the resin into a glass vial. Add 1 mL ammonium hydroxide to the glass vial. Incubate at 55°C overnight.
Day 2: Poly-Pak Purification:
Materials:
 - Glen-Pak DNA purification cartridge (Glen Research)
 - Acetonitrile
 - 2 M triethylamine acetate (TEAA)
 - 2% trifluoroacetic acid (TFA)
 - Ammonium hydroxide (the bottle may not be older than 6 months. Order a new one if it is.)
 - 100 mg/mL NaCl
 - 50% acetonitrile/water (add 50 μL ammonium hydroxide per 10 mL solution to counter TFA and prevent acid-hydrolytic degradation of the DNA)
 - Salt wash solution (5% acetonitrile in 100 mg/mL NaCl (prepare by mixing 5 parts acetonitrile with 95 parts 105.3 mg/mL NaCl)

First add 1 mL 100 mg/mL NaCl solution to the 1 mL deprotected oligo.
Prepare cartridges by first placing onto a vacuum manifold. The pressure should be such that liquid drains noticeably but slowly. Add 0.5 mL acetonitrile, followed by 1 mL TEAA. Apply the oligo/salt mixture to the cartridge (1 mL fits at a time).
Wash the cartridge with 2 x 1mL Salt Wash solution. Then rinse with 2 x 1mL TFA. Then rinse with 2 x 1mL water. Elute with 1 mL 50% acetonitrile with ammonium hydroxide supplement). To do this, I remove the cartridge from the vacuum manifold, then add the 1 mL elution solution, then connect a 3 mL syringe by using a female-female luer. I then pull the plunger out several times to suck the volume through the cartridge and into the syringe. I then transfer the eluent into a 15 mL conical, poke 3 holes into the cap, flash freeze in liquid nitrogen and then immediately place on the lyophilizer overnight.

Day 3: Gel purification:
Materials:
10X TBE (108 g Tris, 55 g Boric Acid, 20 mL 0.5 M EDTA, in 1 L)
Gel elution buffer:
  500 mM Ammonium acetate

10 mM Mg Acetate

1 mM EDTA pH 8.0

Make the 12% acrylamide gels using the following recipe (per gel):

9 mL 40% acrylamide (1:18)

3.75 10X TBE 15 mLs

4.37 mL 100% formamide

15.8 g urea

Heat will be required to get the urea into solution. Then add 0.25 mL APS and 25 μL TEMED and pour gels. If the solution is too warm when you add the APS and TEMED, polymerization will occur so quickly that it will set before you can pour the gels.

Pre-run gels at 300 V for one hour. Dissolve lyophilized oligonucleotides in 0.5 mL formamide and load onto gel. Run the gel for one hour. Remove gels from apparatus and disassemble the glass plates. Place the gel between a sheet of saran wrap (try and make it as flat as possible). Shadow the DNA using a UV lamp and mark using a Sharpie. Cut out the band using a clean razor and then place in a syringe. Crush the gel through the syringe and wash out with 10 mL gel elution buffer into a 50 mL conical. Flash freeze using liquid nitrogen. Let shake overnight at room temperature on a shaker.

Day 4: Reverse phase purification:

Materials:

Sep-Pak Plus C18 Cartridges (Waters)

100% acetylnitrile

30% acetylnitrile, 25 mM triethylammonium bicarbonate (TEAB)

100 mM TEAB

Add 2 mL TEAB to each 10 mL sample that had eluted overnight and use steriflips (Millipore) to separate from the gel matrix. Wash the Sep-Pack column with 10 mL 100% acetylnitrile. Then wash with 10 mL 30% acetylnitrile, 25 mM TEAB. Then wash with 10 mL 100 mM TEAB. Slowly add sample to column, collecting the flow-through, so that you can load it onto the column a second time (at which point the flow-through can be collected in waste). Wash with 30 mL 100 mL TEAB. Elute (slowly) with 30 % acetylnitrile, 25 mM TEAB solution into a 15 mL conical. Poke three holes in the cap, flash freeze in liquid nitrogen, and then immediately put onto the lyophilizer. Lyophilize overnight.

Oligo resuspension and annealing for use in crystallography

Recover samples from the lyophilizer, and resuspend in 100 μL of 10 mM Tris pH 7.9 and 200 mM KCl. Then measure the A_{260} to determine the concentration. Determine the proper volumes

of complementary oligos to mix together to get a 1:1 ratio for the annealed product, and place into a water bath that has been heated to 90°C. Let cool very slowly over the course of several hours, or possibly overnight if you start in the late afternoon. For crystallography, I mix in DNA at a 1.1:1 ratio of DNA:protein for the phosphorothiolated DNA, and a 1.2:1 ratio of DNA:protein for unmodified oligos.